공학박사 학위 논문

자세 변화 최소화 능력이 높고 장애물 극복 능력이 높은 험지 주행 로봇 (RHyMo)의 개발

Development of the Rough Terrain Hybrid Mobile Robot (RHyMo) with Low Posture Variation Index and High Terrainability

2015 년 8 월

서울대학교 대학원
기계항공공학부
최 동 규

자세 변화 최소화 능력이 높고 장애물 극복 능력이 높은 험지 주행 로봇 (RHyMo)의 개발

Development of the Rough Terrain Hybrid Mobile Robot (RHyMo) with Low Posture Variation Index and High Terrainability

지도 교수 김 종 원

이 논문을 공학박사 학위논문으로 제출함

2014 년 10 월

서울대학교 대학원

기계항공공학부

최 동 규

최동규의 공학박사 학위논문을 인준함

2014 년 12 월

위 원 장	주 종 남	(인)
부위원장	김 종 원	(인)
위 원	안 성 훈	(인)
위 원	조 규 진	(인)
위 원	김 화 수	(인)

Abstract

This thesis presents a new mobile robotic platform (RHyMo) which can reduce unexpected variations in height and pitch angle of its main body while traversing rough terrains and also has high terrainability to overcome an obstacle. A new performance metric for a mobile platform called as a posture variation index (PVI) was suggested to evaluate the smoothness of its movement on rugged terrain, which may play an important factor to predict undesired oscillations of a mobile platform while traveling on rugged terrain. The proposed PVI is defined as a combination of height and pitch angle variations of center of mass (CM) of a mobile platform. By using this proposed PVI, the movements of various mobile platforms are exhaustively analyzed.

A new linkage mechanism which has low posture variation was suggested by adopting the inverse four-bar mechanism. Height variation and pitch angle variation of main body of the new linkage mechanism were measured, and the resulting PVI is much smaller than those of other mobile platforms. The new linkage mechanism was optimized by kinematic analysis and the resulting PVI value was significantly reduced by 17.9 % compared to Rocker-Bogie mechanism which showed the smallest PVI value previously.

In order to ensure smooth movement as well as excellent terrainability, a new mobile platform (RHyMo) is proposed based on the kinematic and inverse dynamic analysis results. The extensive experiments are carried out by using Rocker-Bogie and RHyMo on artificial rugged terrain, which validate that in comparison with the Rocker-Bogie, the average and maximum height variations of RHyMo are reduced by 12.72 % and 5.96 %, respectively. Moreover, the average and maximum pitch angle variations of RHyMo are significantly reduced by 65.87 % and 60.53 %, respectively. The terrainability of RHyMo against a step and stairs of high slope is proved to be compatible to those of obstacle climbing mobile platforms with the help of the track mechanism installed at the front linkage

Keyword : mobile platform, posture variation index, terrainability, smooth movement, inverse dynamic analysis, track mechanism

Student Number : 2010-20723

Contents

List of Figures

List of Tables

Chapter 1. Introduction

1.1. Motivation

Various mobile platforms such as wheel−linkage platforms [1−6], track platforms [7−11], leg platforms [12−14] and hybrid platforms [15−19] have been developed to meet an increasing demand for a mobile platform to carry out a lot of tasks regardless of where it is. Therefore, unlike a four−wheeled vehicle to run on a flat road, a mobile platform is highly required to traverse manifold environments efficiently, where many types of obstacles are frequently encountered. For examples, well known Mars Exploration Rovers (MERs) such as Sojourner, Rocky7, Spirit and Opportunity should be able to travel on rugged terrain including different sizes of rocks, holes and humps but to the contrary, service platforms for cleaning and guide in indoor environment should be able to overcome a step or a threshold. From this point of view, it is not surprising that extensive research has focused on improving the capability of mobile platform to overcome an obstacle more effectively [20−23].

For this reason, many researches focus on increasing maneuverability of mobile platform. One of famous mobile platforms for rugged terrains is the MERS Rover equipped with the Rocker−Bogie mechanism which consists of two structural elements called as "Rocker" and "Bogie" [24−26]. The two wheeled Bogie is connected to the Rocker through a pivot and two Rockers on the left and right sides are properly coupled to each other by using a differential joint. With the help of Rocker−Bogie mechanism, all wheels of MER can always keep in contact with rugged terrain and get high traction force to travel on rugged terrain. Based on the Rocker−Bogie mechanism, such mobile platforms as RCL−E, CRAB, SHRIMP and wheeled mobile robot (WMR) have been studied to enhance the obstacle−climbing capability [27−32].

However, many mobile platforms frequently undergo unexpected oscillations while overcoming obstacles on rugged terrain, which may make it difficult for an operator to properly handle a mobile platform

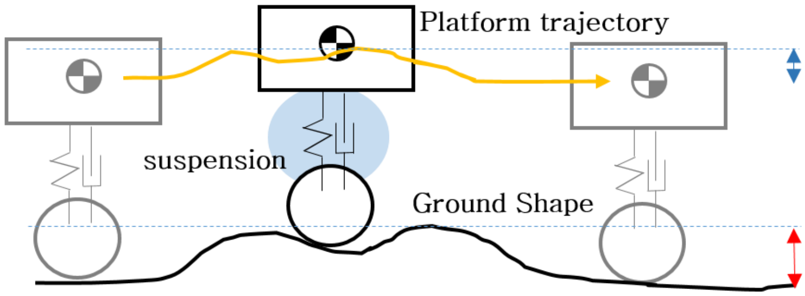

Fig 1.1. A trajectory of a mobile platform on rugged terrain

and lead to failing in a given task on rugged terrain. Since the sizes of obstacles that the platform encounters in such terrains are relatively large compared to wheel size, oscillations cannot be ignored. From the viewpoint of smooth movement, it seems important to minimize the variations of main body of mobile platform while overcoming an obstacle.

A trajectory of platform may be determined depending on ground shape and variation of trajectory can be reduced by using a suspension system between main body and the wheel. (Fig. 1.1) In the case of the four-wheeled automobiles, a spring damper suspension system (Fig. 1.2) is used to reduce the variation because the height of obstacles on road is small compared to the wheel radius (less than 5% of the wheel radius) [33]. However for mobile platforms, the height of obstacles is large and the velocity of platform is low, so the spring damper suspension cannot effectively reduce the variation of the main body efficiently. Therefore, a suspension system by linkage mechanism is more efficient to reduce the variations on mobile platform. With this motivation, this thesis proposes a new linkage suspension system to reduce variation of main body while traveling on a rugged terrain.

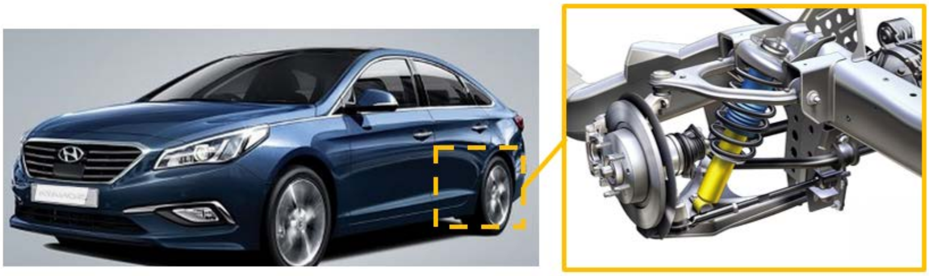

Fig. 1.2. A suspension system in a four-wheel automobile

1.2. Stability metrics on mobile platform

To design a new linkage mobile platform for rugged terrain traveling, comparison between well-known wheel-linkage mobile platforms has to be performed. Metrics on mobile platform can be used for the comparison and most important metric for mobile platform is stability metric. Since mobile platform has to move from place to place in order to carry out a given task, the ability of reaching destination without falling is most important. Two main metrics on stability are used to evaluate the stability of mobile platforms.

1.2.1. A Force angle stability method

The classic stability metric on mobile platform is the minimum distance between a projection point of center of mass (CM) to ground and a side of polygon which is derived from contact points of the platform and ground. If a platform contact with the ground in number of n points, n-polygon can be derived in ground plane. If a projection point of CM is inside in the n-polygon, the platform can maintain its posture and does not fail down. Number of n distances can be measured from the point and the side of the n-polygon, and the shortest distance is used as stability metric (d_2 in Fig. 1.3(a)). If the shortest distance is small, the platform has high possibility of failing [34,35].

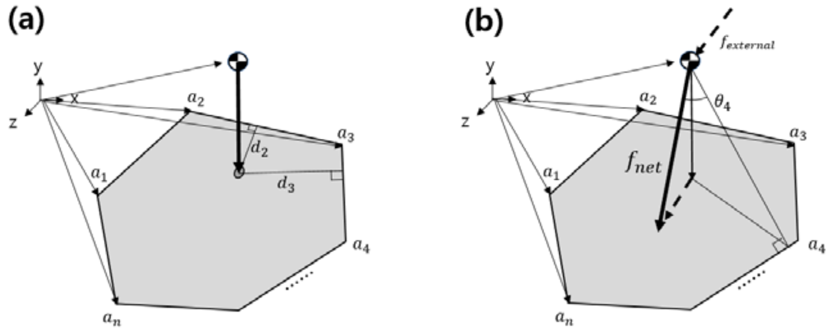

Fig. 1.3. (a) A stability metric (b) a force angle stability method

In Papadopoulos' research study, a Force Angle Stability Method was introduced to improve the classic stability metric [36]. In the Force Angle Stability Method, an external force and moment on main body were considered. The metric is defined by the magnitude of the CM's net force ($\|f_{net}\|$) multiplied by the smallest of the angles between the net force vector and the vector from CM to the side of n−polygon (θ) (Fig. 1.3 (b)). The metric is given by the following equation.

$$\alpha = \theta \cdot \|f_{net}\| \tag{1}$$

If the metric is close to zero, it means the platform is likely to tip−over by a small external force. Since on the force angle stability method, two main elements are multiplied, the metric becomes small value if one of the elements is small.

However, since the CMs of wheel−linkage mobile platform and track platform are close to the ground, the angle value on the metric is large. Therefore value of metric is quite large which means the platforms do not have high possibility of tip−over. Therefore, it seems meaningless comparing wheel−linkage mobile platforms by the stability metric. This metric is usually used for the leg mobile platform, where height of CM is large. Also since the calculation of the angle while traveling on random rugged terrain is quite difficult, the metric cannot be used in real−time control.

1.2.2. A Normalized energy stability margin

Another stability metric used for mobile platform is the Normalized Energy Stability Margin [37]. This metric is defined as a difference between the height of the platform's CM and the minimum distance from the CM to contact point on the ground. The smaller the metric is, the more tip over occurs. (Fig. 1.4)

The metric can easily measure while traveling on rugged terrain because the height of CM and the minimum distance from contact point to CM can be calculated from sensor and geometric condition of platform. Therefore, the stability of the platform can be measured in real time and the metric can be used in mobile platform control [38]. However, similar to the Force Angle Stability Method, the metric is useful for the leg mobile platform, but not for wheel−linkage platform or track platform. It is because if the CM is close to the ground, the metric is too large and it is not useful to warn the risk of tip over.

The metrics for defining stability of mobile platforms already exist, but these metrics can be used for comparing leg mobile platforms and not for comparing wheel−linkage platforms and track platforms.

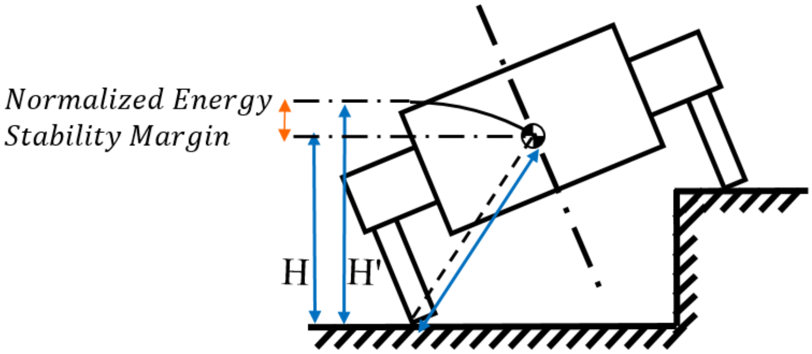

Fig. 1.4. A normalized energy stability margin

1.3. A terrainability metric on mobile platform

In order to evaluate the performance of mobile platform on rugged terrain systematically, the metric called as terrainability has been widely adopted, which is defined as the locomotion's ability to negotiate rough terrain features without compromising the vehicle's stability and forward progress. The minimum friction coefficient required for a mobile platform to climb a step whose height is set equal to the wheel diameter of a mobile platform is defined as quantitative value for terrainability [20−23]. If the minimum friction coefficient is low, following statements are true for the platform.

- The platform needs small traction force to overcome a step.
- The platform can overcomes more slippery steps compared to other mobile platforms.
- The platform can overcomes higher step compared to other mobile platforms in the same ground condition.
- The platform can have large payload than other mobile platforms with same motor.

Recall that previous studies have mainly focused on improving the mobile platform’ s ability of overcoming obstacles without considering the variation of CM of mobile platform. It is noteworthy that a mobile platform with high terrainability does not necessarily ensure acceptable performance in doing tasks on rugged terrain.

1.4. Slip metrics on mobile platform

On mobile platform study, there exist metrics to indicate slip ratio of mobile platform. Slip on wheels has to be eliminated to control platforms' locomotion to desire point. As seen in Fig. 1.5, wheels on platform move in different directions while traveling on rugged terrain, in order to eliminate slips, the velocities of wheels must be given differently based on ground shape. However, on rugged terrain traveling, the shape of ground cannot be measured completely and velocities of wheels on platform cannot be controlled depending on the ground shape in real time so the slip always exists. Therefore, from the viewpoint of locomotion control, a mobile platform which shows less slip on rugged terrain traveling can be regarded as a mobile platform which has high ability.

The slip ratio is widely used to compare mobile platforms, which is defined as dividing the difference between wheel rotation speed and moving velocity by the moving velocity. Also, metric called as velocity constraint violation (VCV) is used, which is defined as average of standard deviation of ideal velocity divide by real velocity [20]. Those metrics can be used for locomotion control on mobile platform, but not for reducing posture variation of main body.

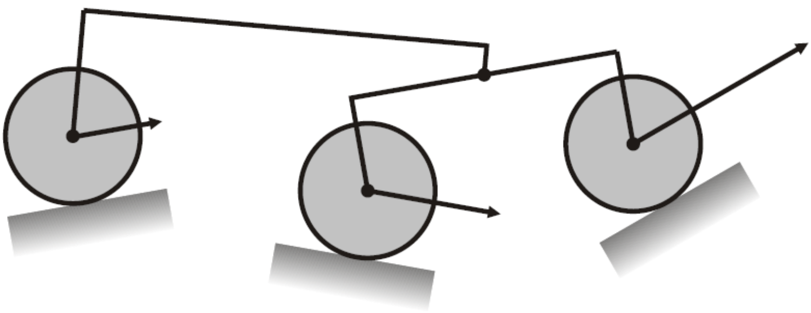

Fig. 1.5. Moving directions of wheels on rugged terrain

1.5. Objective of research

Even though several criteria on mobile platform on various environments have been proposed, a suitable metric for smooth movement of mobile platform has not been defined yet. Since during traveling on rugged terrain, smooth movement plays important role in reducing unexpected oscillation, saving time, energy and increasing control ability, comparison of mobile platforms has to be performed by using a proper metric.

In this study, a new metric for smooth movement is suggested, which is called as a posture variation index (PVI). The proposed PVI consists of variations in height and pitch angle of CM of mobile platform which are likely to experience sudden and significant changes among other parameters of mobile platform when its wheels are lifted up/down on rugged terrain. The PVIs of various mobile platforms are calculated and their movements are analyzed in details.

Based on the evaluation results by using the proposed PVI, a new linkage mobile platform (RHyMo) is constructed to ensure smooth movement as well as excellent terrainability. To this end, the kinematic analysis is applied to the new linkage mechanism combining the Rocker−Bogie mechanism with the inverse four−bar linkage mechanism, which proves that RHyMo can travel on rugged terrain most smoothly compared to well−known mobile platforms. In order to increase the terrainability of proposed mobile platform, the front wheel of Bogie mechanism is replaced with a track mechanism, which can increase terrainability of Bogie mechanism. Then, the dynamic analysis is performed to compare the terrainability of RHyMo with those of well−known mobile platforms. Finally, the experiment using RHyMo and the Rocker−Bogie mechanism on rugged terrain is carried out to verify that the height and pitch angle variations of RHyMo are significantly reduced to ensure the smooth movement against rugged terrain. Other experiments using a step and stairs demonstrate that RHyMo can overcome the obstacle like a step or stairs of high slope with small height and pitch angle variations as well as excellent terrainability

Chapter 2. New metric about posture variation on mobile platform

The smooth movement of the mobile platform seems quite important especially when the additional equipment to perform a task is mounted since the equipment may cause unexpected moment on the mobile platform, which may lead to tip−over at worst or serious oscillations to prevent an operator or a mobile platform itself from completing the given task. Therefore, it is necessary to evaluate the smoothness of mobile platform’ s movement on rugged terrain quantitatively.

However, no suitable measure for these parameters has been derived because the smooth movement of mobile platform is definitely affected by various factors such as the number and height of lifted wheels and the type of linkage mechanism adopted for a mobile platform. In this section, movement of mobile platform on rugged terrain is defined with height and pitch angle variation that change on traveling. From the elements, a new index of posture variation was defined and mobile platforms are compared with the index.

2.1. Definition of height and a pitch angle variation of main body on rugged terrain

Assuming speed of mobile platform is quite small, among other parameters of mobile platform, the height and pitch angle variations of its CM play important roles in determining its smooth movement. Since too many factors such as the number and heights of lifted wheels, and linkage mechanisms, etc will have the effect on the height and pitch angle variations, the basic assumptions are made to simplify the quantitative evaluation of the height and pitch angle variations of mobile platform. To perform a quantitative comparison with mobile platforms on rugged terrain traveling, a height and a pitch angle variation of main body have to be defined. The variations in height

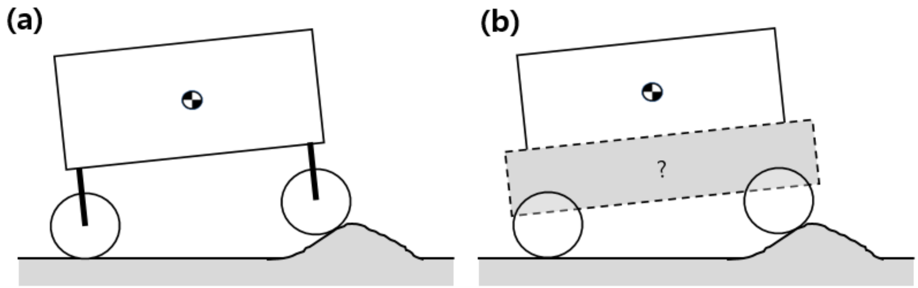

Fig. 2.1. (a) A four−wheel drive and (b) a linkage mechanism

and pitch angles can provide a useful insight into the smooth movement of mobile platform against rugged terrains in that the smooth movement may be considerably improved by reducing undesired caused by drastic variations in height and pitch angle of its main body.

In the case of a four−wheel drive mechanism without any suspension system on it (Fig. 2.1 (a)), the shape of ground directly has the influence to the CM. The height variation of a wheel changes height and pitch angle of CM. However as shown in Fig. 2.1 (b), if some linkage mechanism is attached between wheels and CM to reduce the height and pitch angle variation, the mobile platform can perform more smooth movement on rugged terrain traveling.

Fig. 2.2 shows the schematic diagram of defining the height and pitch angle variations of mobile platform, where H_i and $\emptyset_i$ denote the height and pitch angle variations of CM of mobile platform when the i^{th} wheel is lifted up to a height of d_i above the ground. Since all interactions between linkages and lifted wheels of mobile platform cannot be considered on rugged terrains, for the simplicity of analysis, a single wheel' s lift up is chosen as the alternative of measuring the capability of mobile platform to reduce variations in height and pitch angle. Also, it is impossible to consider all heights of wheel' s lift up, so it is assumed that the height of lift up is set equal to the radius of wheel. Note that the radius of wheel is theoretically the maximum height of obstacle that a mobile platform can overcome without the help of complex control strategy on rugged terrain.

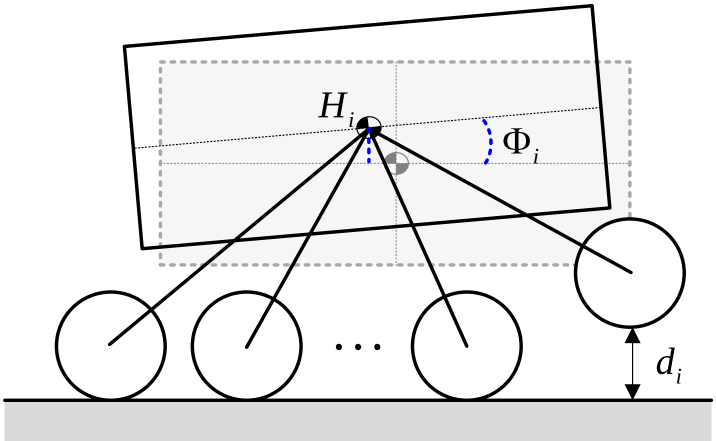

Fig. 2.2. Schematic diagram of defining the height and pitch angle variations.

The number of data related with height and pitch angle is N and N, for a N−wheeled mobile platform. For the index of smooth movement of mobile platform, average, standard deviation and maximum value of height and pitch angle variation were considered. The reason that considering not only average value but also standard deviation and maximum value can be explained in Fig. 2.3.

Consider two mobile platforms, and suppose mobile platform A shows height variation as shown in Fig 2.3 (a), and that of the other mobile platform B is shown in Fig. 2.3 (b). The mobile platform A shows small average of height variation but each values are widely spread. On the other hand, the mobile platform B shows higher average variation than that of the mobile platform A, but each values are not far from the average. If only the average of height variation is considered in the index, the mobile platform A can be regarded as the best mobile platform which has low height variation. However, from the viewpoint of smooth movement, it can be easily imagined that the mobile platform B will show smoother movement on rugged terrain. Therefore, on the index to represent a smooth movement of mobile platform, the standard deviation of height variation must be considered.

Also, maximum height variation has to be considered and the reason can be explained in Fig. 2.3 (c). Even though a mobile platform show low average height variation and low standard deviation, if the maximum variation is large, the mobile platform has high possibility of tip over or drastic variation to CM. Therefore for the index of smooth movement of mobile platform, average, standard deviation and maximum value of height and pitch angle must be considered.

For a mobile platform with N wheels on its one side, the height and pitch angle variations of mobile platform are defined as

$$H_{mobile}^{N} = \sqrt{a \cdot (H_{mobile}^{avg})^2 + b \cdot (H_{mobile}^{std})^2 + c \cdot (H_{mobile}^{max})^2} \quad (2)$$

$$\emptyset_{mobile}^{N} = \sqrt{a \cdot (\emptyset_{mobile}^{avg})^2 + b \cdot (\emptyset_{mobile}^{std})^2 + c \cdot (\emptyset_{mobile}^{max})^2} \quad (3)$$

where H_{mobile}^{avg} ($\emptyset_{mobile}^{avg}$), H_{mobile}^{std} ($\emptyset_{mobile}^{std}$) and H_{mobile}^{max} ($\emptyset_{mobile}^{max}$) correspond to the average height (pitch angle) variation, its standard deviation and the maximum height (pitch angle) variation, respectively. The weighting factors a, b and c are adopted to reflect the effect of each term appropriately since the movement of mobile platform can be affected by a standard deviation as well as a maximum variation even though the average height or pitch angle variation is quite small.

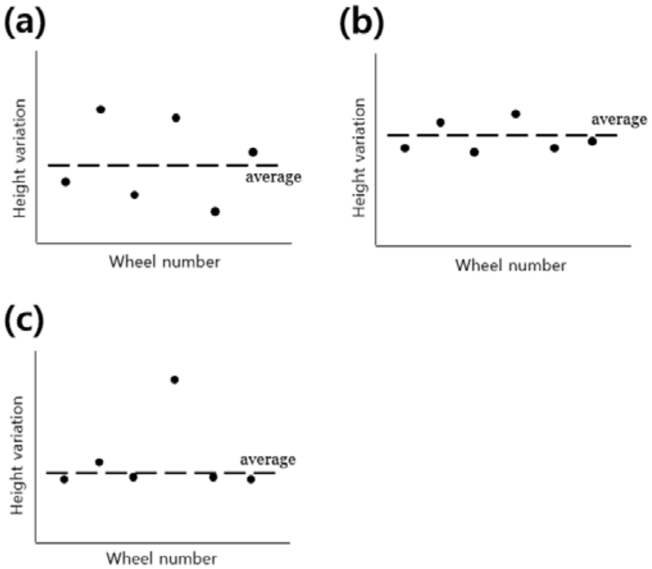

Fig. 2.3. Various height variations of mobile platforms

2.2. Definition of a posture variation index (PVI)

With the definition of height and pitch angle of mobile platform, the posture variation index (PVI) of a mobile platform with N wheels on its one side is defined as

$$PVI = \frac{H_{mobile}^{N}}{H_{4WD}^{2}} \times \frac{\emptyset_{mobile}^{N}}{\emptyset_{4WD}^{2}} \qquad (4)$$

H_{mobile}^{N} : A height variation of a mobile platform
$\emptyset_{mobile}^{N}$: A pitch angle variation of a mobile platform
H_{4WD}^{2} : A height variation of a same size four−wheel drive
$\emptyset_{4WD}^{2}$: A pitch angle variation of a same size four−wheel drive

Note that the proposed PVI is non dimensional and as a PVI of a mobile platform becomes closer to "1", its movement on rugged terrain is very similar to that of four−wheel drive mobile platform of same size so that the movement of mobile platform is liable to suffer from undesired oscillations caused by drastic height or pitch angle variations. If PVI of a mobile platform is closer to zero, the platform is expected to show smooth movement on rugged terrain traveling. By calculating PVI values of mobile platforms, movements of mobile platforms on rugged terrain can be compared.

2.3. Comparison of mobile platforms with posture variation index

To compare the movements of various mobile platforms on rugged terrain with the proposed PVI, it is necessary to scale different sizes of mobile platforms for fair comparison. As the main parameters that mobile platforms have in common, the wheel radius and the distance between wheels are chosen to be 80 mm and 300 mm, respectively and the CM of a mobile platform is assumed to be

150 mm above the center of wheel and also exactly above the middle wheel. Other parameters of mobile platforms are properly adapted so as to make them compatible. Each mobile platform is modeled by using the 3−D modeling tool (Version 2012, SolidWorks, Dassault Systems, Concord, MA, USA) and under the assumption that that the i^{th} wheel of mobile platform is lifted up to height of its radius, the height and pitch angle variations H_i and $\emptyset_i$ are calculated and the results are shown in Table I.

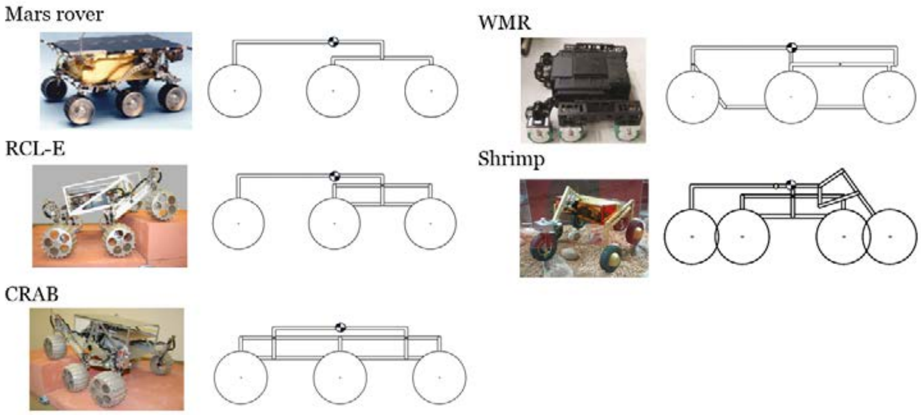

Fig. 2.4. Pictures and schematics of mobile platforms

Table. I. PVI values, height and pitch angle variations of mobile platforms

Mobile Platform	Variation rate when the front wheel was lifted up		Variation rate when the middle wheel was lifted up		Variation rate when the back wheel was lifted up		P V I
	Height [%]	Angle [%]	Height [%]	Angle [%]	Height [%]	Angle [%]	
Mars rover [24]	0.60	0.61	0.60	0.61	0.63	1.36	0.725
RCL−E [27]	0.65	0.67	0.65	0.67	0.61	1.34	0.746
CRAB [28]	0.69	0.92	0.90	0.35	0.69	1.10	0.820
WMR [32]	1.22	0.65	0.18	0.44	1.09	1.28	1.198
Shrimp [30]	0.80	1.00	0.80	1.00	0.20	2.02	1.283

Fig. 2.5 compares the PVIs of stair climbing, track based and wheel−linkage mobile platforms with four−wheel drive mobile platform, where the weighting factors a, b and c are set to be “1”. By the definition of the PVI, the PVI of four−wheel drive mobile platform is equal to “1”. Note that since it is assumed that a four−wheel drive platform has no suspension system, the shape or size of obstacle on rugged terrain will directly affect the movement of mobile platform. As shown in Fig. 2.5, without an active control of tracks of platform, the movements of track based platforms such as Packbot [39], Kenaf [40], and Chaos [41] on rugged terrain are same as that of a four−wheel drive platform suffering from undesired oscillations since the main body of track based mobile platform is directly connected to the tracks so that the height and pitch angle variations of its CM are inevitably deteriorated whenever the track is lifted up.

Unfortunately, the PVIs of stair climbing mobile platforms like Shrimp and WMR are much larger than “1”. Note that the stair climbing mobile platforms are equipped with additional or modified linkage to increase their climbing capability against a structured step or stairs, which may lead to unexpected larger posture variations. In fact, the movement of WMR is less susceptible to the lift up of the middle wheel rather than those of the front and back ones that are connected to its body through a modified four−bar mechanism but as the maximum height variations are too large during the lift ups of the front and the back wheels, the resulting PVI becomes large. As for the Shrimp, the effect of its front fork wheel on the PVI is negligible compared to those of the middle and back wheels since the front fork can naturally elevate the front wheel without causing the height or pitch angle variation. However, since the maximum pitch angle variations are considerably increased when the middle and the back wheels connected by the parallel Bogie are lifted up, the resulting PVI is deteriorated.

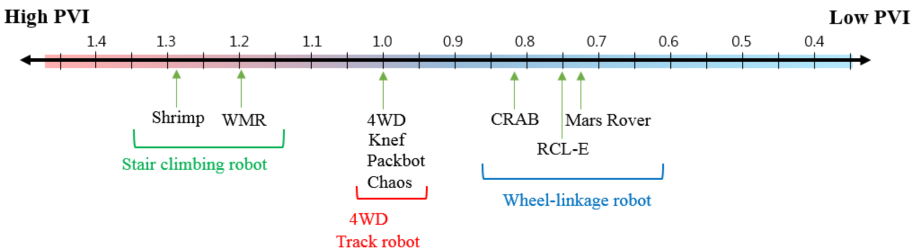

Fig. 2.5. A PVI of mobile platforms

In general, the PVIs of the wheel−linkage mobile platforms are smaller than "1", which implies that the movements of wheel−linkage mobile platforms on rugged terrain are relatively smoother than those of the track based or stair climbing ones. Among them, the PVI of Mars rover based on Rocker−Bogie mechanism is the smallest. RCL−E replaces the Bogie mechanism with the parallel Bogie with the aim of increasing the capability of overcoming sharp obstacles on rugged terrain. CRAB is built upon two parallel Bogies in order to achieve same performances in both forward and backward motions. This two mobile platform was studied to increase maneuverability base from a Rocker−Bogie mechanism, but their posture variation was increased also. It is worthwhile to note that even though RCL−E and CRAB are similar to Shrimp in that the parallel Bogie mechanism is used, the resulting PVIs of RCL−E and CRAB are smaller than that of Shrimp since the geometric relation between the CM of mobile platform and the parallel Bogie is different from each other.

2.4. Terrainability of mobile platforms

The terrainability of mobile platform is the important factor to determine its capability of climbing the obstacle frequently encountered on rugged terrain and defined as the minimum friction coefficient required for a mobile platform to climb a step whose height is equal to its wheel diameter. Since the terrainability is as important as the PVI, the terrainability of mobile platforms was compared.

The terrainability was measured by a motion planning on Solidworks program. Every mobile platforms were modeling in 2D, and by changing friction coefficient between wheels and the ground, the simulation was performed (Fig. 2.6). During the simulation, the minimum friction coefficient to enable a mobile platform to overcome a step was measured. As seen in Fig. 2.7, four-wheel drive car shows the highest friction coefficient, which means that the platform has low terrainability. The friction coefficient of the wheel-linkage mobile platforms is lower than that of the four-wheel drive car.

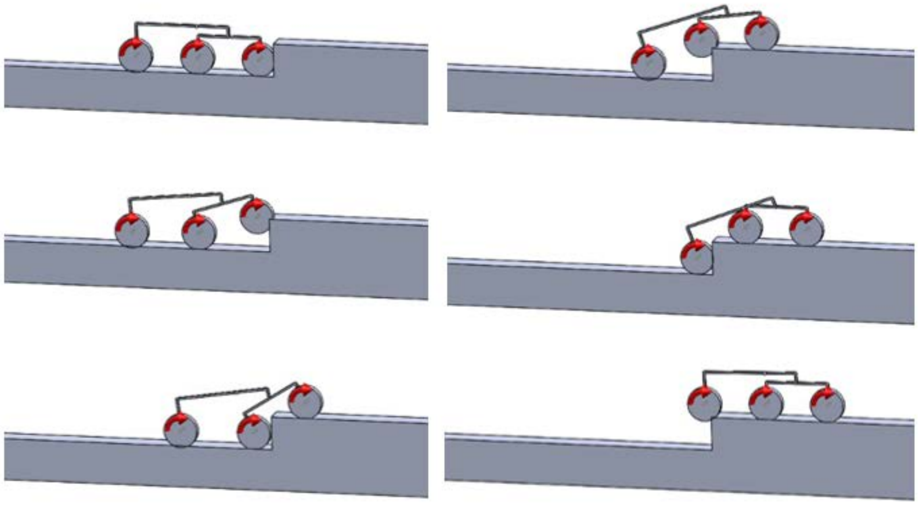

Fig. 2.6. Simulation of overcoming a step

For comparison, track mobile platforms, Packbot, Knef, and CHAOS, was also considered. The friction coefficient of the track mechanism was measured by method introduced in Guangjun Liu’ s research [42,43]. The terrainability of track mechanism increases as the track length becomes longer.

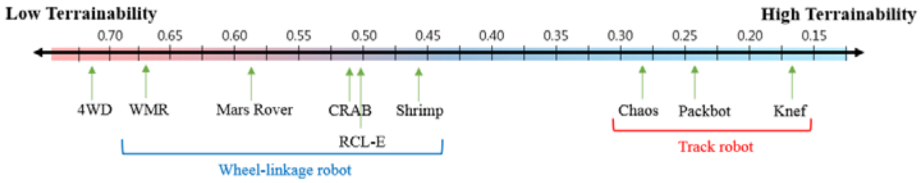

Fig. 2.7. A terrainability of mobile platforms

2.5. A PVI-Terrainability of mobile platforms

By combining the posture variation in Section 2.3 with the terrainability in Section 2.4, a PVI–terrainability of various mobile platforms are obtained as shown in Fig. 2.8, where the X–axes and Y–axes represent the PVI and the terrainability, respectively. When a mobile platform has a much smaller PVI, that is, its movement on rugged terrain becomes smoother, it is located closer to the right side of Fig. 2.8. If a mobile platform has a higher terrainability, that is, it can easily overcome an obstacle without slip, it is located closer to the upper side of Fig. 2.8. In general, the wheel–linkage mobile platforms are located at the lower right side of Fig. 2.8, which indicates that they ensure excellent posture variations on rugged terrain and poor terrainability. In fact, it is revealed that mobile platforms such as the RCL–E and the CRAB focusing on increasing the terrainability of Mars Rover show slightly improved terrainability but the resulting posture variations are relatively increased at the same time. The track based mobile platform are located at the upper left side of Fig. 2.8, which implies that they achieve excellent terrainability but has poor posture variations on rugged terrain.

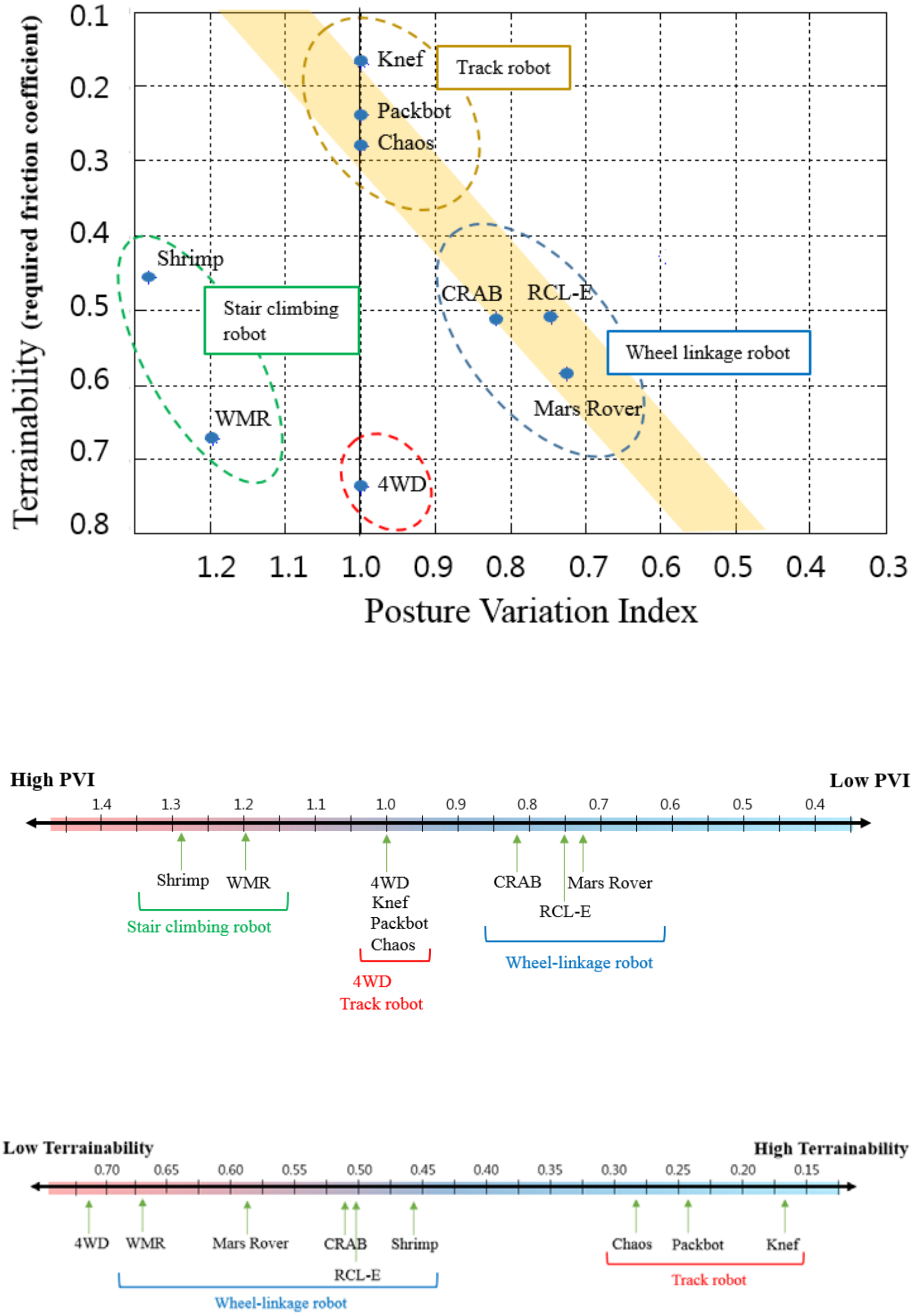

Fig. 2.8. A PVI−terrainability of mobile platforms

Chapter 3. New linkage mechanism

Among various types of mobile platforms, the movement of Rocker−Bogie mechanism on rugged terrain is expected to be much smoother than other platforms. Before building a new mechanism, the detailed kinematic analysis of Rocker−Bogie mechanism on rugged terrain is carried out to investigate the effects of lifted wheels on the resulting height and pitch angle variations, which is tactfully exploited to propose a new mobile platform. The kinematic analysis of the proposed mobile platform is subsequently performed to ensure the smooth movement as well as the terrainability against rugged terrain.

3.1. Analysis of height and pitch angle variations of Rocker-Bogie mechanism

Figs. 3.1 (a) and 3.1 (b) show the schematic diagrams of Rocker−Bogie mechanism and the case that its back wheel is lifted up to the height of its radius, respectively. Under the same conditions on the wheel radius, the distance between wheels and the position of CM assumed for calculating the PVI in the previous section, the height and pitch angle variations of Rocker−Bogie mechanism are obtained when each wheel is lifted up. Table II shows the resulting height and pitch angle variations. It is worthwhile to note that due to the symmetry of Bogie mechanism, $H_1 = H_2$ and $\emptyset_1 = \emptyset_2$ and when the front or middle wheel of Bogie is lifted up, the resulting height and pitch angle variations are relatively smaller than those obtained when the back wheel is lifted up. This is because the CM of Rocker−Bogie mechanism lies on the Rocker linkage which the back wheel is directly connected to so that its lift up naturally deteriorates the height and pitch angle variations H_3 and $\emptyset_3$ as shown in Table II. Therefore, it is possible to achieve much smoother movement than that of Rocker−Bogie mechanism on rugged terrain by reducing the correlation between the back wheel and the CM by virtue of additional mechanism.

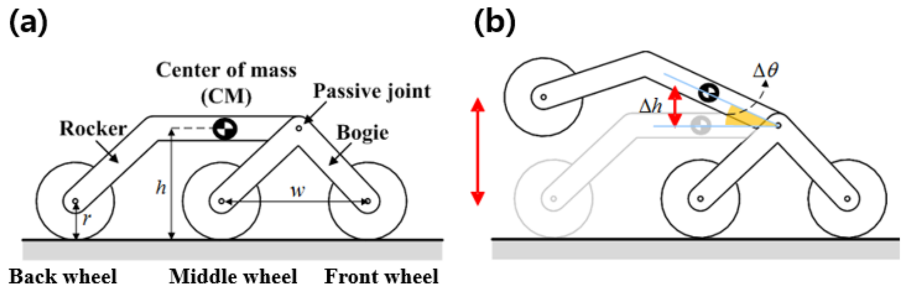

Fig. 3.1. Schematic diagrams of (a) Rocker–Bogie mechanism and (b) case that the back wheel is lifted up.

Table. II. A height and pitch angle variations of Rocker–Bogie mechanism

	Wheel to be lifted up 80 mm		
	front wheel	middle wheel	back wheel
Height variation H_i [mm]	23.97	23.97	25.39
Pitch angle variation $\emptyset_i$ [°]	4.68	4.68	−10.40

3.2. Concept design of new linkage mechanisms

The simplest solution to reduce the detrimental effect of the back wheel of Rocker–Bogie mechanism on the height and pitch angle variations may be to install a revolute joint between the back wheel and its CM, which will prevent the effect of lifted back wheel from being transmitted to the CM. However, by adding the additional joint to Rocker mechanism, the degree of freedom (DOF) of mobile platform increases by one and as a result, the mobile platform cannot maintain its posture so that a new mechanism with an additional linkage should be taken into account.

The schematic diagrams of possible candidates are shown in Fig. 3.2, where two mobile platforms in Figs. 3.2 (a) and 3.2 (b) are built upon the four–bar linkage mechanism while other two mobile platforms in Figs. 3.2 (c) and 3.2 (d) are constructed with the inverse four−bar linkage mechanism. It is worthwhile to note that since the motions of linkages of the four−bar mechanism are highly correlated with each other, it is possible to predetermine the motions of linkages by choosing their lengths properly in such a manner that the height and pitch angle variations caused by lifts up of the back wheel can be reduced. In this study, a new linkage based mobile platform is suggested, which consists of Rocker−Bogie mechanism combined with one of four−bar linkage mechanisms in Fig. 3.2. To evaluate how much the proposed structure of new mobile platform can reduce the height and pitch angle variations on ragged terrain, the kinematic analysis of four−bar linkage mechanism is subsequently carried out.

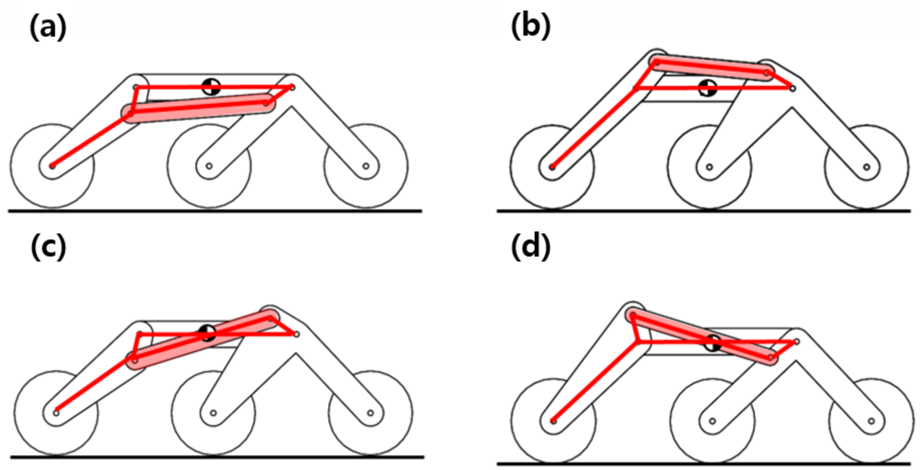

Fig. 3.2. Schematic diagrams of possible candidates with (a) four−bar linkage mechanism 1, (b) four−bar linkage mechanism 2, (c) inverse four−bar linkage mechanism 1 and (d) inverse four−bar linkage mechanism 2.

3.3. Kinematic analysis of four-bar linkage mechanism

To compare these four linkages for new linkage mobile platform, a height and a pitch angle variation of main body was calculated by kinematic analysis assuming that a back wheel was lifted up. The following equations were derived from Freudenstein’s equation [44].

$$A_1 cos\rho_3 - A_2 cos\rho_1 + K_3 = \cos(\rho_1 - \rho_3) \quad (5)$$

$$A_1 cos\rho_2 - A_4 cos\rho_1 + K_5 = \cos(\rho_1 - \rho_2) \quad (6)$$

where

$$A_1 = \frac{l_4}{l_1} \quad (7)$$

$$A_2 = \frac{l_4}{l_3} \quad (8)$$

$$A_3 = \frac{{l_1}^2 - {l_2}^2 + {l_3}^2 + {l_4}^2}{2 l_1 l_3} \quad (9)$$

$$A_4 = \frac{l_4}{l_2} \quad (10)$$

$$A_5 = \frac{{l_3}^2 - {l_4}^2 - {l_1}^2 - {l_2}^2}{2 l_1 l_2} \quad (11)$$

By solving equations (5) and (6), the angles between linkages and the ground can be obtained. The angles are given by

$$\rho_2 = 2\tan^{-1}\left(\frac{-B_2 \pm \sqrt{{B_2}^2 - 4B_1B_3}}{2B_1}\right) \quad (12)$$

$$\rho_3 = 2\tan^{-1}\left(\frac{-B_5 \pm \sqrt{{B_5}^2 - 4B_4B_6}}{2B_4}\right) \quad (13)$$

where

$$B_1 = cos\rho_1 - A_1 + A_4 cos\rho_1 + A_5 \quad (14)$$

$$B_2 = -2sin\rho_1 \quad (15)$$

$$B_3 = A_1 + (A_4 - 1)cos\rho_1 + A_5 \quad (16)$$

$$B_4 = cos\rho_1 - A_1 + A_2 cos\rho_1 + A_3 \quad (17)$$

$$B_5 = -2sin\rho_1 \quad (18)$$

$$B_6 = A_1 - (A_2 + 1)cos\rho_1 + A_3 \quad (19)$$

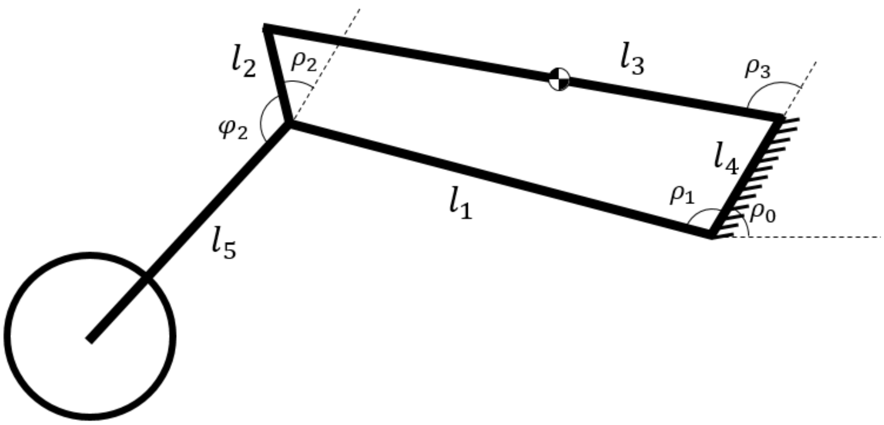

Fig. 3.3. A schematic of four-bar linkage mechanism

ρ_0 is the given value from geometric condition of the Bogie linkage, and φ_2 is fixed value from the mechanism. By setting a value of ρ_1 as input value, the angle between the linkages and the ground can be calculated and height of back wheel from the ground can be also calculated. Furthermore, height variation and pitch angle variation of CM can be calculated when the back wheel is lifted up to the height of wheel radius.

3.4. Comparison of four linkage mechanisms

Under the same conditions on the wheel radius, the distances between wheels and the CM position used in Section 2, the initial values for the linkage lengths $(l_1, l_2, l_3, l_4, l_5,)$, the angles between linkages (φ_2, ρ_0) are chosen properly. Then, when the back wheel of mobile platform in Fig. 3.2 is lifted up to a height of its radius, the height and pitch angle variations of mobile platforms in Fig. 3.2 are simulated by using the kinematic analysis and shown in Fig. 3.4, where the Bogie mechanism is omitted and the cyan and black lines denote before and after the back wheel of mobile platform is lifted up, respectively and the movement of CM is denoted by the blue line.

Fig. 3.4 explicitly implies that when the back wheel is lifted up, the resulting height and pitch angle variations of mobile platforms with the four−bar linkage in Figs. 3.4 (a) and 3.4 (b) are larger than those of mobile platforms with the inverse four−bar linkage in Figs. 3.4 (c) and 3.4 (d).

Fig. 3.5 compares the height and pitch angle variation rates of mobile platforms in Fig. 3.2 with Rocker−Bogie mechanism, which are obtained by dividing the height and pitch angle variations with the lifted height of wheel. As shown in Fig. 3.5, the height and pitch angle variation rates of mobile platforms with four−bar mechanisms in Figs. 3.2 (a) and 3.2 (b) increase in proportion to the lifted height of the back wheel while those of mobile platforms with inverse four−bar mechanisms in Figs. 3.2 (c) and 3.2 (d) are almost constant regardless of lifted height of the back wheel and quite smaller than those of Rocker−Bogie mechanism.

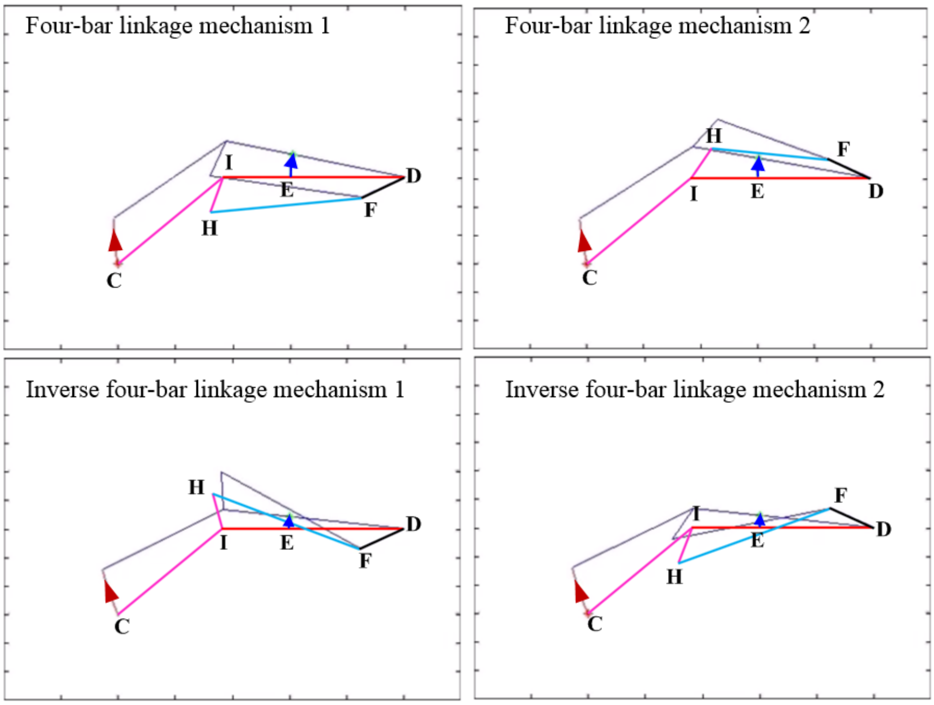

Fig. 3.4. Simulation results of mobile platforms with (a) four−bar linkage mechanism 1, (b) four−bar linkage mechanism 2, (c) inverse four−bar linkage mechanism 1 and (d) inverse four−bar linkage mechanism 2 when the back wheel is lifted up to its radius.

If four−bar mechanisms in Fig. 3.2 (a) and 3.2 (b) is used on new linkage mobile mechanism, the height and the pitch angle variation of main body will be greater than Rocker−Bogie mechanism and a posture variation will be increased. Therefore, the four−bar mechanisms are not suitable for new linkage mobile mechanism.

On the contrary, the inverse four−bar mechanisms in Fig. 3.2 (c) and 3.2 (d) show smaller variation compared to Rocker−Bogie mechanism so that a new linkage mobile mechanism using the inverse four−bar mechanism is expected to show much smoother movement on rugged terrain traveling compared to Rocker−Bogie mechanism.

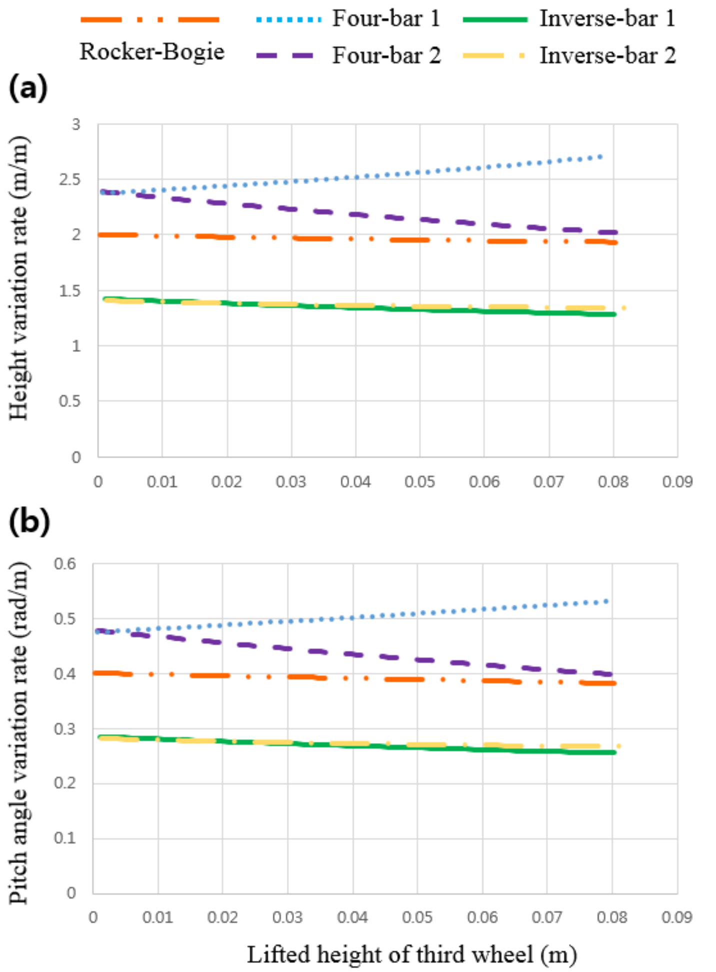

Fig. 3.5. Comparison of simulation results of height and pitch angle variation rates of the platforms and Rocker−Bogie

3.5. Comparison of two inverse four-bar linkage mechanisms

For further comparison of mobile platforms with inverse four−bar linkage mechanisms, the effects of their front and middle wheels on the height and pitch angle variations are investigated. When the lifted height of the front or middle wheel increases, the height of joint D will also increase and Bogie linkage will rotate counter−clockwise or clockwise and as a result, the gap angle changes (see Fig. 3.6 (a)). For the mobile platform with the inverse four−bar linkage mechanism, this gap angle plays an important role in determining the height and pitch angle variations. It is noted that as the gap angle becomes close to zero, the resulting height and pitch angle variations become smaller (Fig. 3.6 (b)).

In the case of mobile platform with the inverse four−bar 1 in Fig. 3.2 (c), when the front wheel is lifted up, the Bogie linkage rotate counter−clockwise so that the CM moves considerably downward as denoted by the red arrow in Fig. 3.7 (a). However, since the gap angle will increase at the same time, the height and pitch angle variations caused by the lift up of the front wheel can be compensated to some extent. From this reason, when the front wheel is lifted up, the height and pitch angle variations of mobile platform with this inverse four−bar linkage 1 can be decreased. When the middle wheel is lifted up, the Bogie linkages rotate clockwise to make the CM move

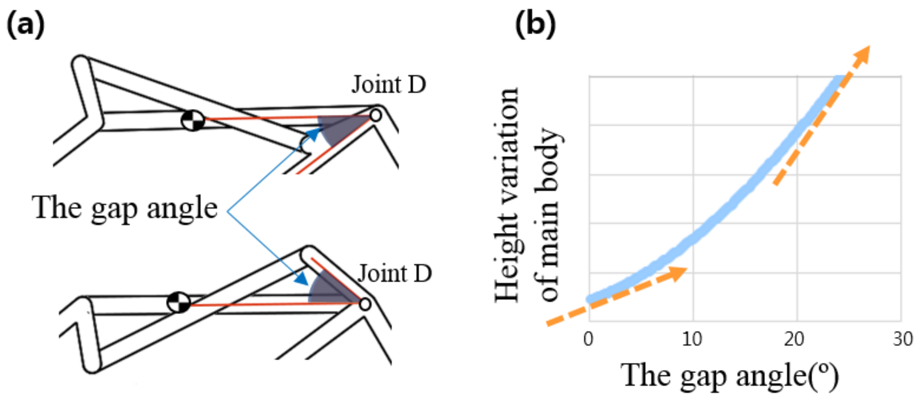

Fig. 3.6. (a) The gap angle on inverse four−bar linkage
(b) the gap angle − a height variation graph

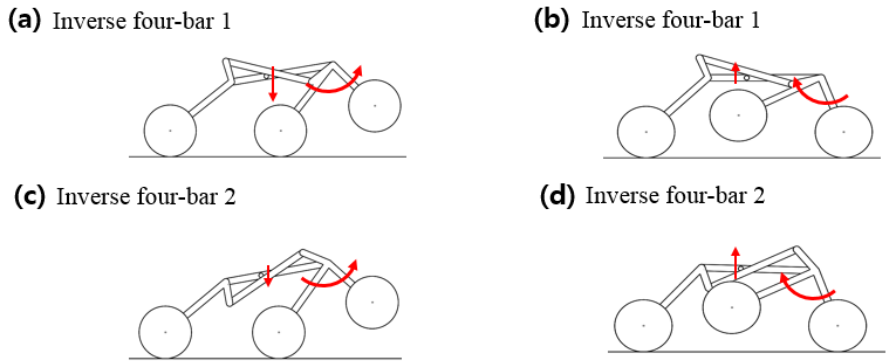

Fig. 3.7. Schematic diagrams of mobile platforms with inverse four-bar linkage 1 ((a),(b)) and inverse four-bar linkage 2 ((c),(d)) when the front or middle wheel is lifted up.

slightly upward and since the gap angle becomes close to zero, the effect of gap angle on the CM can be neglected. (Fig. 3.7 (b))

In the case of mobile platform with the inverse four-bar 2 in Fig. 3.2 (d), when the front wheel is lifted up, the Bogie linkage rotate counter-clockwise and the gap angle decreases to zero as denoted by the red arrow in Fig. 3.7 (c). Therefore, the height and pitch angle variations of mobile platform with the inverse four-bar 2 may be larger than those of mobile platform with the inverse four-bar 1 since the variations caused by the lift up of the front wheel cannot be compensated properly. In a similar manner, when the middle wheel is lifted up, the Bogie linkages rotate clockwise and the gap angle also increases so that the height and pitch angle variations are increased (Fig. 3.7 (d)). As a result, the mobile platform with the inverse four-bar linkage 1 is chosen in this study, which seems more suitable for traveling on rugged terrain with smaller height and pitch angle variations.

3.6. Kinematic analysis of a new linkage mechanism

Kinematic analysis of inverse four−bar linkage 1 was performed for calculating PVI and its schematic diagram is in details shown in Fig. 3.8, where D, F, H and I denote the revolute joints, E represents the CM of main body of mobile platform and, A, B, C correspond to the centers of wheels, respectively. The distances between D and E, D and F, F and H, H and I and, I and D are denoted by L_s, s_9, s_{13}, s_{12} and s_{10}, respectively. The distance between wheels and the lengths of Bogie mechanism are given by s_0, s_1 and s_2, respectively. The contact angles between the i^{th} wheel and the ground are represented by α_i and the angles of the Bogie and Rocker mechanisms with respect to the flat surface are denoted by θ_i, i =1, 2, 3, respectively. The angles between two lines AD and BD, two lines BD and DF and two lines HI and CI are denoted by φ_i, i =1, 2, 3, respectively. Recall that for the given lengths of linkages ($s_1, s_2, s_9, s_{10}, s_{11}, s_{12}, s_{13}$) the angles between linkages (φ_2, φ_3) and the ground conditions (α_i, h_i, i =1, 2, 3), the angles between the linkages and the flat surface (θ_i, i =1~5) can be calculated.

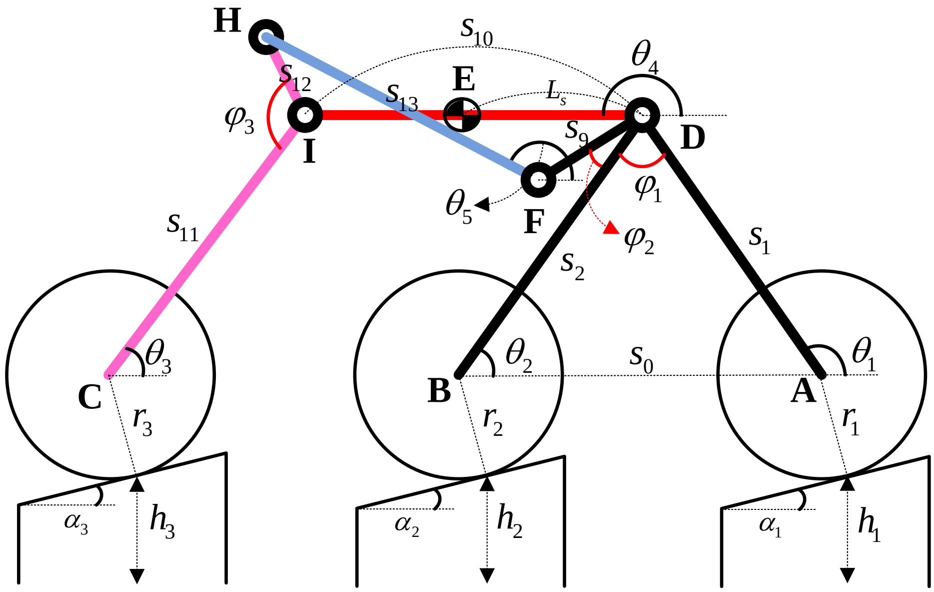

Fig. 3.8. Schematic diagram of proposed mobile platform for kinematic analysis.

From the geometric condition shown in Fig. 3.8, the following relations can be derived.

$$\varphi_1 = cos^{-1}(\frac{{s_1}^2 + {s_2}^2 - {s_0}^2}{2s_1 s_2}) \tag{20}$$

$$\theta_1 = \theta_2 + \varphi_1 \tag{21}$$

The height h_D of joint D can be obtained as follows:

$$\begin{aligned} h_D &= h_1 + r_1 cos\alpha_1 + s_1 \, sin(\pi - \theta_1) \\ &= h_2 + r_2 cos\alpha_2 + s_2 \sin\theta_2 \end{aligned} \tag{22}$$

By combining (21) with (22), θ_1 can be calculated as follows:

$$\theta_1 = \sin^{-1}\frac{h_1 - h_2 + r_1 cos\alpha_1 - r_2 cos\alpha_2}{\sqrt{(s_2 cos\varphi_1 - s_1)^2 + (-s_2 sin\varphi_1)^2}} - \tan^{-1}\frac{-s_2 sin\varphi_1}{s_2 cos\varphi_1 - s_1} \tag{23}$$

Using (23), θ_2 can be easily calculated from (21) and in order to calculate θ_3, θ_4 and θ_5, the following relations can be derived by considering two closed loops D−F−H−I−D and C−I−D−B−C.

$$\begin{aligned} &h_1 + r_1 cos\alpha_1 + s_1 \sin\theta_1 \\ &= h_3 + r_3 cos\alpha_3 + s_{11} \, sin\,\theta_3 + s_{10} \sin(\theta_4 - \pi) \end{aligned} \tag{24}$$

$$\begin{aligned} &-s_{10} \sin(\theta_4 - \pi) + s_{12} \sin(\varphi_3 - \theta_3) \\ &\quad = s_{13} \sin(\pi - \theta_5) - s_9 \sin(\theta_1 - \varphi_1 - \varphi_2) \end{aligned} \tag{25}$$

$$\begin{aligned} &s_{10} \cos(\theta_4 - \pi) + s_{12} \cos(\varphi_3 - \theta_3) \\ &\quad = s_{13} \cos(\pi - \theta_5) + s_9 \cos(\theta_1 - \varphi_1 - \varphi_2) \end{aligned} \tag{26}$$

Rearranging (22) and (24), the following equations are obtained

$$s_{10} \sin\theta_4 = c_1 + s_{11} \, sin\,\theta_3 \tag{27}$$

$$s_{10} \cos\theta_4 = -\sqrt{{s_{10}}^2 - (c_1 + s_{11} \, sin\,\theta_3)^2} \tag{28}$$

where c_1 is given by $c_1 = h_3 - h_0 + r_3 cos\alpha_3$ Similarly, the following equations can be derived

$$s_{13}\sin\theta_5 = sin\theta_3(s_{11} - s_{12}cos\varphi_3) + cos\theta_3(s_{12}sin\varphi_3) + c_1 + c_2 \\ = \sqrt{{c_4}^2 + {c_5}^2}sin(\theta_3 + \emptyset') + c_1 + c_2 \tag{29}$$

$$s_{13}\cos\theta_5 = -\sqrt{{s_{13}}^2 - (\sqrt{{c_4}^2 + {c_5}^2}sin(\theta_3 + \emptyset') + c_1 + c_2)^2} \tag{30}$$

where $c_2 = s_9\sin(\theta_1 - \varphi_1 - \varphi_2)$, $c_4 = s_{11} - s_{12}cos\varphi_3$, $c_5 = s_{12}sin\varphi_3$ and, $\emptyset' = \tan^{-1}{}^{c_5}/_{c_4}$ respectively. By combining (26), (27), (28) and (30), the following equation can be obtained:

$$\sqrt{{s_{13}}^2 - (\sqrt{{c_4}^2 + {c_5}^2}sin(\theta_3 + \emptyset') + c_1 + c_2)^2} + c_3 \\ = \sqrt{{s_{10}}^2 - \left(c_1 + s_{11}\sin\theta_3\right)^2} + s_{12}\cos(\varphi_3 - \theta_3) \tag{31}$$

where $c_3 = s_9\cos(\theta_1 - \varphi_1 - \varphi_2)$. It is worthwhile to note that if θ_3 is calculated from (31), θ_4 and θ_5 can be easily obtained by using (27) and (29). Since (31) consists of a combination of sine and cosine functions, (31) is a nonlinear problem so that the exhaustive search method is used to obtain a precise value for θ_3.

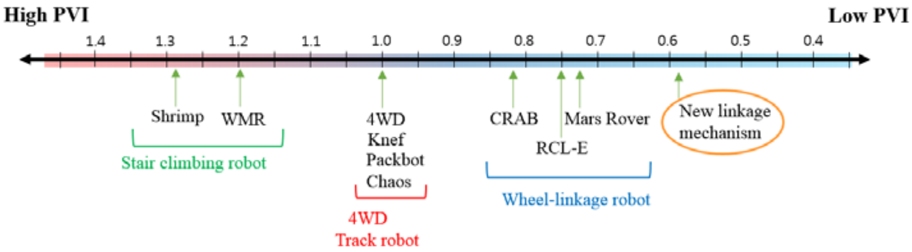

Fig. 3.9. A terrainability of mobile platforms with a new linkage mechanism

Table. III. Optimal parameter values of proposed mobile platform

L_s	s_1	s_2	s_9	s_{10}	s_{11}	s_{12}	s_{13}	φ_2	φ_3
0.2087 m	0.18 m	0.26 m	0.084 m	0.318 m	0.241 m	0.066 m	0.2719 m	13 °	114 °

Table. IV. Height and pitch angle variations and PVIs of Rocker−Bogie mechanism, Rocker−Bogie + inverse four−bar linkage 1 and Rocker−Bogie + inverse four−bar linkage 2

A wheel was lifted up 80 mm	Front wheel		Middle wheel		Third wheel		PVI
	H_1 [mm]	$\emptyset_1$ [°]	H_2 [mm]	$\emptyset_2$ [°]	H_3 [mm]	$\emptyset_3$ [°]	
Rocker−Bogie	23.97	4.68	23.97	4.68	25.39	−10.40	0.725
Rocker−Bogie + Inverse four−bar 1	19.20	8.51	26.17	−2.04	22.35	−6.14	0.595
Rocker−Bogie + Inverse four−bar 2	20.40	9.53	29.07	−1.94	21.94	−5.27	0.709

The parameter values such as linkage lengths and angles between linkages of the mobile platform in Fig. 3.2 (c) are list up in Table III. Tables IV summarizes the resulting height, pitch angle variations and the PVIs of three mobile platforms, where the PVI of inverse four−bar mechanism 1 is smaller than that of Rocker−Bogie mechanism by 17.9 %. Fig. 3.9 shows the posture variation of mobile platforms and new linkage mechanism is located in the rightest side of graph, which implies that the proposed mobile platform can achieve the lowest PVI as well as the smooth movement on rugged terrain traveling. Therefore inverse four−bar mechanism 1 was proposed for new linkage mobile mechanism for rugged terrain traveling.

3.7. A PVI-terrainability of mobile platforms including proposed mobile platform

The PVI and the terrainability of the proposed mobile platform were compared with those of other conventional mobile platforms, and the results are indicated in Fig. 3.10. The terrainability of proposed mobile platform was measured by Motion planning simulation on the Solidworks program.

In Fig. 3.10, the proposed mobile platform demonstrates a lower posture variation compared to the Mars Rover. However, its terrainability was lower than that of Mars Rover. All mobile platforms except for stair climbing platform show a tendency denoted by the yellow line in Fig. 3.10. A mobile platform with low posture variation shows lower terrainability than other platforms. The proposed mobile platform also follows the tendency. It shows lowest posture variation but show lowest terrainability.

Generally, in order to evaluate the terrainability of mobile platform, the normal force acting on its each wheel is analyzed. As seen in Fig. 3.11, Rocker–Bogie mechanism shows same normal force on each wheel because of linkage mechanism. However, unlike other linkage based mobile platform, the proposed mobile platform ensures small posture variation but the normal forces acting on the wheels are not equally distributed and specially, a large normal force acts on the front wheel. Therefore, to guarantee a sufficient traction force for the front wheel of the proposed mobile platform to overcome a step, a high friction coefficient is required, which implies that the terrainability of proposed mobile platform seems quite low.

If the terrainability of the proposed mobile platform can be increased by an additional mechanism, the proposed mobile platform can shows more ability than other mobile platforms.

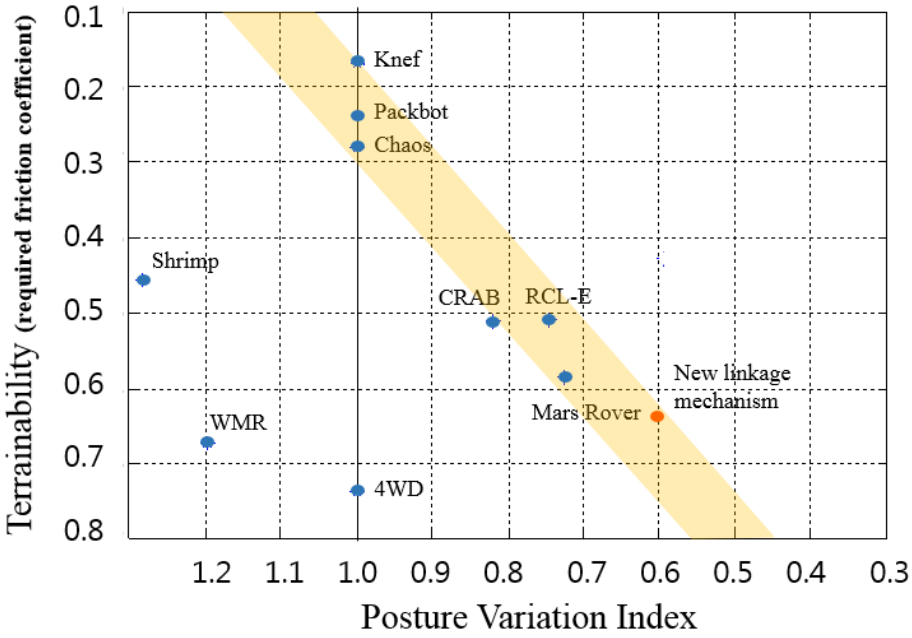

Fig. 3.10. A PVI−terrainability of mobile platforms with a new linkage mechanism

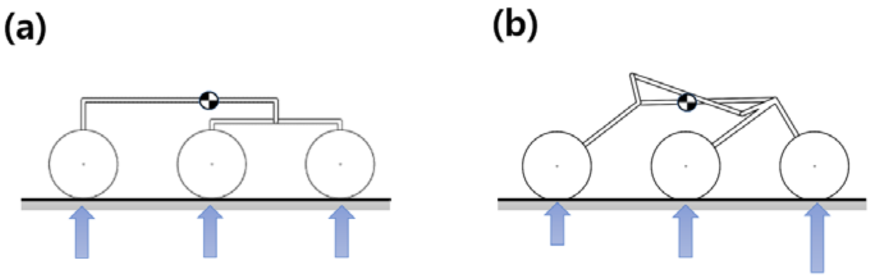

Fig. 3.11. Normal forces on (a) Rocker−Bogie platform and (b) proposed mobile platform

Chapter 4. Dynamic analysis

To analyze terrainability of proposed mobile platform, the variation of friction coefficient while overcoming a step was required. On the simulation by Solidworks motion program, by changing a friction coefficient of the ground, the minimum friction coefficient was obtained to make a mobile platform climb up a step. In this simulation only the minimum value of friction coefficient while overcoming a step can be derived, and the moment when the friction coefficient need or variations of friction coefficient cannot be determined. Therefore, by using the dynamic analysis, a variation of friction coefficient of proposed mobile platform was derived.

4.1. Variation of friction coefficient of the proposed mobile platform by simulation

Variation of friction coefficient can be derived from the normal force and traction force data from the simulation. Normal forces and traction forces of each wheels while overcoming a step can be obtained from the simulation and by dividing a traction force value by a normal force value at a moment, the friction coefficient can be derived. However, on simulation, movement of platforms are calculated by numerical analysis method, so small oscillation on data were observed, which eventually resulted in the large oscillation of friction coefficient.

Tendency of the friction coefficient can be derived from the simulation, but maximum friction coefficient cannot be defined by one value because of large oscillation. Therefore, only simulation data cannot be used for analyzing variation of friction coefficient.

4.2. Previous analysis in mobile platform

To analyze a mobile platform movement on rugged terrain, a quasi−static analysis and Zvi Shillars dynamic analysis were commonly adopted.

4.2.1. Quasi-Static analysis method

The quasi−static analysis is most common method to analyze mobile platforms movement on rugged terrain. Under the quasi−static condition, the mobile platform is supposed to move at a sufficiently low and constant speed as if its movement consists of consecutive static equilibriums [25−33]. Therefore, static equilibrium of a mobile platform is analyzed in every moment during its traveling and the dynamic effect on a mobile platform is ignored. For example, the quasi−static analysis can be adopted to analyze the behavior of Mars Exploration Rovers (MERs) which travel on rugged terrain at speeds of 3~5 m/min. However, for indoor mobile platforms whose moving speeds are maximally up to a few dozen meters per minute, their dynamic effects cannot be neglected in order to predict their behavior with high fidelity so that the quasi−static analysis does not seem suitable for the force/torque analysis of high−speed mobile platforms.

4.2.2. Dynamic analysis method by Zhi Shillar

Zvi Shillar et al suggested a dynamic analysis method to consider the velocity and acceleration of CM of mobile platform along the moving direction, where feasible ranges of velocuty and acceleration of CM of mobile platform are determined to satisfy a set of dynamic constraints. For examples, a normal force on a wheel must be positive for a mobile platform to keep contact with the ground and the ratio of

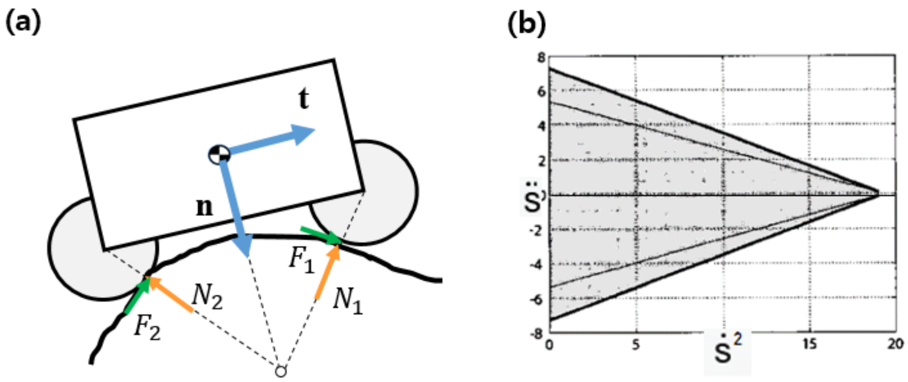

Fig. 4.1. (a) A free body diagram of four−wheel drive and (b) FSA graph in Zvi Shillar research

traction force to normal force must be smaller than friction coefficient of ground for a mobile platform to move without slip [45,46]. In a static analysis, a force equilibriums and a moment equilibriums are used and right sides of equilibrium set to zero because a platform does not have any movement or any acceleration except gravity. On the Zvi Shillars analysis, a velocity and an acceleration of CM of a mobile platform in moving direction was considered. Force equilibriums and a moment equilibriums are written in following manner.

$$J^T(s)\begin{pmatrix} N_1 \\ F_1 \\ N_2 \\ F_2 \end{pmatrix} = \begin{pmatrix} m(t_x\ddot{s} + k_x\dot{s}^2 - g_x) \\ m(t_y\ddot{s} + k_y\dot{s}^2 - g_y) \\ I(\theta_s\ddot{s} + \theta_{ss}\dot{s}^2) \end{pmatrix} \tag{32}$$

where $\dot{s}$ is velocity, $\ddot{s}$ is acceleration in moving direction and J^T is trans matrix of Jacobian which relating between the velocity of the CM and the velocity of the contact point. To calculate normal forces and traction forces of wheels, Zvi Shillar set ranges of a velocity and acceleration of platform. By selecting one velocity value and one acceleration value in the range, normal forces and traction forces were obtained by solving the dynamic equation. If the normal forces are larger than zero, and ratios of the traction force and the normal force are smaller than friction coefficient from the ground, a mobile platform can move with selected velocity and selected acceleration without slip or tip over. By substituting all values in the range of velocity and acceleration, feasible speed and acceleration (FSA) graph can be derived as shown in Fig. 4.1 (b). A black area in the FSA graph means a velocity and an acceleration to move a mobile platform without slip or tip over. For example, on the convex surface, a shape of FSA graph is triangle shape like Fig. 4.1 (b), and a maximum velocity exists. A FSA graph can be derived every moment while traveling a rugged terrain, and a maximum velocity can be determined not to slip or tip over.

By analyzing FSA graphs, a maximum velocity of a mobile platform can be determined, but normal forces and traction forces while traveling cannot be uniquely determined even though ranges of a normal forces and traction forces can be determined. To calculate a variation of friction coefficient, a normal force and a traction force must be determined. Therefore dynamic analysis method by Zvi Shillar cannot be used to calculate variation of friction coefficient of proposed platform while overcoming a step.

4.3. Concept of inverse dynamic analysis

To calculate the variation of friction coefficient, inverse dynamic analysis was performed in this research. In dynamic analysis in generally, with given single position data and all forces and moments on platform, a next position or movement of platform can be derived. On the other hand, the inverse dynamic analysis produces a force and momentum on the single state with three position data of platform.

$$\textbf{Force on a moment} \underset{\text{Inverse dynamic}}{\overset{\text{dynamic}}{\rightleftarrows}} \textbf{Robot movement}$$

Fig. 4.2. Concept of dynamic analysis and inverse dynamic analysis

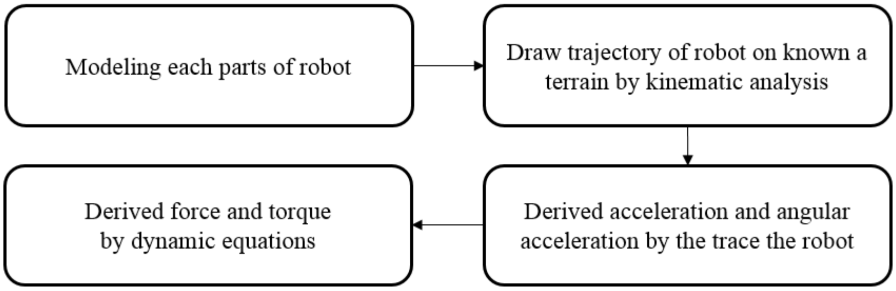

Fig. 4.3. Flow chart of inverse dynamic analysis

To perform inverse dynamic analysis, for the first, the posture of the platform on random ground condition has to be defined by kinematic analysis. A trajectory of platform while traveling on known terrain can be derived from the kinematic analysis and the trajectory will be used in inverse dynamics. On a random rugged terrain, a movement of mobile platform cannot be determined in advance so that the inverse dynamic analysis cannot be applied. However, in the case of overcoming a step, since all wheels of platform are supposed to contact the ground every moment, a movement of a mobile platform is uniquely determined and as a result, the inverse dynamic analysis can be performed.

The inverse dynamics analysis can calculate linear/angular accelerations of each parts of platforms from the platform movement, and dynamic equations related with the force and moment balances can be solved with this values. With two position data on the trajectory, linear/angular velocities of each part on a mobile platform can be calculated. In addition, with three position data, linear/angular accelerations of each part on a mobile platform can be calculated. Force and moment equilibriums can be derived for every parts of a mobile platform and normal/traction forces on every wheels and motor torques can be calculated.

4.4. Characteristics of platform parts

The characteristic data such as size, mass, and inertia of each parts of proposed mobile platform are modeled for inverse dynamic analysis. The platform is consist of three wheels and inverse four-bar linkage combined with bogie mechanism on a side. The linkage mechanism consists of four sub-linkage parts and each joint is connected via a revolution joint.

The proposed mobile platform was designed by Solidworks program and mechanical parts such as motor, bearing, and gears are considered for manufacturing. Length of linkages set as optimized value in Table III in Section 3. The positions of CM, weight, and inertia value of each linkages can be analyzed in Solidworks program and the results are in Table V. Fig. 4.4 shows the position of CM of the linkage 0 for example.

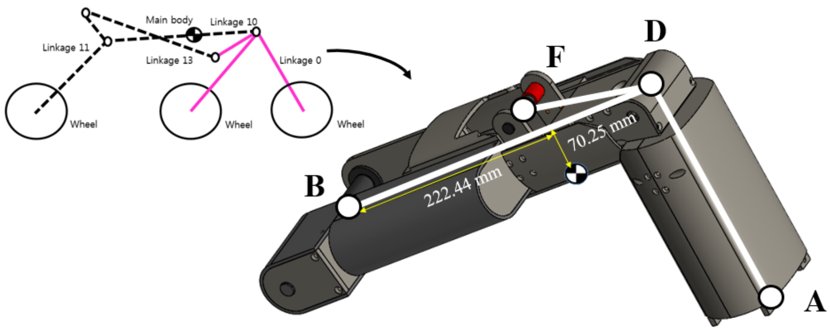

Fig. 4.4. Location of center of mass of the linkage 0

Table. V. Weight and moment of inertia of each part

	Weight [kg]	Moment of inertia [kg m^2]
Linkage 0	5.870	0.138
Linkage 10	1.305	0.031
Linkage 11	3.390	0.045
Linkage 13	1.415	0.019
Main body	25.300	0.943
Wheel	0.680	0.003

4.5. Algorism to draw a trajectory of mobile platform

A trajectory of the proposed mobile platform while overcoming a step is required to analyze by inverse dynamic analysis and a new algorism was used. The steps of the algorithm are as follow: first, choose the reference points on a step terrain. Front wheel will move from the first reference point to the last reference point and posture of proposed mobile platform will be drawn for every points. When the front wheel placed one of the reference point, a location of the middle wheel can be calculated through the geometric condition and the location is function of the angle between the linkage 1 and the ground (θ_1 in Fig. 3.8). The angle of the linkage 1 is initially set as 90 degree and the angle increase gradually until the middle wheel touches the terrain.

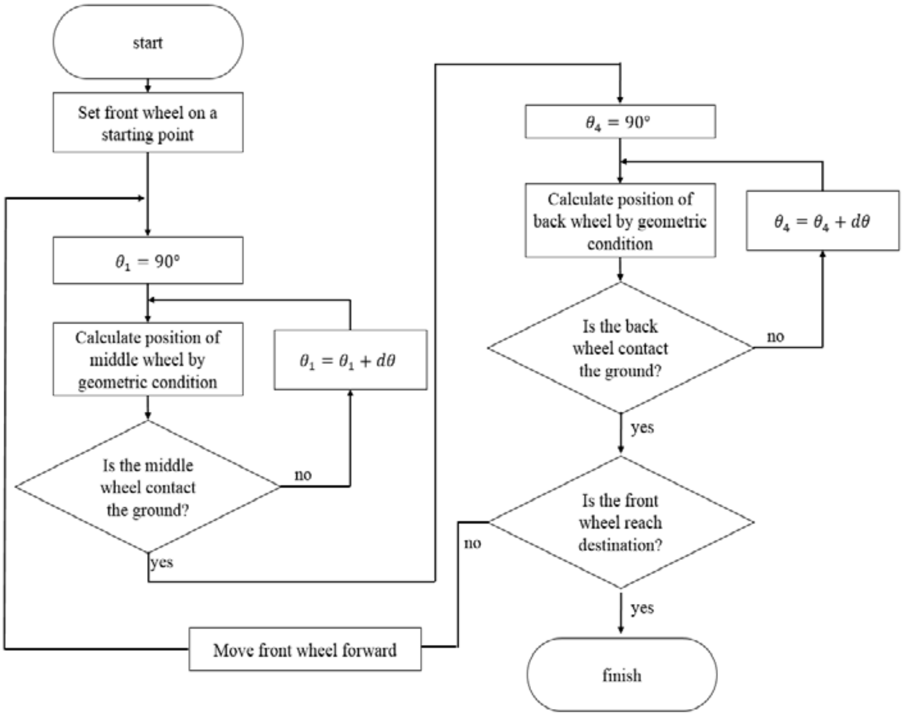

Fig. 4.5. An algorism to derive trajectory of a mobile platform

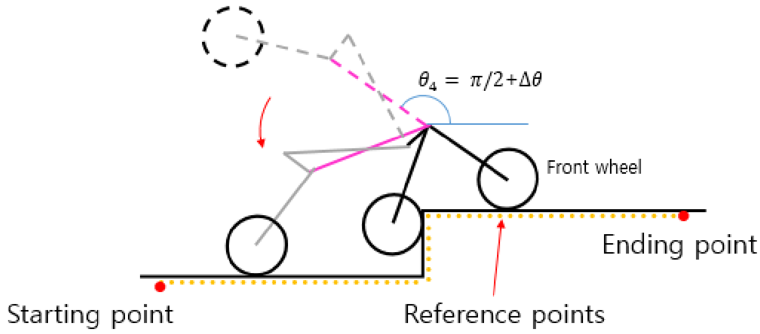

Fig. 4.6. Searching a location of back wheel in the algorism

In the same way, a location of the back wheel can be calculated through the geometric condition of inverse four−bar linkage and thelocation is function of the angle between the linkage 10 and the ground (θ_4 in Fig. 3.8). The angle of the linkage 10 is initially set as 90 degree also and the angle increase gradually until the back wheel touches the terrain (Fig. 4.6). In this way the locations of all parts of the platform on a reference point can be determined.

The trajectory of CM of the platform while climbing up a step is shown in Fig. 4.7, where the circle denote the moments when the track and wheels climb the step and the green line represents the corresponding trace of CM. The height of CM changes whenever the wheels touch and climb up a step. There is a section during the trajectory in which CM did not proceed and moved backward. This section is occurred when the front wheel climbed a vertical face of step, and the main body of the platform was lifted backward as the front linkage moved upward.

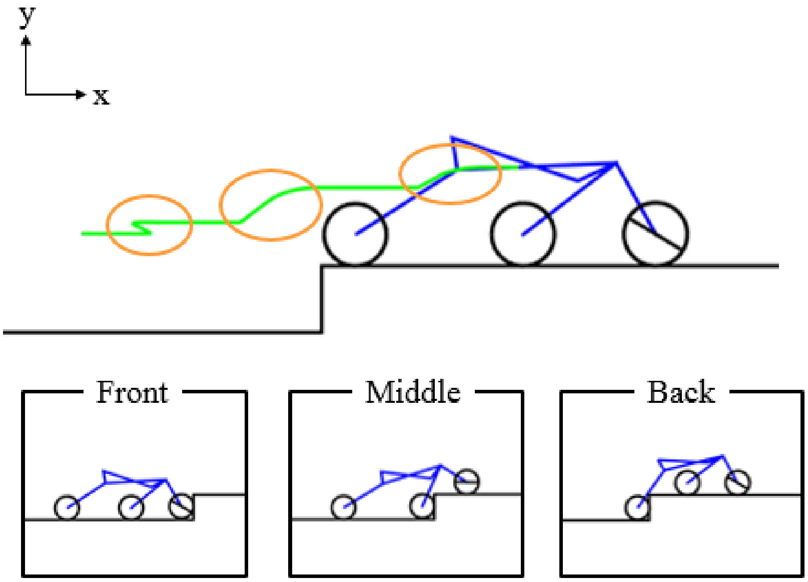

Fig. 4.7. Trajectory of proposed mobile platform on step climbing

4.6. Accelerations and angular accelerations of linkages

When the wheel climb up the step, posture of each part of the mobile platform changes and its linear/angular accelerations occur, which are caused by the reaction forces from the ground and joints. With two position data on the trajectory, linear/angular velocities of each part of a mobile platform can be calculated and with three position data, linear/angular accelerations of each part of a mobile platform can be calculated. The moving velocity of platform can be selected by changing value of time difference between two position data.

Linear/angular velocities of CM were derived from the trajectory and the results are shown in Fig. 4.8 and linear/angular accelerations are shown in Fig. 4.9. The moving velocity of the proposed mobile platform was set to be 10 m/min (1.66 m/s). When the wheels contact and climb up the step, the velocities and accelerations change. The largest acceleration change was occurred when the front wheel comes in contact with the step. (-2.58 m/s^2 on X direction)

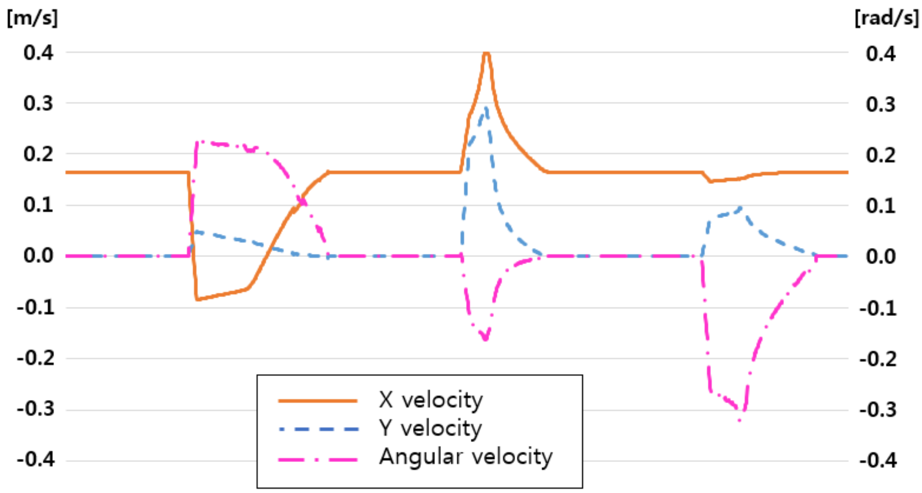

Fig. 4.8. Velocity and angular velocity of CM on step climbing

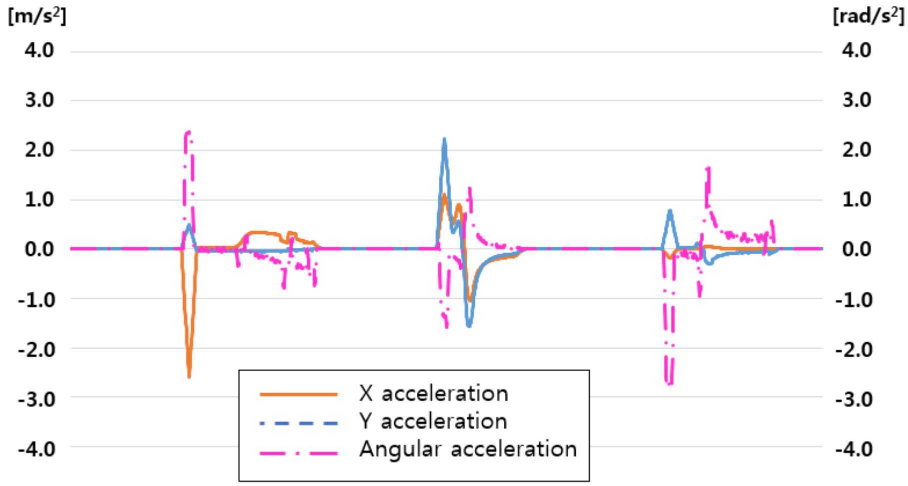

Fig. 4.9. Acceleration and angular acceleration of CM on step climbing

4.7. Dynamic analysis of the proposed mobile platform

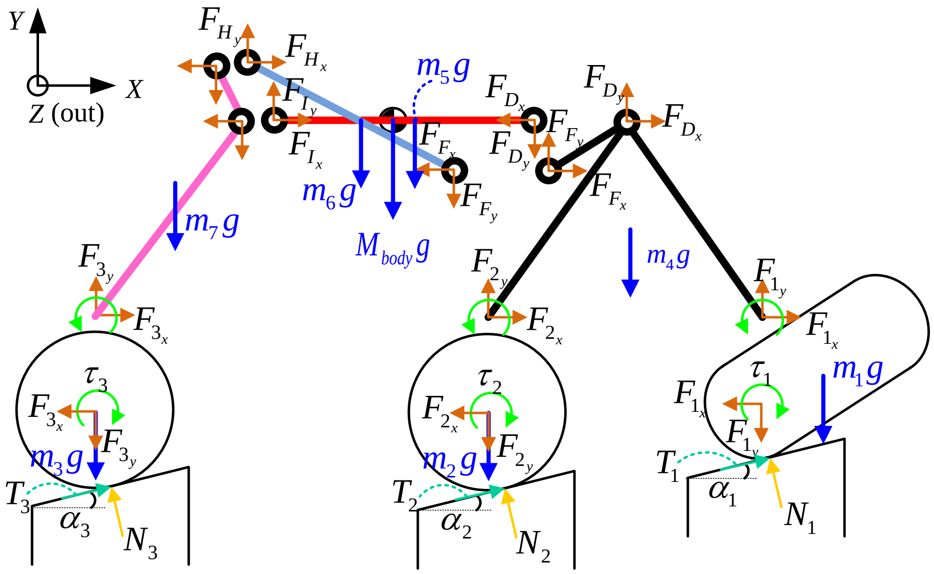

Fig. 4.10. Free body diagram of proposed mobile platform

Dynamic force and moment equations can be derived from the linear/angular acceleration data from the trajectory analysis. There are three wheels and four linkage groups on a side of the proposed mobile platform. Dynamic force and moment equations of each part are given as follow:

Force and moment equations of the front wheel are

$$-F_{Ax} + \mu_1 N_1 cos\alpha_1 - N_1 sin\alpha_1 = m_1 a_{1x} \tag{33}$$

$$-F_{Ay} - m_1 g + \mu_1 N_1 sin\alpha_1 + N_1 cos\alpha_1 = m_1 a_{1y} \tag{34}$$

$$-\tau_1 + \mu_1 N_{1_1} r_1 = I_1 \dot{\omega}_1 \tag{35}$$

Force and moment equations of the middle wheel are

$$-F_{Bx} + \mu_2 N_2 cos\alpha_2 - N_2 sin\alpha_2 = m_2 a_{2x} \tag{36}$$

$$-F_{By} - m_2 g + \mu_2 N_2 sin\alpha_2 + N_2 cos\alpha_2 = m_2 a_{2y} \tag{37}$$

$$-\tau_2 + \mu_2 N_2 r_2 = I_2 \dot{\omega}_2 \tag{38}$$

Force and moment equations of the back wheel are

$$-F_{Cx} + \mu_3 N_3 cos\alpha_3 - N_3 sin\alpha_3 = m_3 a_{3x} \tag{39}$$

$$-F_{Cy} - m_3 g + \mu_3 N_3 sin\alpha_3 + N_3 cos\alpha_3 = m_3 a_{3y} \tag{40}$$

$$-\tau_3 + \mu_3 N_3 r_3 = I_3 \dot{\omega}_3 \tag{41}$$

Force and moment equation of the linkage group with linkage 1, linkage 2 and linkage 9 are

$$F_{Ax} + F_{Bx} + F_{Dx} + F_{Fx} = m_4 a_{4x} \tag{42}$$

$$F_{Ay} + F_{By} + F_{Dy} + F_{Fy} - m_4 g = m_4 a_{4y} \tag{43}$$

$$\begin{aligned}&\tau_1 + \tau_2 + F_{Ax}\Delta_{m_4}^{F_{Ax}} + F_{Ay}\Delta_{m_4}^{F_{Ay}} + F_{Bx}\Delta_{m_4}^{F_{Bx}} - F_{By}\Delta_{m_4}^{F_{By}} \\ &-F_{Dx}\Delta_{m_4}^{F_{Dx}} + F_{Dy}\Delta_{m_4}^{F_{Dy}} + F_{Fx}\Delta_{m_4}^{F_{Fx}} - F_{Fy}\Delta_{m_4}^{F_{Fy}} = I_4 \dot{\omega}_4\end{aligned} \tag{44}$$

Force and moment equations of the linkage group with linkage 10 are.

$$-F_{Dx} + F_{Ix} = m_5 a_{5x} + M_{body} a_{5x} \tag{45}$$

$$-F_{Dy} + F_{Iy} - m_5 g - M_{body} g = m_5 a_{5y} + M_{body} a_{4y} \tag{46}$$

$$F_{Dx}\Delta_{m_5}^{F_{Dx}} - F_{Dy}\Delta_{m_5}^{F_{Dy}} + F_{Ix}\Delta_{m_5}^{F_{Ix}} - F_{Iy}\Delta_{m_5}^{F_{Iy}} - M_{body} g \Delta_{m_5}^{F_{Mg}} = I_5 \dot{\omega}_5 + I_M \dot{\omega}_5 \tag{47}$$

Force equations and moment equation of the linkage group with linkage 13.

$$-F_{Fx} + F_{Hx} = m_6 a_{6x} \tag{48}$$

$$-F_{Fy} + F_{Hy} - m_6 g = m_6 a_{6y} \tag{49}$$

$$-F_{Fx}\Delta_{m_6}^{F_{Fx}} - F_{Fy}\Delta_{m_6}^{F_{Fy}} + F_{Hx}\Delta_{m_6}^{F_{Hx}} - F_{Hy}\Delta_{m_6}^{F_{Hy}} = I_6 \dot{\omega}_6 \tag{50}$$

Force and moment equations of the linkage group with linkage 11 and linkage 12 are

$$F_{Cx} - F_{Ix} - F_{Hx} = m_7 a_{7x} \tag{51}$$

$$F_{Cy} - F_{Iy} - F_{Hy} - m_7 g = m_7 a_{7y} \tag{52}$$

$$\tau_3 + F_{Cx}\Delta_{m_7}^{F_{Cx}} - F_{Cy}\Delta_{m_7}^{F_{Cy}} + F_{Ix}\Delta_{m_7}^{F_{Ix}} - F_{Iy}\Delta_{m_7}^{F_{Iy}} + F_{Hx}\Delta_{m_7}^{F_{Hx}} + F_{Hy}\Delta_{m_7}^{F_{Hy}} = I_7 \dot{\omega}_7 \tag{53}$$

$$A_{6\times 6}$$

$$\begin{pmatrix}
-sin\alpha_1 & -sin\alpha_2 + \mu_2 cos\alpha_2 & -sin\alpha_3 + \mu_3 cos\alpha_3 & cos\alpha_1 & 0 & 0 \\
cos\alpha_1 & cos\alpha_2 + \mu_2 sin\alpha_2 & cos\alpha_3 + \mu_3 sin\alpha_3 & sin\alpha_1 & 0 & 0 \\
0 & 0 & 0 & 0 & \Delta_{F_{Ix}}^{F_{Dx}} & -(\Delta_{F_{Iy}}^{F_{Dy}}) \\
0 & 0 & \begin{matrix} sin\alpha_3\left(\Delta_{F_{Hx}}^{F_{Fx}}\right) - cos\alpha_3\left(\Delta_{F_{Hy}}^{F_{Fy}}\right) \\ -\mu_3(cos\alpha_3\left(\Delta_{F_{Hx}}^{F_{Fx}}\right) + sin\alpha_3\left(\Delta_{F_{Hy}}^{F_{Fy}}\right)) \end{matrix} & 0 & \Delta_{F_{Hx}}^{F_{Fx}} & \Delta_{F_{Hy}}^{F_{Fy}} \\
0 & 0 & \begin{matrix} -sin\alpha_3\left(\Delta_{F_{Cx}}^{F_{Hx}}\right) - cos\alpha_3\left(\Delta_{F_{Cy}}^{F_{Hy}}\right) \\ +\mu_3(cos\alpha_3\left(\Delta_{F_{Cx}}^{F_{Hx}}\right) - sin\alpha_3\left(\Delta_{F_{Cy}}^{F_{Hy}}\right) + r_3) \end{matrix} & 0 & \Delta_{F_{Hx}}^{F_{Ix}} & \Delta_{F_{Iy}}^{F_{Hy}} \\
\begin{matrix} -sin\alpha_1\left(\Delta_{F_{Ax}}^{m_4} - \Delta_{F_{Ax}}^{m_1}\right) \\ +cos\alpha_1\left(\Delta_{F_{Ay}}^{m_1} + \Delta_{F_{Ay}}^{m_4}\right) \end{matrix} & \begin{matrix} -sin\alpha_2\left(\Delta_{F_{Bx}}^{m_4}\right) - cos\alpha_2\left(\Delta_{F_{By}}^{m_4}\right) \\ +\mu_2(cos\alpha_2\left(\Delta_{F_{Bx}}^{m_4}\right) - sin\alpha_2\left(\Delta_{F_{By}}^{m_4}\right) + r_2) \end{matrix} & \begin{matrix} sin\alpha_3\left(\Delta_{F_{Fx}}^{m_4}\right) - cos\alpha_3\left(\Delta_{F_{Fy}}^{m_4}\right) \\ +\mu_3(-cos\alpha_3\left(\Delta_{F_{Fx}}^{m_4}\right) - sin\alpha_3\left(\Delta_{F_{Fy}}^{m_4}\right)) \end{matrix} & cos\alpha_1\left(\Delta_{F_{Ax}}^{m_4} - \Delta_{F_{Ax}}^{m_1}\right) + sin\alpha_1\left(\Delta_{F_{Ay}}^{m_1} + \Delta_{F_{Ay}}^{m_4}\right) + r_1 & \Delta_{F_{Fx}}^{m_4} & \Delta_{F_{Fy}}^{m_4}
\end{pmatrix}$$

$$
\begin{array}{ccc}
X_{6\times 1} & & B_{6\times 1} \\
\begin{bmatrix} N_1 \\ N_2 \\ N_3 \\ T_1 \\ F_{Ix} \\ F_{Iy} \end{bmatrix} & = & \begin{pmatrix}
m_1a_{1x} + m_2a_{2x} + m_3a_{3x} + m_4a_{4x} + m_5a_{5x} + m_6a_{6x} + m_7a_{7x} + M_{body}a_{5x} \\
m_1a_{1y}' + m_2a_{2y}' + m_3a_{3y}' + m_4a_{4y}' + m_5a_{5y}' + m_6a_{6y}' + m_7a_{7y}' + M_{body}a_{5y}' \\
I_5\dot{\omega}_5 + I_M\dot{\omega}_5 + \left(m_5a_{5x} + M_{body}a_{5x}\right)\Delta_{m_5}^{F_{Dx}} - (m_5a_{5y}' + M_{body}a_{5y}')\Delta_{m_5}^{F_{Dy}} \\
I_6\dot{\omega}_6 - (m_6a_{6x})\Delta_{m_6}^{F_{Fx}} - \left(m_6a_{6y}'\right)\Delta_{m_6}^{F_{Fy}} - (m_3a_{3x} + m_7a_{7x})\Delta_{F_{Fx}}^{F_{Hx}} - (m_3a_{3y}' + m_7a_{7y}')\Delta_{F_{Fy}}^{F_{Hy}} \\
I_3\dot{\omega}_3 + I_7\dot{\omega}_7 + (m_3a_{3x})\Delta_{F_{Cx}}^{F_{Hx}} - \left(m_3a_{3y}'\right)\Delta_{F_{Cy}}^{F_{Hy}} + (m_7a_{7x})\Delta_{m_7}^{F_{Hx}} - (m_7a_{7y}')\Delta_{m_7}^{F_{Hy}} \\
I_1\dot{\omega}_1 + I_2\dot{\omega}_2 + I_4\dot{\omega}_4 + m_1a_{1x}\left(\Delta_{F_{Ax}}^{m_4} - \Delta_{F_{Ax}}^{m_1}\right) + m_1a_{1y}'\left(\Delta_{F_{Ay}}^{m_4} + \Delta_{F_{Ay}}^{m_1}\right) + (m_2a_{2x})\Delta_{m_4}^{F_{Bx}} - (m_2a_{2y}')\Delta_{m_4}^{F_{By}} \\
-(m_3a_{3x} + m_6a_{6x} + m_7a_{7x})\Delta_{m_4}^{F_{Fx}} - (m_3a_{3y}' + m_6a_{6y}' + m_7a_{7y}')\Delta_{m_4}^{F_{Fy}}
\end{pmatrix}
\end{array}
\qquad (54)
$$

where N_i denotes the normal force acting on the i_{th} wheel, and the μ_i is the friction coefficient which is defined as the normal force over the traction force on the i_{th} wheel. τ_i is the torque on the i_{th} wheel motor. $\Delta_{mi}^{F_x}$ is the shortest distance between the force vector F_x and the i_{th} center of mass. Equations (33)~(53) can be arranged as shown in Eq. (54) where $a_{iy}' = a_{iy} + g$

The equation (54) can be rewrite as this equation.

$$A_{6\times6} \cdot X_{6\times1} = B_{6\times1} \tag{55}$$

By solving this equation, the normal and traction forces on each wheel can be calculated. The unknown parameters in the equation (55) are $(N_1, N_2, N_3, T_1, F_{Ix}, F_{Iy})$ of matrix X and two friction coefficient (μ_2, μ_3) of matrix A. However, since the number of equation is six, it is indeterminate equation.

4.8. Solving an indeterminate equation problem

On the dynamic analysis, 23 unknowns exist: three normal forces of wheels, three traction forces of wheels, three motor torques, and 14 forces on seven joints. However, there are only 21 equations. After re-arranged, there is 8 unknowns with 6 equations in the matrix equation (54) so that it is an indeterminate problem. In a mobile platform case, let the mobile platform has number of n wheels, there are number of n normal forces and number of n traction forces as unknown value (Fig. 4.11). However, equations for the mobile platform are only three; force equilibriums along the x- and y-axes and moment equilibrium. For this reason, the mobile platform with n wheels has $2\text{n} - 3$ degree-of-freedom inevitably [47]. The degree-of-freedom can be reduced by specification of linkage mechanism, but usually it is bigger than zero which means the system is indeterminate problem. Therefore, normal forces and traction

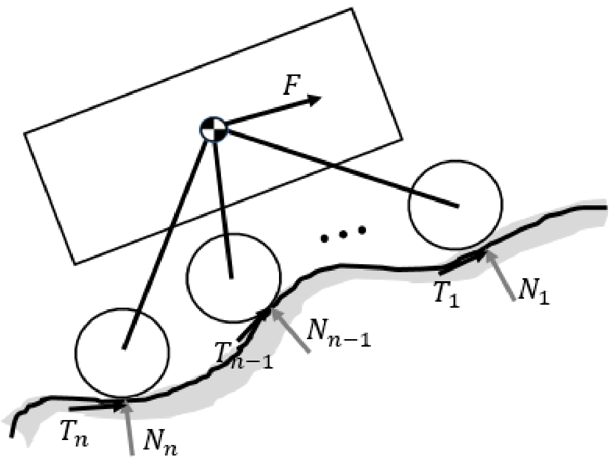

Fig. 4.11. Normal forces and traction forces on mobile platform in rugged terrain

forces cannot be determined uniquely. In order to solve indeterminate equation problem, a various researches were performed.

4.8.1. Solving an indeterminate equation by pseudo inverse matrix

From the equation (33)~(53), 21 × 23 matrix can be derived and it is not a square matrix. Therefore, the inverse matrix cannot exist. To calculate normal force and traction force values, the pseudo inverse of matrix can be used [48]. A pseudo inverse is the method to make rectangular matrix to square matrix by following equation.

$$A\,X = B \tag{56}$$

$$X = A^{\#}B \tag{57}$$

$$A^{\#} = (A^T A)^{-1} A^T \tag{58}$$

By using the pseudo inverse matrix ($A^{\#}$), the force matrix X can be determined. An indeterminate equation, there are too many answers for the equation. By using the pseudo inverse matrix method, an answer that minimize difference between square values of entries in answer matrix is chosen. The force matrix is composed of normal forces and traction forces, so that the pseudo inverse matrix selects an answer in such a manner that square of normal forces and traction forces have similar value. Therefore, the friction coefficient defined as traction force divided by normal force becomes close to ‘1’ in every moments. Also, because square values are considered in pseudo inverse matrix the force values can be negative value. However, normal forces cannot be smaller than zero, the pseudo method is not suitable to solve mobile platform problem.

4.8.2. Solving an indeterminate equation by linkage characteristic condition

Some studies of Rocker−Bogie mechanism tactfully used linkage characteristic to solve an indeterminate problem [49]. As seen in Fig. 4.12, a joint on the bogie linkage (point P) is located in middle of front wheel and middle wheel. A CM of platform is located above middle wheel and a distance between front wheel and middle wheel and a distance between middle wheel and back wheel are same. Therefore, this study assumes a normal force of front, middle, and back wheel

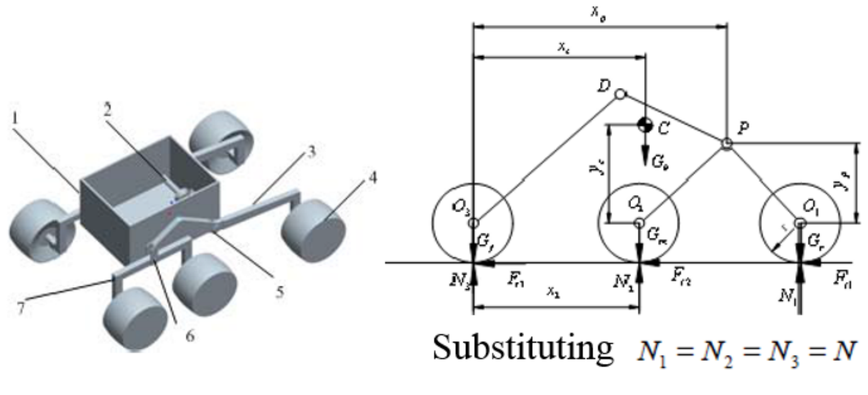

Fig. 4.12. A schematic and normal forces of Rocker−Bogie mechanism in study [49]

as same value. However, on a flat surface, this supposition can be valid, but not on a rugged terrain. Solving an indeterminate equation by linkage characteristic is highly depending on the ground condition and a posture of the platform. Therefore, on rugged terrain analysis, this method cannot be used.

4.8.3. Solving an indeterminate equation by supposing traction force on wheels as maximum force

To solve an indeterminate equation by setting force value as its maximum was done by researchers [32]. On this study, forces on the platform was calculated while the platform climb up a stair. First, all cases of postures were classified into 11 cases as seen in Fig. 4.13. In the indeterminate equation, traction forces of wheels were supposed to be maximum value except for the wheel contacting a side of stair. For example, in case 3 in Fig. 4.13, because middle wheel contacts the side of stair, traction forces of front wheel and back wheel are supposed to have maximum traction values from the ground.

$$F_1 = \mu^* N_1,\ \ F_2 \neq \mu^* N_2,\ \ F_3 = \mu^* N_3 \tag{59}$$

where μ^* is friction coefficient between wheel and the ground. With two additional equation in (59), indeterminate equation can be solved. If a traction force divided by a normal force on the middle wheel is smaller than friction coefficient of the ground, the platform can maintain its posture, which means there will be a solution satisfying static equilibrium. The platform can overcome a stair, if all posture cases satisfy static equilibrium. With this analysis method, a possibility that a platform can overcomes a stair or not can be determined, but the values of normal forces and traction forces cannot be determined uniquely. Therefore, variation of friction coefficient cannot be derived from this method.

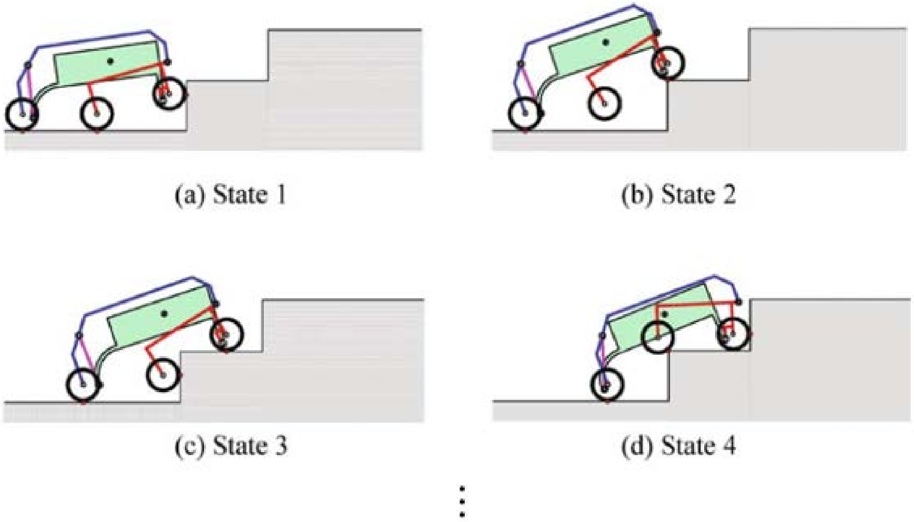

Fig. 4.13. Sequence of WMR overcoming a stair

4.8.4. Solving an indeterminate equation by minimizing energy

An optimization method to minimize a maximum friction coefficient on wheels was studied to solve an indeterminate equation [50]. Friction coefficient of each wheel can be calculated by traction force divided by normal force and three friction coefficients can be derived from calculation. On the study in Roland Siegwart, by minimizing the friction coefficient, an energy for operating a mobile platform can be reduced. Objective function can be written as follows.

$$\text{Objective function} = \min(\max\left(\frac{F_1}{N_1}, \frac{F_2}{N_2}, \frac{F_3}{N_3}\right)) \qquad (60)$$

There are numerous number of force solutions satisfying the equations (60), so by a exhaustive search method, a force to minimize a maximum friction coefficient on wheels was selected. If maximum friction coefficient is minimized, the three friction coefficient became similar. Variation of friction coefficient can be derived from this method, so terrainability of proposed mobile platform was calculated by this method.

4.9. The terrainability of the proposed mobile platform

The variation of friction coefficient of the proposed mobile platform while overcoming a step was calculated by using the minimizing energy method. The inverse dynamic analysis result can be seen in Fig. 4.14 and Fig 4.15. Maximum friction coefficient was occurred when a front wheel contact a side of step and the value is 0.78. When middle wheel and back wheel contact a side of step, friction coefficient is smaller than 0.78, so terrainability of proposed mobile platform is 0.78. Note that the platform model in dynamic analysis is not same as model used in Section 3 simulation, so terrainability of proposed mobile platform is by simulation and dynamic analysis are little different. If an additional mechanism which can reduce the friction coefficient when the front wheel contact a side of step, a terrainability of new linkage mechanism can be improved.

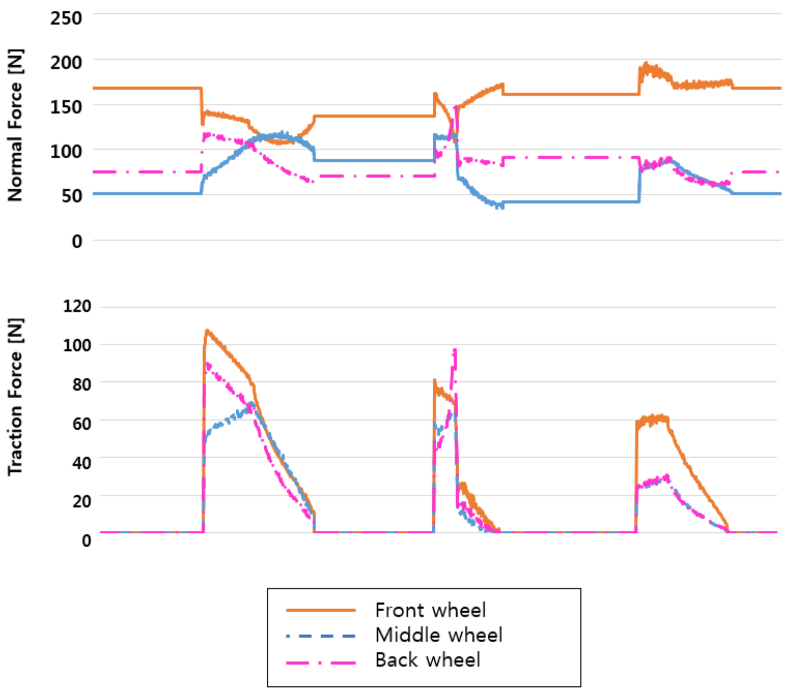

Fig. 4.14. Normal force and traction force on wheels

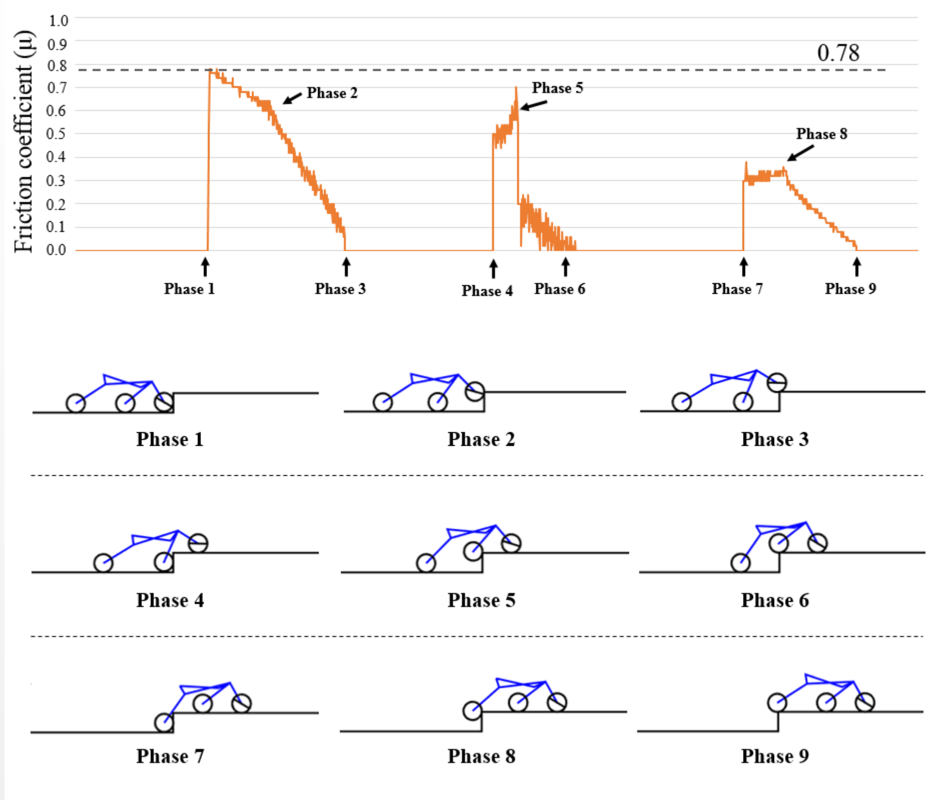

Fig. 4.15. The friction coefficient of proposed mobile platform

Chapter 5. Track mechanism in front of platform

For the design of a mobile platform, increasing the terrainability is one of the most important issues while traveling on rugged terrain. To increase terrainability of proposed mobile platform, replacing the front wheel with track was considered. Side of a track can be regarded as part of large wheel, so track can make platform easy to overcome obstacles. For this reason, in the PVI−terrainability in section 2, mobile platforms with track ensure high terrainability. Therefore, in this section, study of increasing terrainability by using a track was performed.

5.1. Previous research: Rocker-Bogie mechanism with track

In the previous research, increasing a terrainability of a Rocker−Bogie by replacing front wheel with track was studied. As seen in Fig. 5.1 (a) and (b), a Rocker−Bogie with wheel and a Rocker−Bogie with track were manufactured for comparison of stair climbing capability. Simulation was performed for all size of stairs in urban environment, and climbing ability of two platforms are shown in Fig. 5.1 (c) and (d). X−axis and y−axis denote a length of stair and a height of stair, respectively. The red area corresponds to stairs which the platform cannot overcome, and the blue area represents stairs which the platform can overcome, which are analyzed by geometric condition and static analysis of platforms [53]. As seen in the graphs, the Rocker−Bogie with track can overcomes more various size of stairs than the Rocker−Bogie with wheel.

Experiment was performed to verify an improvement of stair climbing ability. A stair used in experiment has 300 mm in length and 100 mm in height and it is marked as black star in the graphs. The stair was marked in red area on the Rocker−Bogie with wheel which means the platform cannot overcome the stair. On the other hand, the stair was marked in blue area on the Rocker−Bogie with track which means the platform can overcome the stair. A picture of experiment is shown in Fig. 5.2. The Rocker−Bogie with wheel did not get enough traction force from the stair and the platform slipped on the stair and did not overcome. On the other hand, the Rocker−Bogie with track overcome the stairs easily. Without any additional actuators, a terrainability of platform increases by replacing front wheel with track.

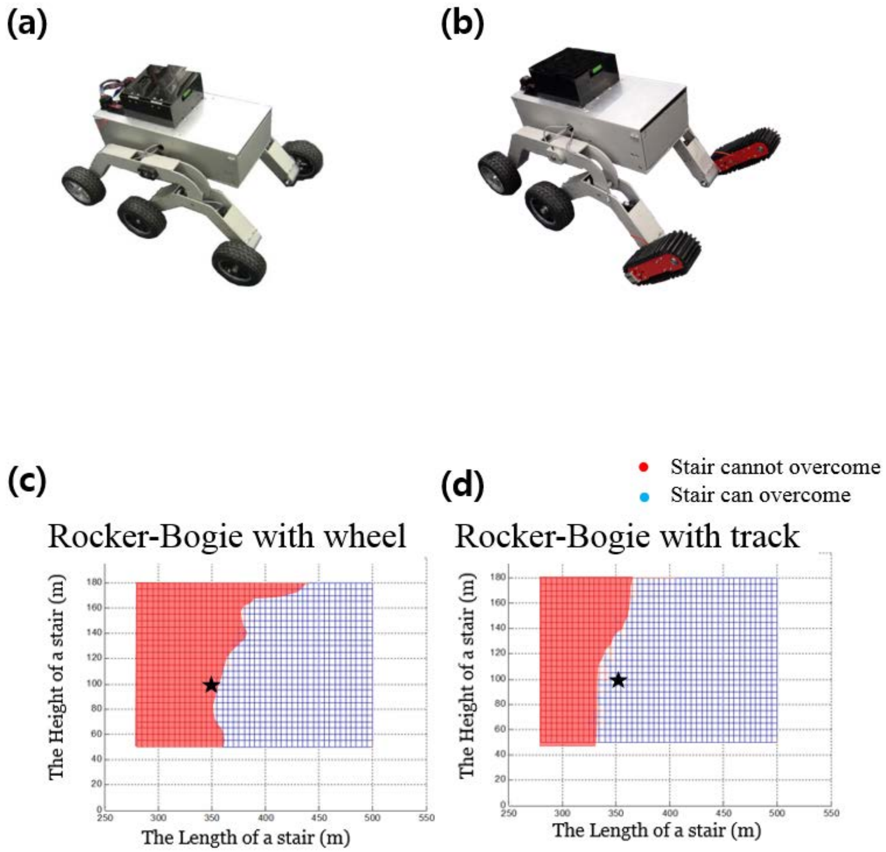

Fig. 5.1. (a) A Rocker−Bogie with wheel (b) A Rocker−Bogie with track (c)(d) Stair climb possibility graph of two platforms

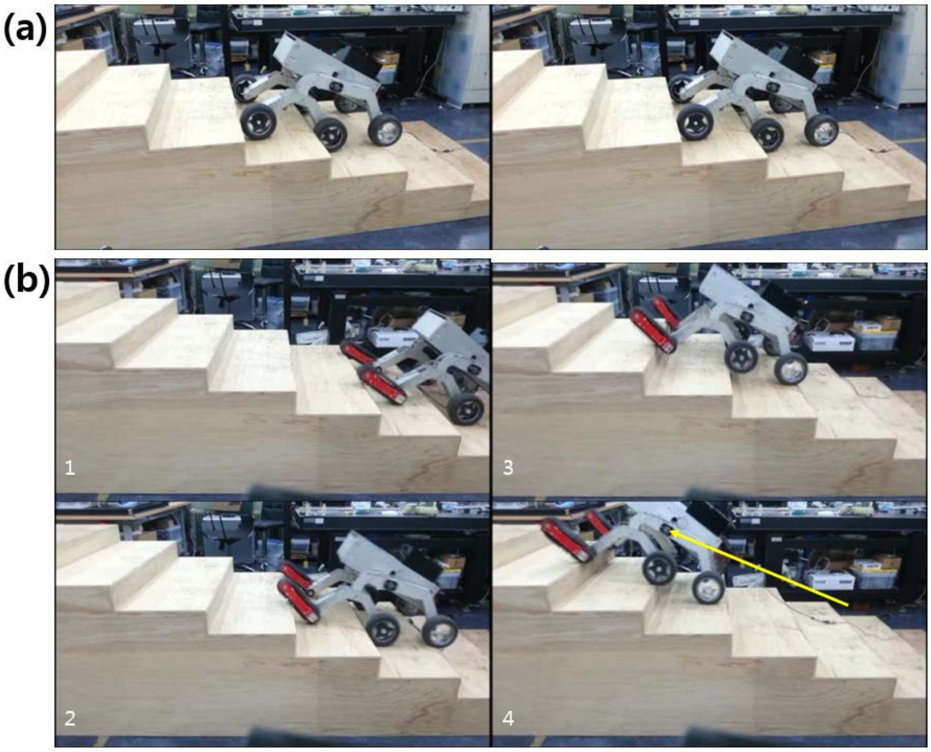

Fig. 5.2. Sequence of Rocker−Bogie (a) with wheel and (b) with track on stair climbing

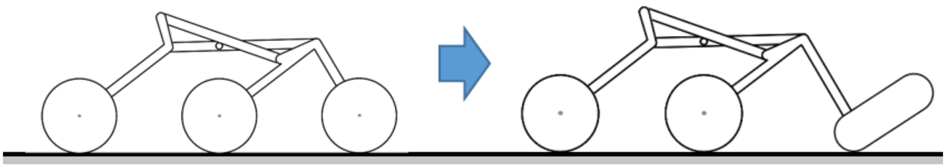

Fig. 5.3. Concept design of the proposed mobile mechanism with track

5.2. Terrainability of the proposed mobile platform with track

Base on the previous research, a new mobile platform with inverse four−bar linkage and a track was proposed and the concept design is shown in Fig. 5.3. The wheel on the front is replaced by a track. A terrainability of proposed mobile platform with inverse four−bar linkage and a track was analyzed by inverse dynamic analysis. A trajectory of new proposed mobile platform was derived first by the algorism in Section 4.4, and the trajectory is shown in Fig. 5.4. Note that when the mobile platform is equipped with six wheels, the backward movement of its CM is observed which is known as one of defects of the Rocker−Bogie mechanism. On the contrary, the path of CM of mobile platform with tracks does not show such backward movement and the platform continuously moves forward

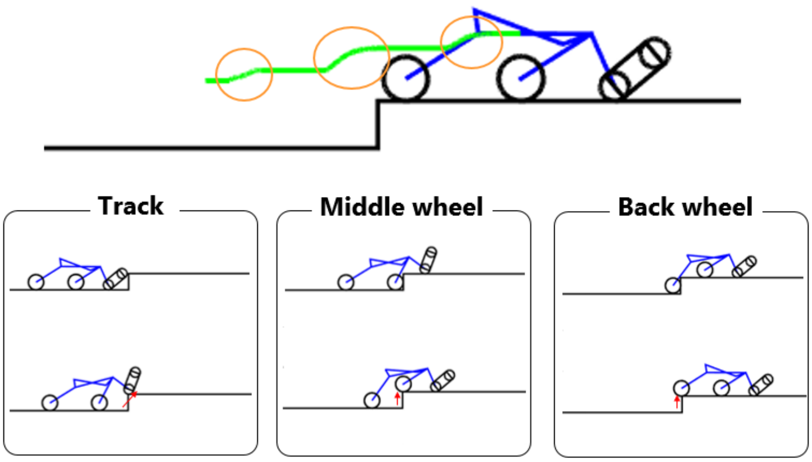

Fig. 5.4. A trajectory of new proposed mobile platform while overcoming a step

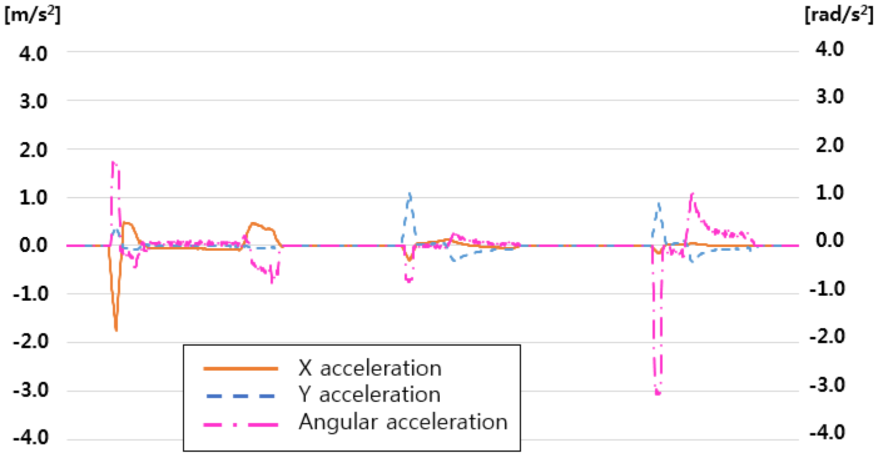

Fig. 5.5. Acceleration and angular acceleration of CM of proposed mobile platform on step climbing

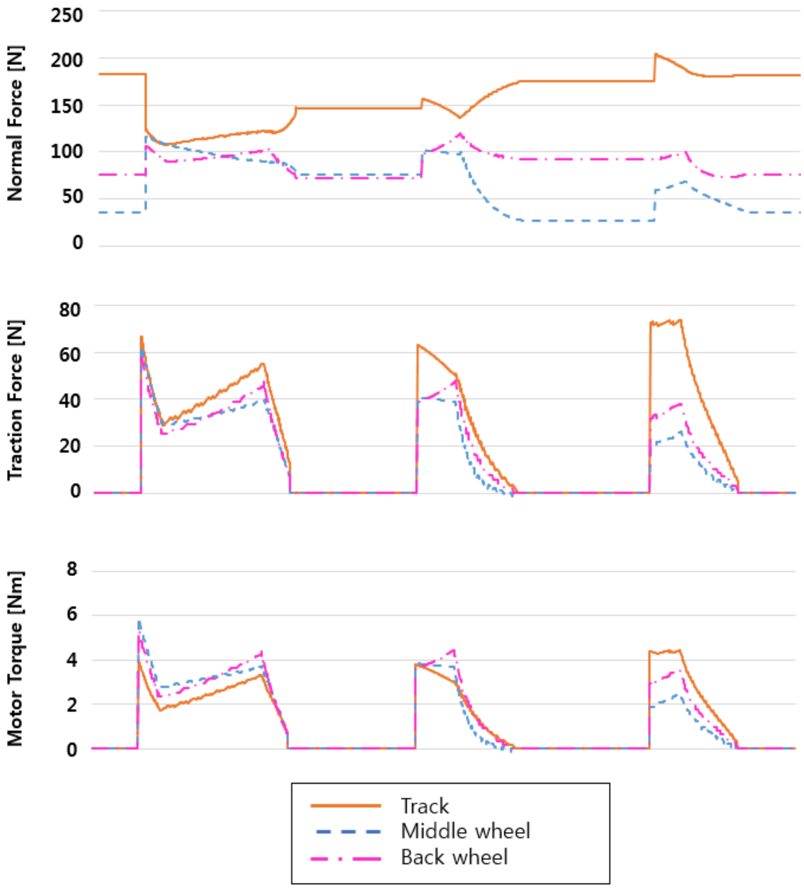

Fig. 5.6. Normal force, traction force, and motor torque of proposed mobile platform

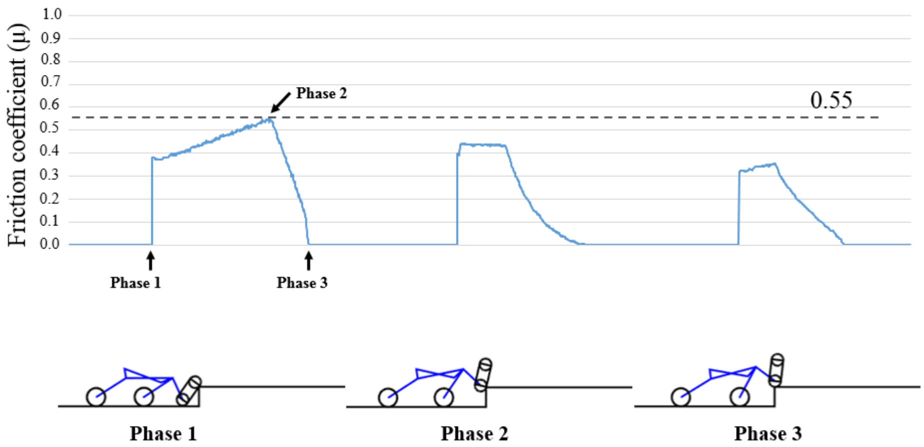

Fig. 5.7. The friction coefficient of proposed mobile platform

According to Fig. 5.6, the normal force for the track is larger than those of middle and rear wheels, which implies that compared to the Rocker-Bogie mechanism, the normal force distribution of proposed mobile platform is relatively concentrated upon the front track, the rear and middle wheel in the order. Different from the normal force, the trends of traction force and motor torque are very similar to each other. Note that the traction force of front track is larger than those of middle and rear wheels while the required motor torque of front track is smaller than those of other wheels, which implies the efficiency of track mechanism.

Acceleration and angular acceleration of each linkage were derived from the trajectory and normal force, traction force and motor torque were derived by inverse dynamic analysis. (Fig. 5.5 and Fig. 5.6) Also, friction coefficient of proposed mobile platform while overcoming step was derived and the result can be seen in Fig. 5.7. When the front of platform climb up the step, the shape of friction coefficient was changed because of track. The maximum friction coefficient of proposed mobile platform with four wheels plus two tracks occurs at the moment when the front track completes climbing a step.

5.3. Optimization of the contact angle between the track and the ground

It is noted that the contact angle of track mechanism may have the detrimental effect on the resulting friction coefficient of proposed mobile platform. If the contact angle of track mechanism is too small, the trend of the resulting friction coefficient may be very similar to that of the six wheel mobile platform so that the maximum friction coefficient will occur at the initial contact moment because the height of contact point between the track and the step is similar to that of contact point between the wheel and the step. Therefore, the contact angle of track mechanism should be optimally chosen in order not to deteriorate the terrainability of proposed mobile platform. Through the extensive simulations in Fig. 5.8, the contact angle of track mechanism of proposed mobile platform is set be 53.8 °. This is the angle that height of the end of track is same as step height.

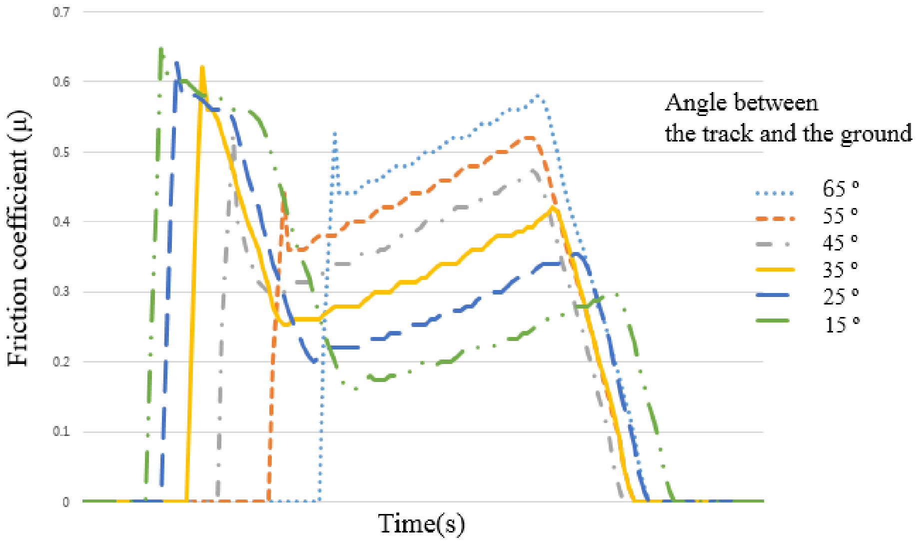

Fig. 5.8. Friction coefficient depend on the angle between the track and the ground

5.4. Comparison between new linkage mechanism and new linkage mechanism with track

Fig. 5.9 compares the friction coefficients of two different mobile platforms to climb a step whose height is equal to the wheel diameter. The graph describes the resulting friction coefficients of mobile platforms with six wheels and four wheels plus two tracks, which are denoted by the orange dash and blue solid lines, respectively. For both mobile platforms, the resulting friction coefficients become the largest when the front wheel or track climbs a step. It is worthwhile to note that the maximum friction coefficient of mobile platform with six wheels occurs at the moment when the front wheel starts to climb a step. On the other hand, the maximum friction coefficient of proposed mobile platform with four wheels plus two tracks occurs at the moment when the front track completes climbing a step.

Compared to that of six-wheel mobile platform, the maximum friction coefficient of mobile platform with track is reduced from 0.78 to 0.55, which implies that the mobile platform with four wheels plus two tracks enables to climb a step with smaller traction force without suffering from slip. As a result, its terrainability is considerably improved with the help of the track mechanism.

The proposed mobile platform combining the inverse four-bar linkage with the track mechanism is call as “RHyMo”, which corresponds to the acronym for “Rugged terrain Hybrid Mobile platform”

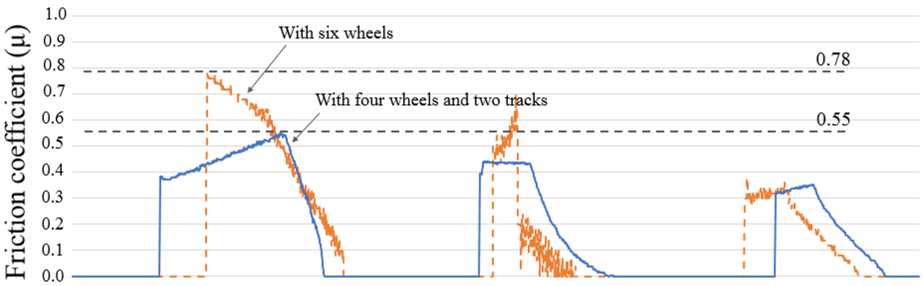

Fig. 5.9. The friction coefficient of proposed mobile platform with six wheels and four wheels and two track

5.5. A PVI-Terrainability of mobile platforms

The PVI−terrainability of various mobile platforms are compared with that of RHyMo as shown in Fig. 5.10. As mentioned before, the wheel−linkage mobile platforms are located at lower right side of the graph, which indicates that they ensure low posture variation and poor terrainability. The track−based mobile platform are located at the upper left side of the graph, which implies that they achieve excellent terrainability and poor posture variations on rugged terrain.

The proposed mobile platform RHyMo is located at the upper right side of the graph, which means that it has much lower posture variation and also has higher terrainability. The terrainability of RHyMo may not be higher than that of the track−based mobile platforms but with respect to the posture variation, RHyMo guarantees the excellent capability of overcoming obstacles smoothly on rugged terrain and seems to be more suitable for traveling and carrying out manifold tasks on rugged terrain.

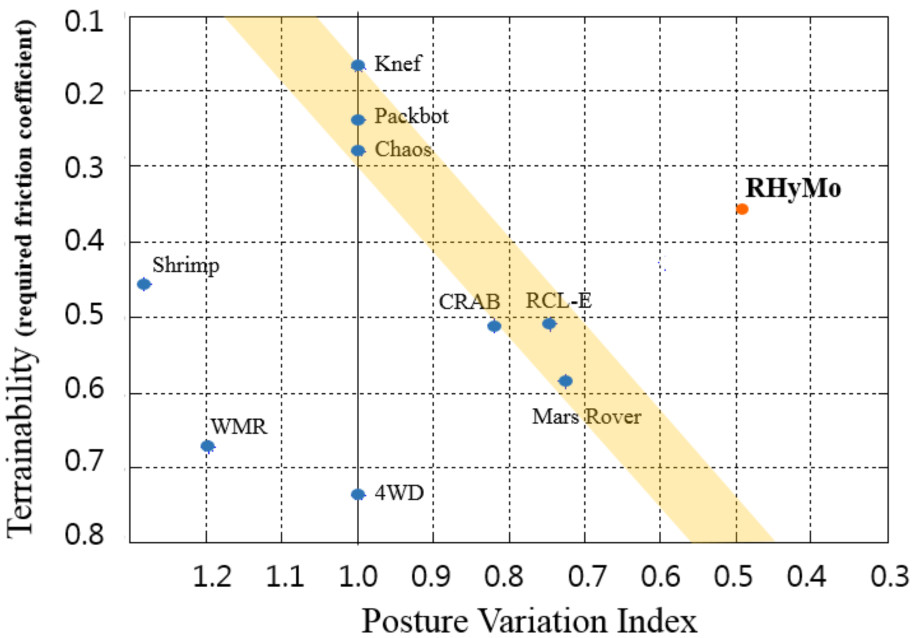

Fig. 5.10. A PVI−terrainability of mobile platforms with RHyMo

Chapter 6. Simulation of RHyMo

Simulation was performed to compare the movements of mobile platforms on rugged terrain. From analyzing rugged terrain shape on a real world, a rugged terrain for simulation was designed. The heights variation, the pitch angles variation and the PVI values of mobile platforms were measured while mobile platforms traveling on a rugged terrain and the data were compared. Also, performances of RHyMo and Rocker–Bogie were compared.

6.1. Modeling of rugged terrain

On the Rescue Robot League [51], a rugged terrain is artificially manufactured with combination of wooden blocks as shown in Fig. 6.1 (a). A wooden blocks have different heights and they are randomly placed. Since the rectangular shape terrain is most challenging terrain for mobile platforms, the rugged terrain used in Rescue Robot League is representing a harsh rugged terrain in real world. Similar to the terrain, a rugged terrain with rectangular shape was modeled for simulation (Fig. 6.1 (b)). The rugged terrain was made of blocks with two different heights: one is same as wheel radius and the other is same as half of the wheel radius. Blocks are randomly placed to make a rugged terrain as similar as real world.

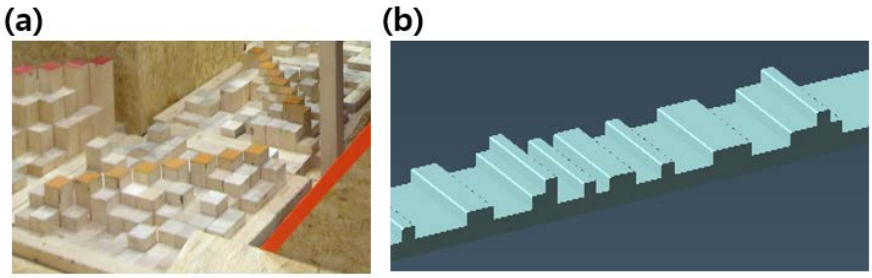

Fig. 6.1. (a) The rescue robot league terrain (b) The rugged terrain modeling.

6.2. Comparison of mobile platforms movement on rugged terrain

The height variation, pitch angle variation and traveling time of mobile platforms were measured while traveling the rugged terrain by simulation. Four−wheel drive car, Rocker−Bogie, RCL−E, and CRAB were compared in simulation (Fig. 6.2). The mobile platforms travel on the rugged terrain at a speed of 3 m/min.

The simulation results are shown in Table VI. In the section 2, the PVI value of each mobile platform was calculated and the PVI value of four−wheel drive car shows the highest value. After the four−wheel drive car, CRAB, RCL−E and Rocker−Bogie show high PVI value in order. Since the PVI value is a function of height and pitch angle variation of main body, a mobile platform with low PVI value can be expect to show low height and pitch angle variation while traveling on the rugged terrain, which guarantees smooth movement of the CM. In Table VI, the order of average height variations of main body shows the same tendency as the order of PVI values of mobile platforms. The order of pitch angle variations of main body also shows the same tendency as the order of PVI values except for CRAB. Due to an interaction of linkages of CRAB, CRAB shows the low pitch angle variation on a rugged terrain traveling. However, unlike the pitch angle variation, a height variation of main body shows the large value so that CRAB does not show smooth movement on the rugged terrain.

The order of traveling times on the rugged terrain shows the same tendency as the order of PVI values of mobile platforms. If height and pitch angle variations of a mobile platform are low, it means the mobile platform moves along the horizontal line of the ground and the moving distance will be minimized. Therefore, if traveling speed of mobile platforms are same, the traveling time will be proportional to the PVI value. As shown in Table VI, 58.68 second was necessary for four−wheel drive car to travel the rugged terrain, and 56.73 second was necessary for Rocker−Bogie.

On the definition of PVI in Section 2, for the simplicity of analysis, a single wheel' s lift up is chosen as the alternative of measuring the capability of mobile platform. The simulation result shows the PVI value represents mobile platforms movement on a rugged terrain. ,

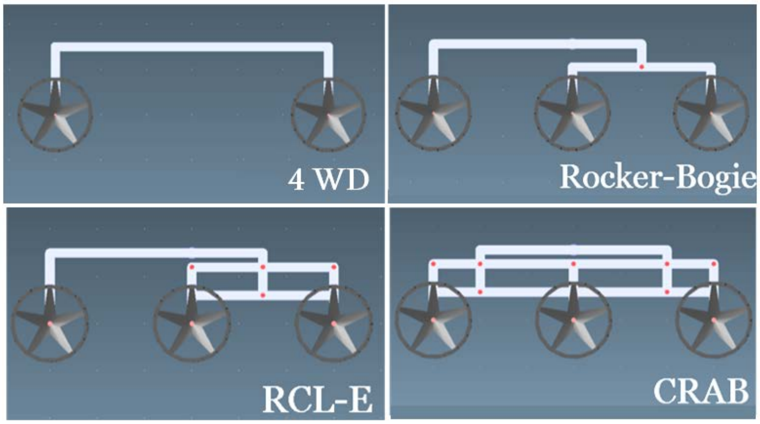

Fig. 6.2. Modeling of a four−wheel drive, Rocker−Bogie, RCL−E and CRAB

Table. VI. PVI, traveling time, height and pitch angle variation of the platforms

Mobile Platform	4WD	Rocker-Bogie	RCL-E	CRAB
PVI	1.000	0.725	0.746	0.820
	- 4 -	- 1 -	- 2 -	- 3 -
Traveling time [sec]	58.68	56.73	57.09	58.35
	- 4 -	- 1 -	- 2 -	- 3 -
Δh avg [mm]	20.51	13.86	14.14	17.65
	- 4 -	- 1 -	- 2 -	- 3 -
Δθ avg [degree]	3.95	3.44	3.71	3.43
	- 4 -	- 2 -	- 3 -	- 1 -

6.3. Comparison of Rocker-Bogie and RHyMo

A simulation using RHyMo on the rugged terrain was performed for comparison. Rocker−Bogie was used for comparison because Rocker−Bogie mechanism shows lowest posture variation. Fig. 6.3 shows traveling movements of Rocker−Bogie and RHyMo on rugged terrain. A pitch angle variation of main body is observed in a Fig. 6.3 (a). On the other hand, in Fig. 6.3 (b), a pitch angle of RHyMo seems to maintain its initial value even though the terrain is quite rugged.

The height and pitch angle variation of Rocker−Bogie and RHyMo while traveling are shown in Fig. 6.4 and Table VII. In the case of height variation of main body, the height variation of RHyMo always shows low value compared to that of Rocker−Bogie. The average height variation of Rocker−Bogie was 38.89 mm. The average height variation of RHyMo was 34.99 mm and it is decreased by 14.57 % compared to the height variation of Rocker−Bogies'. The maximum height variation of Rocker−Bogie is 54.05 mm and that of RHyMo is 51.63 mm, and the value was decreased by 4.48 %.

In the case of pitch angle variation of main body, the pitch angle variation of RHyMo does not always show low value compared to that of Rocker−Bogie, but the average and the maximum angle are lower than Rocker−Bogie. The average pitch angle variation of Rocker−Bogie was 2.01 degree, and the average pitch angle variation of RHyMo was 1.65 degree. The maximum pitch angle variation of Rocker−Bogie was 7.10 degree, and the maximum pitch angle variation of RHyMo was 4.89 degree. The average value was decreased by 17.74 % and the maximum value was decreased by 31.13 %. In the simulation of Rocker−Bogie, the large peak pitch angle variation was observed and this variation can cause moment shock to the main body or some stuff on the main body. On the other hand, the pitch angle variation of RHyMo does not show large peak variation on rugged terrain, which reduces the damage on main body.

From the simulation result, RHyMo shows low posture variation compared to Rocker−Bogie mechanism.

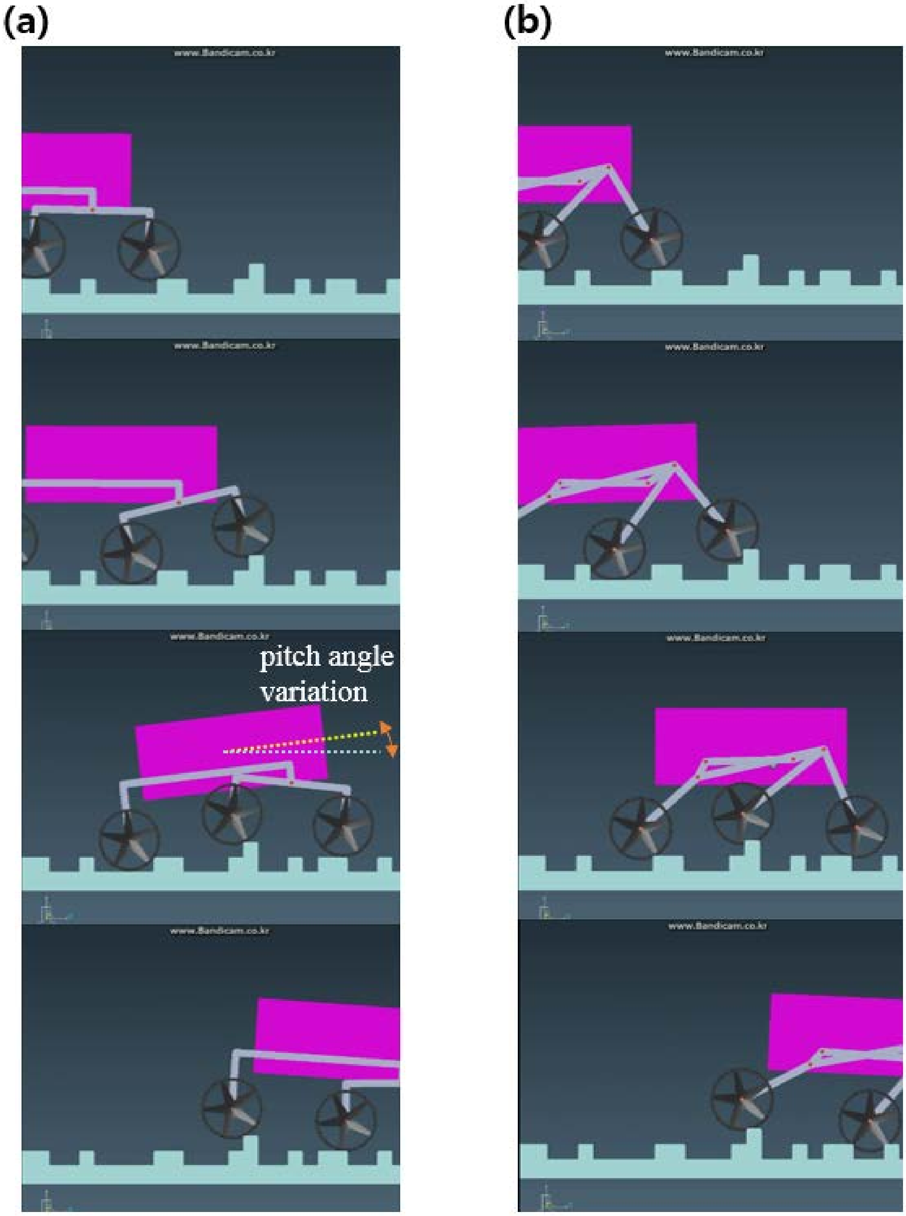

Fig. 6.3. Sequences of simulation on rugged terrain traveling of (a) Rocker−Bogie and (b) RHyMo

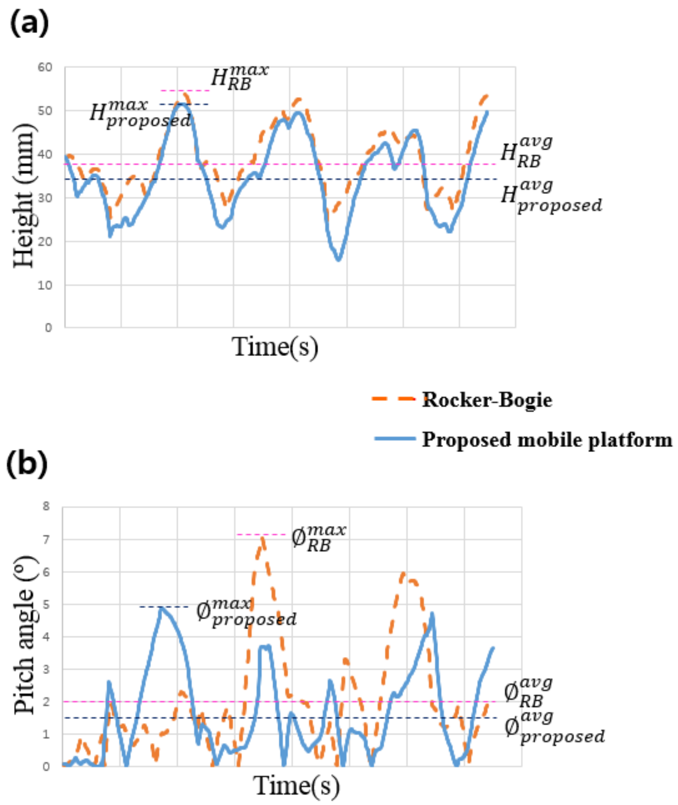

Fig. 6.4. (a) A height variation and (b) a pitch angle variation of Rocker−Bogie and RHyMo

Table. VII. PVI, height and pitch angle variation of Rocker−Bogie and RHyMo on simulation

		Rocker-Bogie	RHyMo	Decrement rate
Height term in PVI		0.623	0.540	13.34 %
Pitch angle term in PVI		1.163	0.918	21.07 %
Height [mm]	Average	38.89	34.99	10.04 %
	Maximum	54.05	51.63	4.48 %
Pitch angle [°]	Average	2.01	1.65	17.74 %
	Maximum	7.10	4.89	31.13 %

Chapter 7. Design of RHyMo

To conduct experiments evaluating the proposed mobile platform's performance, a prototype of RHyMo was assembled. The new inverse four-bar linkage mechanism was implemented and the front wheel is replaced with a track. Main issue for the design was to avoid interferences between linkages to make the platform smooth movement on a rugged terrain. Heights of six wheels will be changed during traveling and in all case, the linkages will not interfere with other linkages.

For the detail, the front linkage was designed to make it easy to replace a wheel module with a track module. Batteries are included in the platform body and all power lines from batteries to motors are hidden in linkages. Control units are located on a front of main body to be easily modified and check errors. Also, RHyMo was made for Multi Scale Robot System, therefore spaces to load a quadcopter and small robots are prepared

7.1. Outline of RHyMo

CAD design of RHyMo is shown in Fig. 7.1. Tracks and wheels are commercial items and other parts are designed in the scale of 1:1 by CAD program and manufactured. The size of RHyMo is 1000 mm in length, 700 mm in width and 450 mm in height. Two direct current (DC) motors (RE-30 60 W, Maxon, Switzerland) were used for the track, and four DC motors (RE-40 150 W, Maxon, Switzerland) were used for the rotating wheels. Weight of the platform is 53 kg including batteries and all parts are manufactured with aluminum to reduce the weight. Arduino Mega (Italy) [54] and Wii wireless classic controllers (Nintendo, Japan) were used to control RHyMo.

The mobility of RHyMo on a flat surface was tested first. RHyMo traversed at 20 m/min at maximum and can move forward and backward.

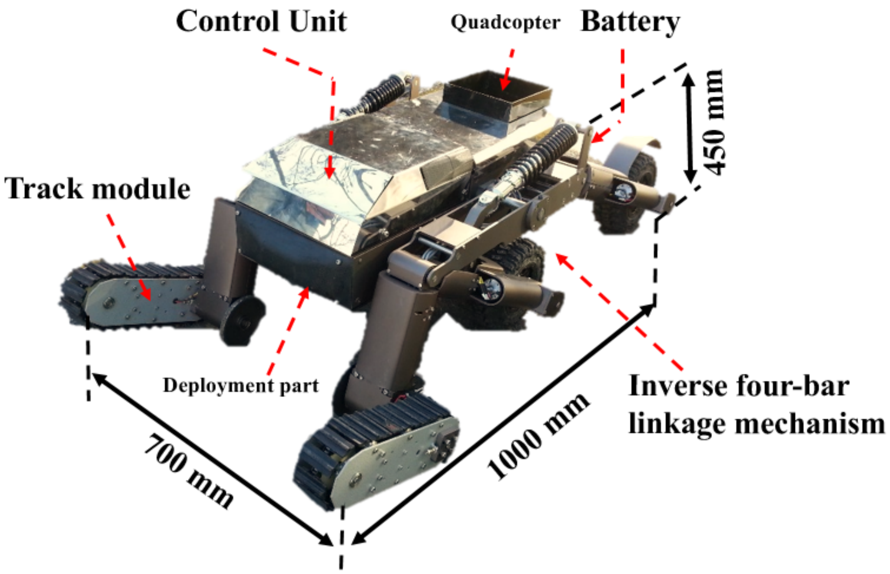

Fig. 7.1. A new mobile platform RHyMo.

It could rotate in a narrow space by driving the left and right wheels in opposite directions. RHyMo is able to move with 60 kg payload.

7.2. Description of mechanical parts

Each model parts of RHyMo are described in this section. RHyMo are composed of a platform body, a linkage part, a track module part and a control unit. All parts are designed not to interference with other parts.

7.2.1. A platform body

The platform body was designed to include much stuff on it and to easily balance left and right linkages. Control unit, batteries, quadcopter and small robots are loaded on the main body. Since the quadcopter has large wings larger than width of main body, a space for quadcopter was placed on a back side. Small robots have to deploy from the main body, a space for small robots was located in front of main body. To make it easy to repair and check error, the control unit was placed on top of front of main body. In the last, batteries were located on bottom of back of main body. Four 13.2 V 6600mAh batteries for motor power and one 13.2 V 910 mAh battery for operating Arduino are located inside of platform.

For the quadcopter, the open box of 165 mm(W) * 165 mm(L) * 120 mm(H) size was designed.(Fig. 7.3) When a quadcopter is loaded on the box, half of the quadcopter body will be go inside of the box. Quadcopter can easily take off from RHyMo by moving upward. To prevent the damage by vibrations while traveling, sponges are located inside the box.

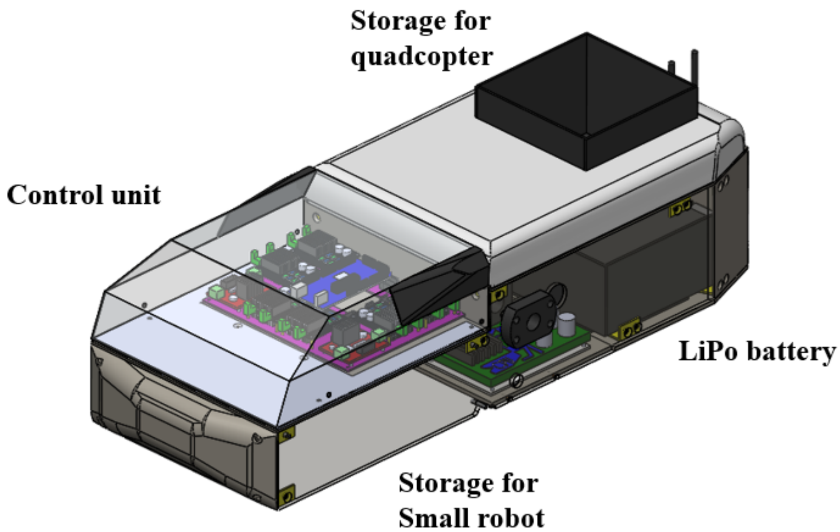

Fig. 7.2. A platform body of RHyMo

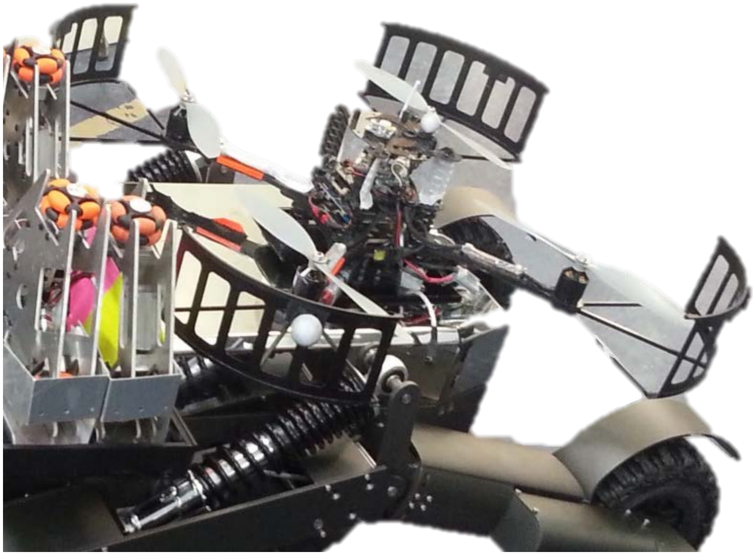

Fig. 7.3. RHyMo with quadcopter on it.

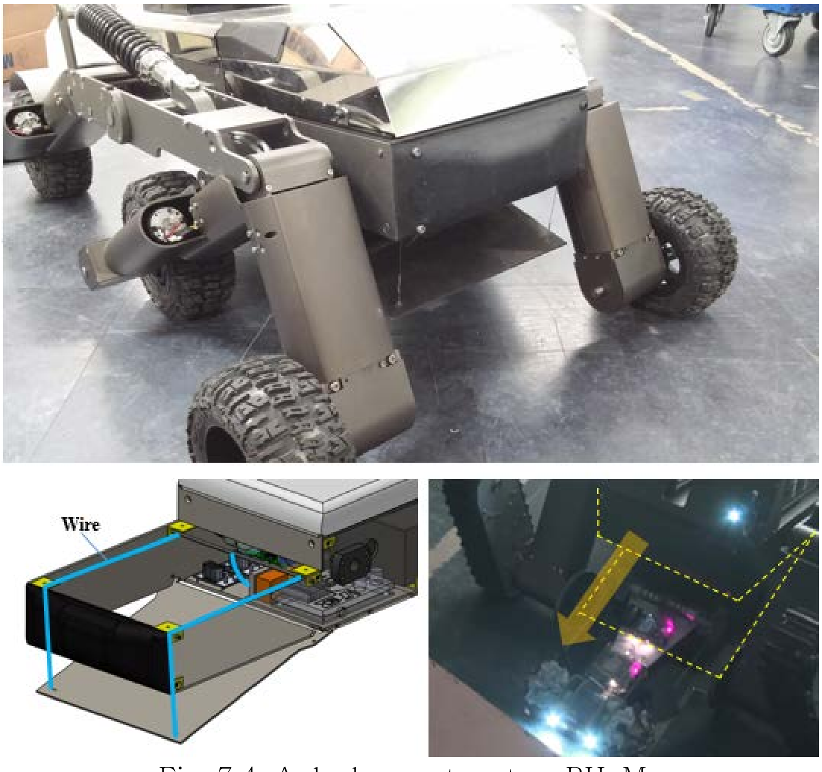

Fig. 7.4. A deployment part on RHyMo

The bottom plate of RHyMo is opened downward to deploy small robots inside of RHyMo. A wire is attached to the bottom plate, and length of the wire is controlled by a motor. By changing motor speed, an opening speed of the bottom plate can be changed. After the bottom plate is opened, small robots can be deployed from RHyMo with their movement capability. The design of deployment part is shown in Fig. 7.4.

The main body needs a balancing mechanism because the left and right linkages may move in different ways. On the rugged terrain, the path of the left wheels and the path of the right wheels are different so that height variations and pitch angle variations of left and right linkage are different. When the heights of left and right linkages are different, the main body may rotate on a roll direction. However, height difference between two linkages are quite small compared to width of RHyMo, a roll angle variation will not be the issue while the RHyMo travels on the rugged terrain.

To the contrary, in the case of pitch angle, the pitch angle difference between two linkages is large and cannot be ignored. If the left linkage and the right linkage are connecting by one solid axis, the axis will be twisted. If the left linkage and the right linkage are connected by two separate axes and rotating joint, RHyMo can be free from the axis-twisted problem but the main body could not maintain its pitch angle and rotate freely. Therefore differential mechanism was used on the main body.

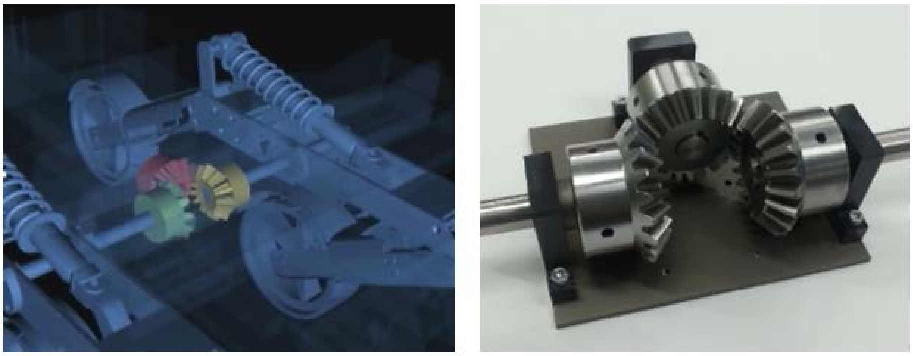

Fig. 7.5. A differential gear mechanism on RHyMo

Differential mechanism is the mechanism consisting of three bevel gears as shown in Fig. 7.5. The left and right bevel gears are connected with left and right linkage, and middle bevel gear is connected with main body. When the left linkage is fixed and the right linkage rotates, the middle bevel gear rotates by half of right linkage pitch angle. As a result, the pitch angle of main body is at the average value of the pitch angles of left and right linkages. With the help of this mechanism, the pitch angle of RHyMo can make smooth movement on a rugged terrain where the left and right wheel paths are different.

7.2.2. A linkage mechanism design

The linkage mechanism is designed on the basis of the inverse four-bar mechanism and all linkages will not interfere with other linkages. In the simulation, interference between each linkage is not considered even though all linkages are located on same plane. However, in real application, linkages have to be placed at different

Fig. 7.6. A linkage mechanism on RHyMo

planes to avoid interference between the linkage 10 and the linkage 13. On the inverse four-bar-linkage mechanism, intersection of two linkages is unavoidable. Therefore linkage 10 was designed to consist of two parts and the middle of the linkage 10 is empty. The linkage 13 intersects with this empty space. The front linkage was designed to attach the wheel module and the track module. The motors for tracks and wheels are installed inside a hollow link. Details of linkage part is shown in Fig. 7.6.

7.2.3. A wheel module and a track module design

Details of the wheel module and the track module are shown in Fig. 7.7. The wheel module is composed of wheel, bevel gears and one driven motor. The inside of linkage 1 has a space for a motor and the motor will be placed inside of linkage 1 as shown in Fig. 7.8. The track module is composed of track, bevel gears and one driven motor and one angle motor. Driven motor is located inside of the track. The angle motor is located in the linkage 1 and it changes the angle between the track and the ground. The wheel module and the track module will be changed depending on the experiment.

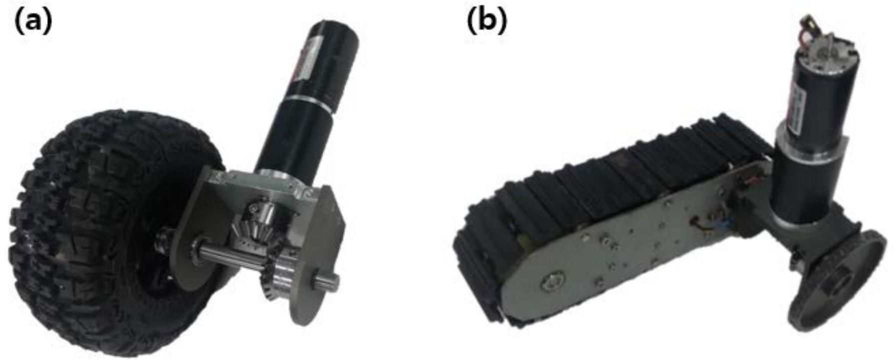

Fig. 7.7. (a) A wheel module and (b) a track module

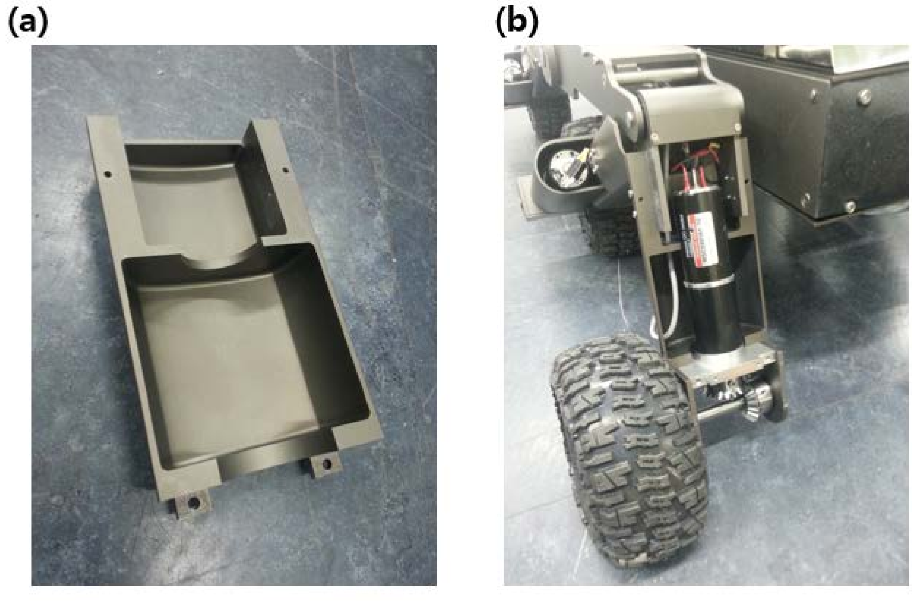

Fig. 7.8. (a) The front linkage on RHyMo (b) a front linkage with wheel module

7.3. A control unit

An Arduino Mega was used for RHyMo control [54]. The Arduino is the control module with Atmega 128 on it, and it receives sensor data and send PWM signal to motor drivers. Six motor drivers are attached for driven motors, two motor drivers are attached for the angle motors and one motor driver is attached for deployment. PCB board was designed for each motor driver.

A Wii wireless controller was used for user input (Fig. 7.9). The Wii wireless controller has transmission unit and reception unit, and these two units are connecting with Bluetooth. The transmission unit transmit x- and y-axes data given by the joystick, pitch angle data, roll angle data and two button data. According to joystick data, RHyMo could move forward, backward, and rotate in same position. According to two button data and pitch data, the left and right track moves upward and downward and the bottom plate move upward and downward. Motors are controlled by open loop control.

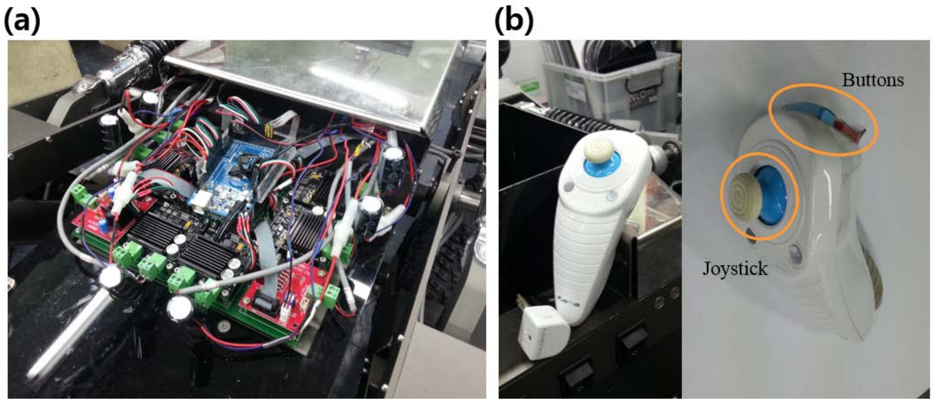

Fig. 7.9. (a) An Arduino and control unit (b) a Wii wireless controller

Chapter 8. Experiment and discussion

Experiments were performed to evaluate the posture variation and terrainability of RHyMo. A rugged terrain and a step were made for experiment, and a Rocker−Bogie platform, RHyMo with wheel module and RHyMo with track module were used for the experiment.

8.1. Posture variation experiment on rugged terrain

Rocker−Bogie platform is manufactured as shown in Fig. 8.1 (a) for comparison with RHyMo, whose overall size is 600 mm x 450 mm x 800 mm (width x height x length). In order to ensure fairness of experiments, the track mechanism of front linkage of RHyMo is replaced with the wheel of same diameter because the purpose of the experiment is to measure the effect of new linkage mechanism on smooth movement.

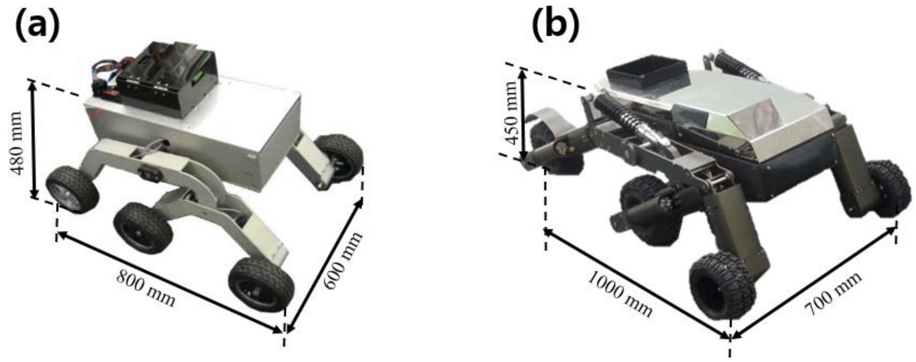

Fig. 8.1. (a) Rocker−Bogie platform and (b) Proposed RHyMo with six wheels,

8.1.1. A rugged terrain design

To design a rugged terrain for experiment, the shape of a real rugged terrain in Fig. 8.2 (a) was analyzed. The HC-sr04 ultra-sonic sensor and linear guide are used in the measuring device. Length of the linear guide is 800 mm similar to the length of the platforms. Three points of rugged terrain was measured and roughness average (Ra), maximum height of profile (Rmax) and instance maximum height change of rugged terrains are shown in Table VIII.

Shape of the artificial rugged terrain for experiment was designed based on the data in Table VIII. The artificial rugged terrain is artificially constructed with three types of rectangular wood blocks whose heights are 50 mm, 100 mm and 150 mm, respectively. As

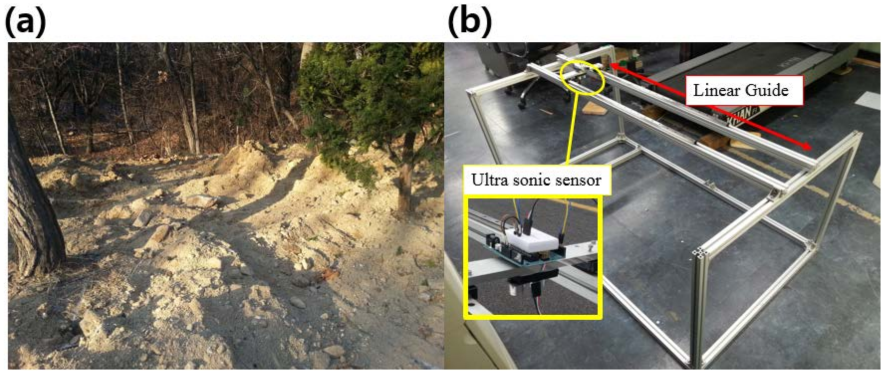

Fig. 8.2. (a) A rugged terrain in real world (b) The measuring device

Table. VIII. Ra, Rmax and instance maximum height variation of rugged terrains

	Real rugged terrain #1	Real rugged terrain #2	Real rugged terrain #3	Artificial rugged terrain #1	Artificial rugged terrain #2
Roughness average (Ra)	17	13	23	23	24
Maximum height of profile (Rmax) [mm]	102	104	110	100	100
Instance maximum height change [mm/mm]	49	55	55	50	50

shown in Fig. 8.3, wood blocks are placed randomly in order to reproduce roughness of rugged terrain. The total length of rugged terrain is 3000 mm and the surface roughness (Ra) is 25 mm. Roughness average (Ra), maximum height of profile (Rmax) and instance maximum height change were set similar to real rugged terrain. It is worthwhile to note that two paths for the left and right wheels of mobile platform are different from each other. During experiments, the trajectory of CM of mobile platform is captured by using a high-speed camera and the height and pitch angle variations of Rocker-Bogie and the proposed RHyMo are measured by using a pro-analyst program (Xcitex).

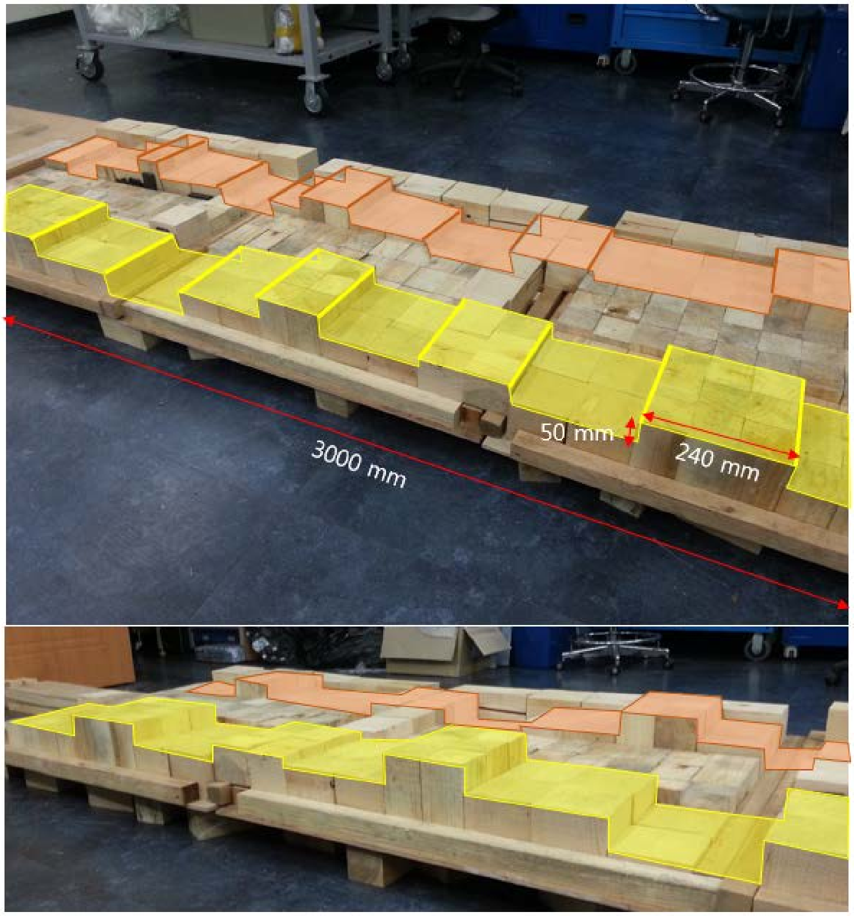

Fig. 8.3. The artificial rugged terrain constructed with rectangular wood blocks.

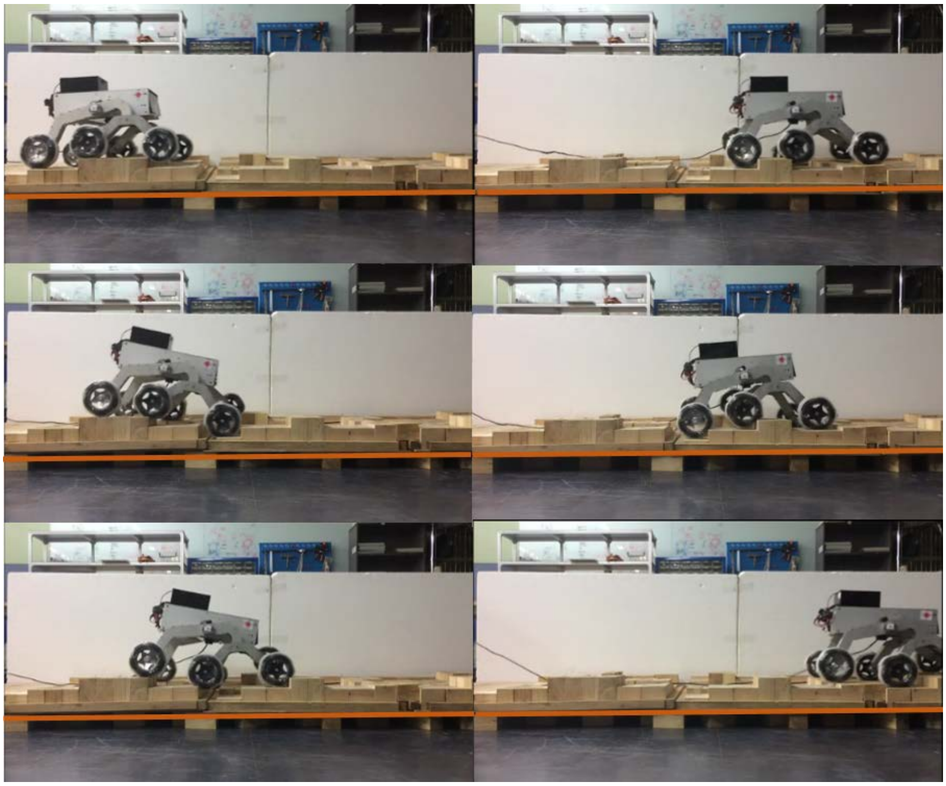

Fig. 8.4. Trajectories of CMs of Rocker−Bogie platform on manufactured rugged terrain

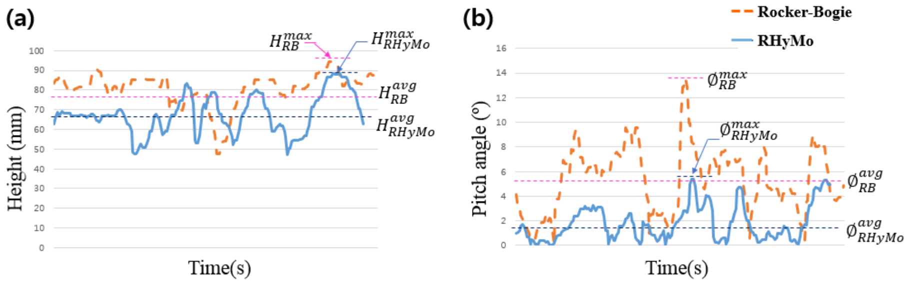

Fig. 8.6. (a) A height variations and (b) a pitch angle variations of Rocker−Bogie and RHyMo

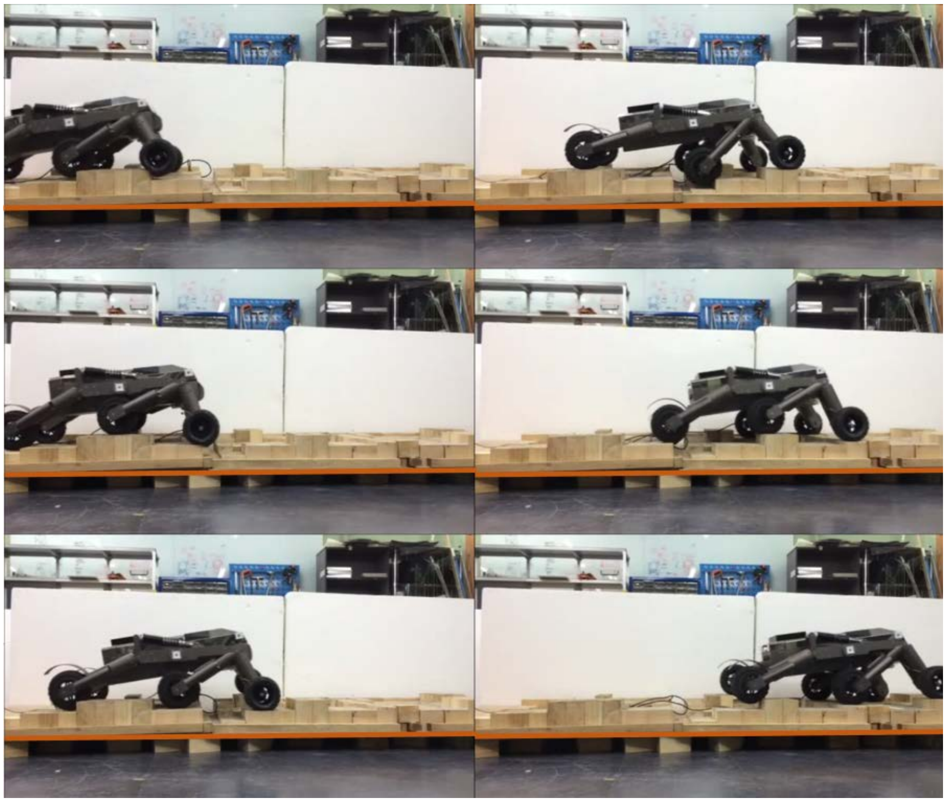

Fig. 8.5. Trajectories of CMs of RHyMo with six wheels on manufactured rugged terrain

Table. IX. PVI, height and pitch angle variation of Rocker–Bogie and RHyMo on experiment

		Rocker-Bogie	RHyMo	Decrement rate
Height term in PVI		0.623	0.540	13.34 %
Pitch angle term in PVI		1.163	0.918	20.07 %
Height [mm]	Average	77.56	67.69	12.72 %
	Maximum	94.18	88.58	5.96 %
Pitch angle [°]	Average	5.21	1.78	65.87 %
	Maximum	13.61	5.37	60.53 %

8.1.2. Experiment result on the rugged terrain

While traveling on the artificial rugged terrain in Fig. 8.3, the resulting trajectories of CMs of Rocker–Bogie and RHyMo are measured and shown in Figs. 8.4 and 8.5, respectively. The resulting height and pitch angle variations of Rocker–Bogie and RHyMo are shown in Fig. 8.6 (a) and 8.6 (b), respectively and in Table IX. The experimental results in Fig. 8.6 (a) verify that the average and maximum height variations of Rocker–Bogie are 77.56 mm and 94.18 mm, respectively. On the contrary, the average and maximum height variations of RHyMo are 67.69 mm and 88.58 mm, respectively. Therefore, compared to Rocker–Bogie, RHyMo reduced the average and maximum height variations by 12.72 % and 5.96 %, respectively.

The experimental results in Fig. 8.6 (b) imply that the average pitch angle variations of Rocker–Bogie and RHyMo are 5.21 º and 1.78 º, and their maximum pitch angle variations are 13.61 º and 5.37 º, respectively, which demonstrates that in comparison with Rocker–Bogie, RHyMo reduced the average and maximum pitch angle variations by 65.87 % and 60.53 %, respectively. The reason why the decrease of pitch angle variation of RHyMo is quite larger than that of its height variation is mainly because the pitch angle variation of inverse four–bar mechanism is small. The movement of RHyMo on rugged terrain is much smoother than that of Rocker–Bogie so that undesired oscillations or drastic changes in its height or pitch angle can be effectively prevented to considerably extend its viability on rugged terrain.

8.2. Terrainability experiment on a single step

The terrainability of RHyMo is investigated against a step whose height is up to 200 mm, same as wheel diameter.(Fig. 8.7) For experiments, the friction coefficient between the step and wheels of RHyMo is set to be 0.6, which is smaller than the friction coefficient required for RHyMo with six wheels to overcome the step (Recall that according to the dynamic analysis in Section 4, the maximum friction coefficient of RHyMo with six wheels is up to 0.78 while the maximum friction coefficient of RHyMo with two tracks and four wheels is 0.55).

The experimental results using RHyMo with six wheels and two tracks plus four wheels against the step are shown in Figs. 8.8 and 8.9, respectively. As shown in 8.8, RHyMo with six wheels cannot climb up the step and suffers from slip because RHyMo with six wheels does not have sufficient traction force required to climb the step. On the other hand, RHyMo with two tracks can overcome the step since the height of its contact point with the step is increased by using the track, so without slip, RHyMo with two tracks can climb the step with much smaller traction force. As discussed previously, the contact angle between the track and the step should be properly chosen so as to minimize the maximum friction coefficient because the pose of mobile platform is highly affected by the contact angle while climbing a step. From the experiment, the terrainability of mobile platform can be improved by replacing front wheel to a track.

Fig. 8.7. A step on experiment.

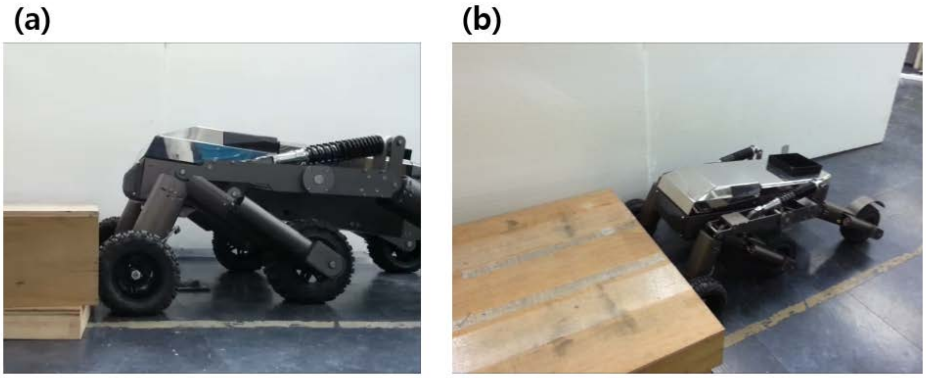

Fig. 8.8. Experimental results of climbing a step by using RHyMo with six wheels on (a) side view and (b) isometric view

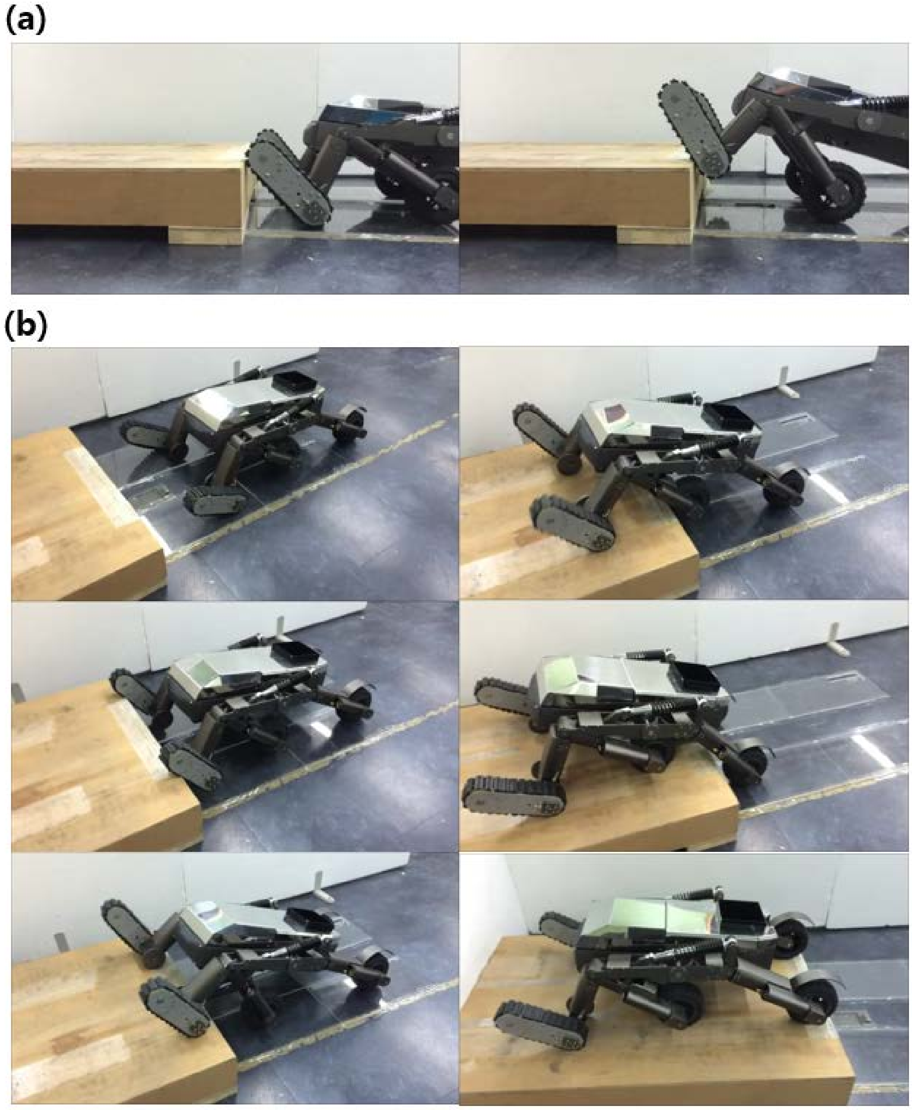

Fig. 8.9. Experimental results of climbing a step by using RHyMo with two tracks plus four wheels on (a) side view and (b) isometric view

8.3. Stair climbing experiment

The other experiment to examine the climbing capability of RHyMo is carried out against the stairs as shown in Fig. 8.10. Stairs are the most challenging terrain for mobile platform, because a platform has to not only overcome the high slope stairs, but also overcome the stair smoothly. Since the linkage mechanism of RHyMo is able to reduce the height and the pitch angle variation of the main body, RHyMo overcame all of the stairs successfully and smoothly without large vibrations. The tracks help RHyMo to contact the edges of stair, not to be stuck or hindered by the stairs.

The stair with overall size of 300 mm x 160 mm (length x height) and 28.1 ° slope was used for experiment. As confirmed in Fig. 8.10, RHyMo can climb the stairs of high slope successfully without any complex control strategy. Also, even at the speed of 20 m/min, RHyMo maintains its movement on stairs as smooth as possible, which can be observed from the fact that the trajectory of CM is very similar to the dotted line whose slope is same as that of stairs. This is possible due to the inverse four-bar linkage mechanism combined with the track mechanism of RHyMo.

For comparison with RHyMo, Rocker-Bogie with track was tested on a low slope stair. The overall size of stairs is 300 mm x 100 mm (length x height) and the corresponding slope is 18.4 º (Fig. 8.11). Since a track was installed in front of platform, Rocker-Bogie with track overcomes the stair with high terrainability. However, RHyMo shows much smoother movement on stair climbing movement because the PVI value of RHyMo is better compared to the PVI value of Rocker-Bogie. Fig. 8.11 and 8.12 show the camera views while two platforms overcome the stair and the video from Rocker-Bogie with track highly vibrate while overcome the stair. The light on a ceiling in video was appeared and disappeared due to large vibration. On the other hand, the video from RHyMo shows constant picture in all moment because of smooth movement.

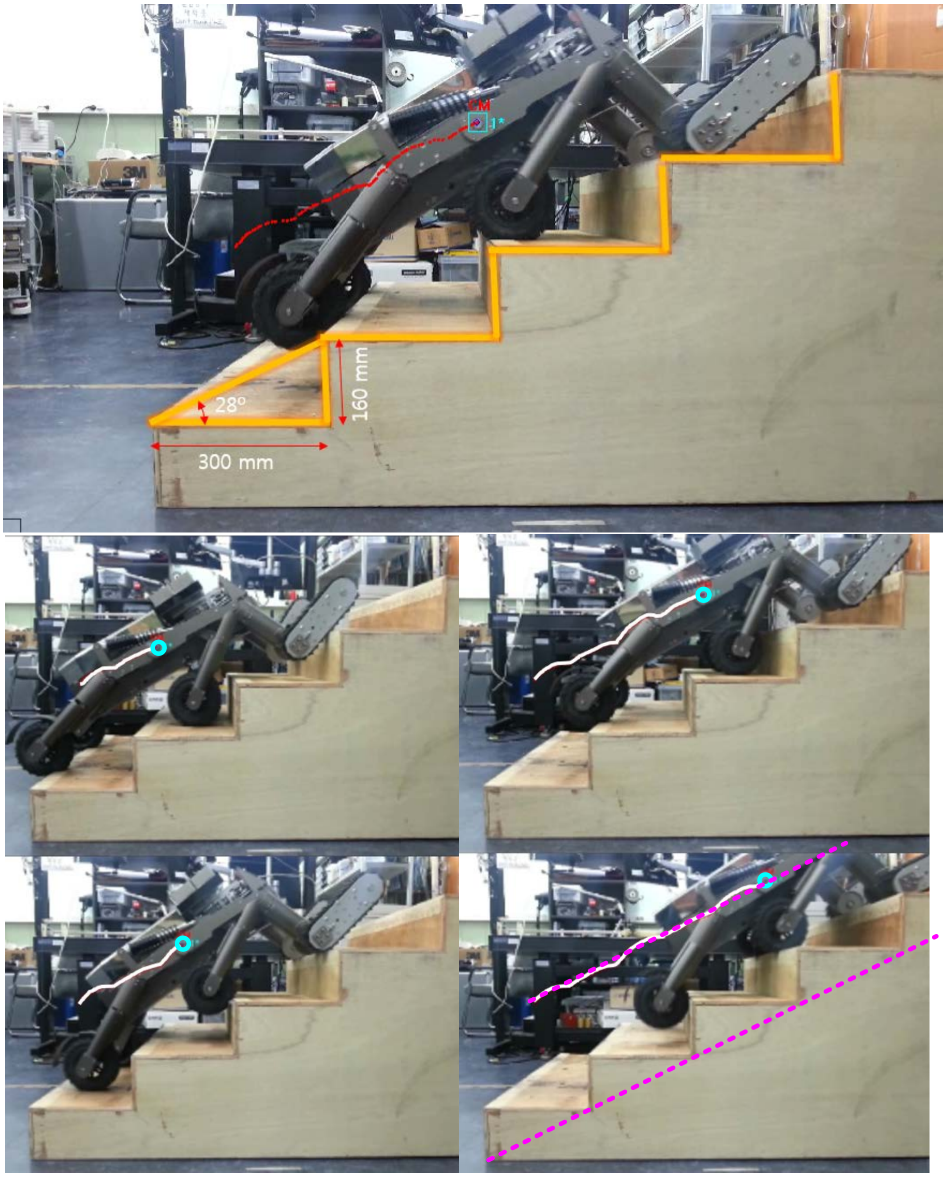

Fig. 8.10. Experimental result of climbing stairs of steep slope by using RHyMo

Fig. 8.11. Pictures from Rocker-Bogie with track while climbing stair

Fig. 8.12. Pictures from RHyMo while climbing stair

8.4. Summary of experimental results

Three experiments were performed to verify a performance of new mobile platform RHyMo: on the rugged terrain, on the step and on the stair. The posture variation of RHyMo and Rocker−Bogie platforms were compared and RHyMo was expected to shows much smoother movement than Rocker−bogie on rugged terrain. RHyMo had a 12.72 % decrease in the average height variation 5.96 % decrease in the maximum height variation compared to Rocker−Bogie on rugged terrain traveling. Also RHyMo had a 65.87 % decrease in the average pitch angle variation and 60.53 % decrease in the maximum pitch angle variation compared to Rocker−Bogie.

In the second experiment, terrainability of RHyMo with track and RHyMo with wheel were compared in step overcoming experiment. RHyMo with wheel cannot overcome the step with 0.6 friction coefficient, but RHyMo with track can overcome the step. The track in front helps RHyMo to contact the edge of the step and it makes RHyMo overcome the step with low friction coefficient.

Finally, RHyMo and Rocker−Bogie with track were tested on the stair. Two platforms easily overcome the stair by using the track. However, since posture variation index values of two platforms were different, performances of two platforms are quite different. RHyMo show much smoother movement on the stair and video from RHyMo shows constant picture.

As a result of experiments, the new mobile platform RHyMo not only shows low posture variation which guarantees smooth movement on rugged terrain traveling but also shows high terrainability. It is worthwhile to note that even though smooth movement of mobile platform on rugged terrain may not be the main factor to determine its mobile stability, the smooth movement on rugged terrain can supply the insight into the current state of mobile platform so that if the movement of mobile platform is fluctuated frequently while traveling on rugged terrain, it implies that the mobile platform is prone to be unstable. Therefore, the smoothness of movement of mobile platform can be used as the effective metric for predicting the state of mobile platform on rugged terrain and RHyMo shows smoothest movement compare to other mobile platforms in simulation and in experiment.

Chapter 9. Conclusion

While a mobile platform travels on rugged terrain, small posture variation and high terrainability play important roles in determining the performance of mobile platform such as manipulation, inspection and rescue etc. In this study, the posture variation index (PVI) is suggested as a new metric to evaluate the smoothness of movement of mobile platform. By using the proposed PVI, the smoothness of movements of various mobile platforms on rugged terrain are analyzed, which shows that among various platforms, Rocker–Bogie mechanism ensures much smoother movement on rugged terrain. Based on this observation, a new linkage based mobile platform is proposed to reduce the height and pitch angle variations by performing the kinematic analysis. Also, by replacing the front wheel with the track mechanism, the terrainability of mobile platform was improved and inverse dynamic analysis was performed for optimizing a track angle.

Finally, the new mobile platform called as "RHyMo" is constructed by combining the inverse four–bar linkage with Rocker–Bogie mechanism. The extensive experiments using Rocker–Bogie platform and RHyMo on an artificial rugged terrain, step, and stairs validate that the height and pitch angle variations of RHyMo are considerably reduced compared to those of Rocker–Bogie platform, which implies that RHyMo guarantees much smoother movement while traveling on rugged terrain. 12.72 % of average height variation was decreased and 65.87 % of pitch angle variation was decreased.

Also, the terrainability of RHyMo has been significantly enhanced to easily overcome the step or stairs of high slope without any complex control strategy with track in front.

The PVI–terrainability was derived for mobile platforms, and RHyMo shows lowest posture variation and high terrainability on the graph which means RHyMo is the most suitable mobile platform for rough terrain task. For the future work, RHyMo will load a Quad copter and small robots and cooperate with these robots for executing search and rescue missions on rough terrain tasks.

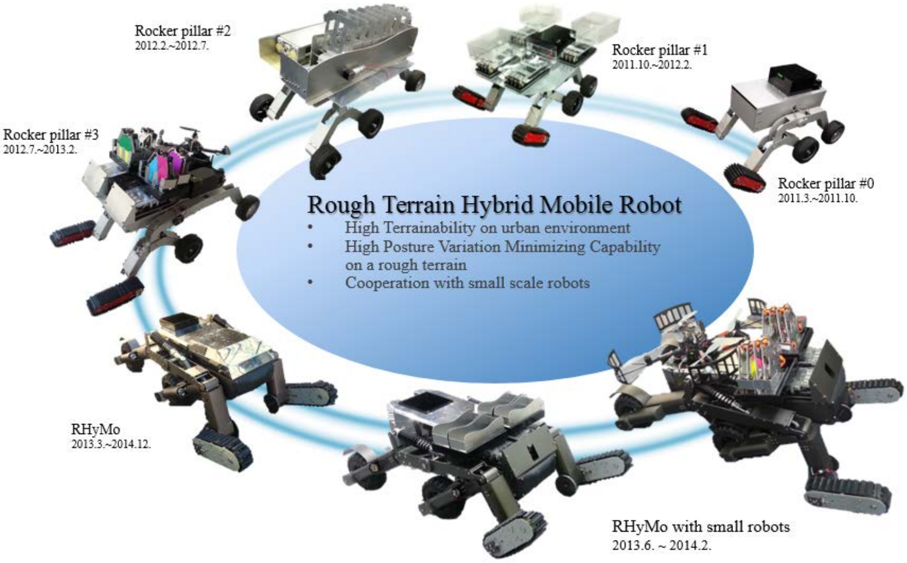

Fig. 9.1. History of Rough terrain hybrid mobile robot

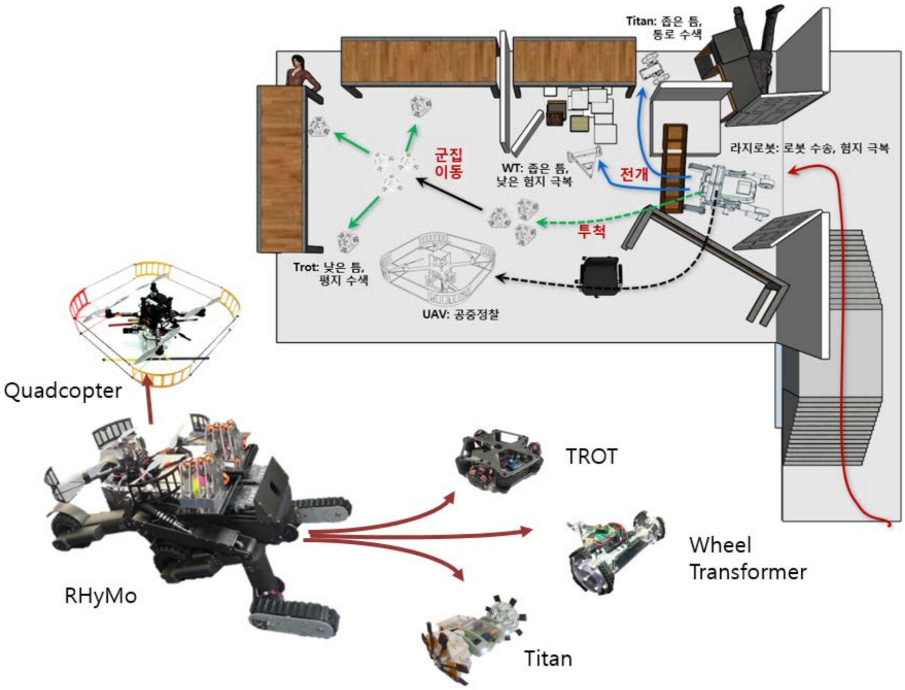

Fig. 9.2. Rescue mission on MRL project

Bibliography

[1] Iagnemma, K. D., Rzepniewski, A., Dubowsky, S., Pirjanian, P., Huntsberger, T. L., & Schenker, P. S. "Mobile robot kinematic reconfigurability for rough terrain." *Intelligent Systems and Smart Manufacturing*. International Society for Optics and Photonics, 2000.

[2] Kubota, T., Kuroda, Y., Kunii, Y., & Nakatani, I. "Small, light-weight rover “Micro5” for lunar exploration."*Acta Astronautica* 52.2 (2003): 447-453.

[3] Barlas, Fırat. *Design of a Mars rover suspension mechanism*. Diss. Izmir Institute of Technology, 2004.

[4] Freitas, G., Lizarralde, F., Hsu, L., & Dos Reis, N. R. S.. "Kinematic reconfigurability of mobile robots on irregular terrains." *Proceedings of the 2009 IEEE international conference on Robotics and Automation*. IEEE Press, 2009.

[5] Lauria, M., Y. Piguet, and R. Siegwart. "Octopus: an autonomous wheeled climbing robot." Proceedings of 5th International Conference on Climbing and Walking Robots (CLAWAR). 2002.

[6] Jaulin, Luc. "Control of a wheeled stair-climbing robot using linear programming." Robotics and Automation, 2007 IEEE International Conference on. IEEE, 2007.

[7] Lee, W., Kang, S., Kim, M., & Shin, K. "Rough terrain negotiable mobile platform with passively adaptive double-tracks and its application to rescue missions." Robotics and Automation, 2005. ICRA 2005. Proceedings of the 2005 IEEE International Conference on. IEEE, 2005.

[8] Koh, Doo-Yeol, Soo-Hyun Kim, and Kyung-soo Kim. "Design and modeling of an image stabilizing device for small unmanned ground vehicle." Control, Automation and Systems (ICCAS), 2012 12th International Conference on. IEEE, 2012.

[9] Yoneda, Kan, Yusuke Ota, and Shigeo Hirose. "High-grip stair climber with powder-filled belts." The International Journal of Robotics Research 28.1 (2009): 81-89.

[10] Kadous, Mohammed Waleed, Raymond Ka-Man Sheh, and Claude Sammut. "Caster: A robot for urban search and rescue." Proceedings of the 2005 Australasian Conference on Robotics and Automation. 2005.
[11] Tao, Weijun, Yi Ou, and Hutian Feng. "Research on Dynamics and Stability in the Stairs-climbing of a Tracked Mobile Robot." Int J Adv Robotic Sy 9.146 (2012).
[12] Raibert, M., Blankespoor, K., Nelson, G., & Playter, R. "Bigdog, the rough-terrain quadruped robot." Proceedings of the 17th World Congress. 2008.
[13] Birkmeyer, Paul, Andrew G. Gillies, and Ronald S. Fearing. "CLASH: Climbing vertical loose cloth." Intelligent Robots and Systems (IROS), 2011 IEEE/RSJ International Conference on. IEEE, 2011.
[14] Birkmeyer, Paul, Kevin Peterson, and Ronald S. Fearing. "DASH: A dynamic 16g hexapedal robot." Intelligent Robots and Systems, 2009. IROS 2009. IEEE/RSJ International Conference on. IEEE, 2009.
[15] Saranli, Uluc, Martin Buehler, and Daniel E. Koditschek. "RHex: A simple and highly mobile hexapod robot." The International Journal of Robotics Research20.7 (2001): 616-631.
[16] Huang, K. J., Chen, S. C., Chou, Y. C., Shen, S. Y., Li, C. H., & Lin, P. C. . "Experimental validation of a leg-wheel hybrid mobile robot Quattroped." *Robotics and Automation (ICRA), 2011 IEEE International Conference on*. IEEE, 2011.
[17] Herbert, Sam D., Andrew Drenner, and Nikolaos Papanikolopoulos. "Loper: A quadruped-hybrid stair climbing robot." *Robotics and Automation, 2008. ICRA 2008. IEEE International Conference on*. IEEE, 2008.
[18] Hunt, A. J., Bachmann, R. J., Murphy, R. R., & Quinn, R. D. "A rapidly reconfigurable robot for assistance in urban search and rescue." *Intelligent Robots and Systems (IROS), 2011 IEEE/RSJ International Conference on*. IEEE, 2011.
[19] Dunker, P. A., Lewinger, W. A., Hunt, A. J., & Quinn, R. D. "A biologically inspired robot for lunar in-situ resource

utilization." *Intelligent Robots and Systems, 2009. IROS 2009. IEEE/RSJ International Conference on*. IEEE, 2009.

[20] Thueer, Thomas, and Roland Siegwart. "Mobility evaluation of wheeled all−terrain robots." *Robotics and autonomous systems* 58.5 (2010): 508−519.

[21] Thueer, Thomas, Ambroise Krebs, and Roland Siegwart. "Comprehensive locomotion performance evaluation of all−terrain robots." *Intelligent Robots and Systems, 2006 IEEE/RSJ International Conference on*. IEEE, 2006.

[22] Thueer, T., Krebs, A., Siegwart, R., & Lamon, P.. "Performance comparison of rough-terrain robots—simulation and hardware." *Journal of Field Robotics* 24.3 (2007): 251−271.

[23] Krebs, A., Thueer, T., Michaud, S., & Siegwart, R. "Performance optimization of all−terrain robots: a 2D quasi−static tool." *Intelligent Robots and Systems, 2006 IEEE/RSJ International Conference on*. IEEE, 2006.

[24] Chottiner, Jeffrey E. *Simulation of a six wheeled martian rover called the rocker bogie*. Diss. The Ohio State University, 1992.

[25] Hacot, Herve. *Analysis and traction control of a rocker−bogie planetary rover*. Diss. Massachusetts Institute of Technology, 1998.

[26] Hacot, Herv, Steven Dubowsky, and Philippe Bidaud. "Analysis and simulation of a rocker−bogie exploration rover." *COURSES AND LECTURES−INTERNATIONAL CENTRE FOR MECHANICAL SCIENCES* (1998): 95−102.

[27] Kucherenko, Vladimir, Alexei Bogatchev, and Michel Van Winnendael. "Chassis concepts for the ExoMars rover." *The 8th ESA Workshop on Advanced Space Technologies for Robotics and Automation (ASTRA'04)*. 2004.

[28] Thueer, Thomas, Pierre Lamon, and Ambroise Krebs. *CRAB−Exploration rover with advanced obstacle negotiation capabilities*. Swiss Federal Institute of Technology (ETHZ), Autonomous Systems Lab, 2006.

[29] Krebs, Ambroise, Thomas Thueer, and Edgar Carrasco. *Towards torque control of the CRAB rover*.

Eidgenössische Technische Hochschule Zürich, Autonomous Systems Lab, 2008.

[30] Woo, C. K., Do Choi, H., Yoon, S., Kim, S. H., & Kwak, Y. K. "Optimal design of a new wheeled mobile robot based on a kinetic analysis of the stair climbing states." *Journal of Intelligent and Robotic Systems* 49.4 (2007): 325-354.

[31] Meghdari, A., Pishkenari, H. N., Gaskarimahalle, A. L., Mahboobi, S. H., & Karimi, R. "A novel approach for optimal design of a rover mechanism." *Journal of Intelligent and Robotic Systems* 44.4 (2005): 291-312.

[32] Siegwart, R., Lamon, P., Estier, T., Lauria, M., & Piguet, R. "Innovative design for wheeled locomotion in rough terrain." *Robotics and Autonomous systems* 40.2 (2002): 151-162.

[33] Jeachul Joo, "A Study of the automobile 's Ride Comfort Influence according to the shape of the road" 2001.08.

[34] Freitas, G., Lizarralde, F., Hsu, L., & Dos Reis, N. R. S. "Kinematic reconfigurability of mobile robots on irregular terrains." *Proceedings of the 2009 IEEE international conference on Robotics and Automation*. IEEE Press, 2009.

[35] Peters, Steven C., and Karl Iagnemma. "An analysis of rollover stability measurement for high-speed mobile robots." *Robotics and Automation, 2006. ICRA 2006. Proceedings 2006 IEEE International Conference on*. IEEE, 2006.

[36] Papadopoulos, Evangelos, and Daniel A. Rey. "The force-angle measure of tipover stability margin for mobile manipulators." *Vehicle System Dynamics* 33.1 (2000): 29-48.

[37] Hirose, Shigeo, Hideyuki Tsukagoshi, and Kan Yoneda. "Normalized energy stability margin and its contour of walking vehicles on rough terrain." *Robotics and Automation, 2001. Proceedings 2001 ICRA. IEEE International Conference on*. Vol. 1. IEEE, 2001.

[38] Nagatani, K., Yamasaki, A., Yoshida, K., Yoshida, T., & Koyanagi, E. "Semi-autonomous traversal on uneven terrain for a tracked vehicle using autonomous control of active flippers." *Intelligent*

Robots and Systems, 2008. IROS 2008. IEEE/RSJ International Conference on. IEEE, 2008.

[39] Yamauchi, Brian M. "PackBot: a versatile platform for military robotics."*Defense and Security*. International Society for Optics and Photonics, 2004.

[40] Okada, Yoshito, Keiji Nagatani, and Kazuya Yoshida. "Semi-autonomous operation of tracked vehicles on rough terrain using autonomous control of active flippers." *Intelligent Robots and Systems, 2009. IROS 2009. IEEE/RSJ International Conference on*. IEEE, 2009.

[41] Lewis, P. J., Flann, N., Torrie, M. R., Poulson, E. A., Petroff, T., & Witus, G. "Chaos, an intelligent ultra-mobile SUGV: combining the mobility of wheels, tracks, and legs." *Defense and Security*. International Society for Optics and Photonics, 2005.

[42] Liu, Yugang, and Guangjun Liu. "Track--Stair Interaction Analysis and Online Tipover Prediction for a Self-Reconfigurable Tracked Mobile Robot Climbing Stairs." *Mechatronics, IEEE/ASME Transactions on* 14.5 (2009): 528-538.

[43] Liu, Guangjun, and Yugang Liu. "Track-stair and vehicle-manipulator interaction analysis for tracked mobile manipulators climbing stairs." *Automation Science and Engineering, 2008. CASE 2008. IEEE International Conference on*. IEEE, 2008.

[44] Freudenstein, Ferdinand. *Design of Four-link Mechanisms*. University Microfilms, 1954.

[45] Shiller, Zvi, and Moshe P. Mann. "Dynamic stability of off-road vehicles."*Intelligent Robots and Systems, 2004.(IROS 2004). Proceedings. 2004 IEEE/RSJ International Conference on*. Vol. 2. IEEE, 2004.

[46] Mann, Moshe P., and Zvi Shiller. "Dynamic stability of a rocker bogie vehicle: longitudinal motion." *Robotics and Automation, 2005. ICRA 2005. Proceedings of the 2005 IEEE International Conference on*. IEEE, 2005.

[47] Iagnemma, Karl, and Steven Dubowsky. "Mobile robot rough-terrain control (RTC) for planetary exploration." *Proceedings of*

the 26th ASME Biennial Mechanisms and Robotics Conference, DETC. Vol. 2000. 2000.

[48] Wikidepia Retrieved Dec 02. 2014. from http://en.wikipedia.org/wiki/Generalized_inverse

[49] Li, Suojun, Haibo Gao, and Zongquan Deng. "Mobility performance evaluation of lunar rover and optimization of rocker-bogie suspension parameters."*Systems and Control in Aerospace and Astronautics, 2008. ISSCAA 2008. 2nd International Symposium on*. IEEE, 2008.

[50] Lamon, P., Krebs, A., Lauria, M., Siegwart, R., & Shooter, S. "Wheel torque control for a rough terrain rover." *Robotics and Automation, 2004. Proceedings. ICRA'04. 2004 IEEE International Conference on*. Vol. 5. IEEE, 2004.

[51] Robocup rescue Retrieved Dec. 02. 2014. from http://en.wikipedia.org/wiki/Rescue_Robot_League

[52] Chen, B., Wang, R., Jia, Y., Guo, L., & Yang, L. "Design of a high performance suspension for lunar rover based on evolution." *Acta Astronautica* 64.9 (2009): 925-934.

[53] Dongkyu Choi, Jongkyun Oh, and Jongwon Kim. "Analysis method of climbing stairs with the rocker-bogie mechanism." Journal of Mechanical Science and Technology 27.9 (2013): 2783-2788.

[54] Arduino, Retrieved May. 10, 2014 from http://arduino.cc

Abstract in Korean

본 논문에서는 험한 지형에서 주행 시에 본체의 자세 변화가 작고 장애물 극복 능력도 높은 모바일 플랫폼 (RHyMo)의 개발에 대한 내용을 다룬다. 주행 시 발생 할 수 있는 의도하지 않은 진동을 예측하기 위하여, 울퉁불퉁한 지형에서의 모바일 플랫폼의 자세 변화를 측정하기 위한 지표(PVI)가 제안되었다. 이 지표는 본체의 높이 변화와 각도 변화의 식으로 이루어져 있으며 이 지표를 통하여 다양한 모바일 플랫폼들의 안정적인 주행이 분석되었다.

모바일 로봇의 비교 데이터를 바탕으로 역 사절구조를 이용한 새로운 링크 구조가 제안되었다. 새로운 링크 구조는 다른 링크 구조에 비하여 더 적은 높이 각도 변화를 보였다. 기구학 해석을 통하여 링크 길이가 최적화 되었으며 기존에 자세 변화가 가장 적었던 라커-보기 구조보다 17.9 % 더 적은 변화를 보였다.

기구학 해석과 역 동역학 해석을 바탕으로 자세 변화가 적으며 장애물 극복 능력도 높은 모바일 플랫폼 (RHyMo)이 개발되었다. 동일한 크기의 라커-보기 플랫폼과 험지 모형에서 주행 실험이 이루어졌으며 RHyMo 는 기존의 자세 변화 최소화 능력이 가장 높은 라커-보기 로봇에 비하여 12.72 % 적은 평균 높이변화와 5.96 % 적은 최대 높이 변화 값을 보였다. 또한 RHyMo 의 평균 각도 변화와 최대 각도 변화 값 역시 65.87 % 와 60.53 % 감소하였다. 또한 RHyMo 는 앞에 장착된 트랙을 통하여 다른 모바일 플랫폼에 비하여 더 높은 턱과 더 가파른 계단을 극복하는 모습을 보였다.

주요어 : 모바일 플랫폼, 자세 변화 지표, 험지 극복 능력, 안정적인 주행, 역 동역학 해석, 트랙 구조

학번 : 2010-20723